LEWIS-ACIDIC TRIARYLBORANES: OPTOELECTRONIC APPLICATIONS AND UNUSUAL REACTIVITIES

by

Christina Sun

A thesis submitted to the Department of Chemistry

In conformity with the requirements for

the degree of Master of Science

Queen's University

Kingston, Ontario, Canada

(June, 2012)

Abstract

A new electron-transport material using a triarylboron-functionalized 2,4,6-triphenyltriazine core has been synthesized. This compound exhibits reversible reduction with low-lying HOMO and LUMO energy levels, as well as a high-energy triplet state. Preliminary experiments incorporating this material into phosphorescent OLEDs as an electron transport layer gave devices with high current and external quantum efficiencies at brightness levels appropriate for applications in the display industry.

Furthermore, a nitrogen-containing alkynyltriarylboron compound, 2-(2'-(dimesitylboryl)phenylethynyl)pyridine, has been found to undergo a facile alkyne hydration reaction in the presence of copper(I) iodide and triethylamine. The copper(I)-catalyzed addition of water occurs at room temperature, and produces a brightly luminescent boron-enol compound that is stable under air. Studies of the reaction mechanism were carried out by monitoring product formation under different conditions using ^{1}H NMR. The cooperativity between the Lewis acidic triarylboryl group and Lewis basic pyridyl group is determined to be vital in promoting the hydration process and in stabilizing the enol structure of the product.

Finally, we have discovered that diarylplatinum(II) complexes of 2-(2'-(dimesitylboryl)phenylethynyl)pyridine are capable of undergoing an unusual intramolecular double aryl migration/cyclization reaction, resulting in the formation of a unique bicyclic organometallic scaffold. The structures of these remarkable products have been characterized by X-ray crystallography, as well as by 1D and 2D ^{1}H NMR. The reaction mechanism was established by ^{1}H NMR studies and by DFT calculations. The complementary electronic properties of the electron-deficient triarylborane and the electron-rich platinum centers were found to play a key role in this unprecedented transformation.

Acknowledgements

First, I would like to express my sincerest gratitude to Dr. Suning Wang. She has been my supervisor for the past three years while I worked in her group as a fourth-year thesis student, and as a graduate student. Dr. Wang is an excellent teacher and researcher that inspired many students, including myself, to pursue studies in inorganic chemistry. She has always made herself available to her students and is always open to scientific discussion. Throughout my graduate studies, Dr. Wang not only helped me develop research ideas, but also motivated me to pursue challenging projects. It is with her guidance and encouragement that I am able to accomplish this thesis. Her dedication to the well-being of her students and to the advancement of science is truly remarkable. It has been a privilege to work for Dr. Wang.

I would also like to thank members of the Wang group for their guidance, assistance and comedic relief: Dr. Chul Baik, Dr. Barry Blight, Dr. Yi Sun, Hazem Armarne, Yufei Li, Louis Lu, Ying-Li Rao, Maria Varlan, Nan Wang, Xiang Wang and Vlad Zlojutro. In particular, I am thankful to Zac Hudson for providing me with meticulous training as a synthetic chemist and as a scientific writer. His unwavering support, companionship and correction of my subject-verb agreements have been invaluable to me.

Moreover, I am grateful to many faculty members in the department in my six years at Queen's University. Dr. Diane Beauchemin gave me my first opportunity as an undergraduate researcher; she brought me to my first conference and encouraged me to pursue studies in chemistry. I have been very fortunate to have Dr. Ralph Whitney and Dr. David Zechel as advisors, teachers and committee members. They have truly made a positive impact on my experience as a student and as a researcher. The success of my projects is in no small part due to Dr. Sauriol's expertise and patient teachings in NMR spectroscopy. In addition, I would like to thank Dr. Henryka Tilk and Lindsay Hull for giving me a fantastic teaching experience.

Of course, my time at Queen's has been made all the more wonderful by my friends. I have also been extraordinarily lucky to live with a bunch of high-spirited girls who are inspiring in their generosity and compassion. Courtney, thank you for feeding me and reading Harry Potter to me. Angie, I always look forward to your care packages. Sarah, we are going to get there. Nicole, we'll be alright. To my friends, thank you all for your encouragement and your steadfast belief in me.

Finally, to my dearest mom, you are my role model. I am able to achieve my dreams today because of your perseverance and determination to build a good life for us. Thank you for trusting me and supporting me even when I falter. I hope I will always make you proud.

Table of Contents

List of Figures

List of Tables

List of Abbreviations

A	ampere, absorbance
Å	Angstrom
B3LYP	Becke 3-Parameter Exchange, Lee, Yang and Parr
calcd	Calculated
cm	Centimeters
CH_3CN	Acetonitrile
CH_2Cl_2	methylene chloride
COSY	correlation spectroscopy
CV	cyclic voltammetry
d	Doublet
dd	doublet of doublets
DFT	density functional theory
DMF	Dimethylformamide
DMSO	Dimethylsulfoxide
EL	Electroluminescent
EML	emitting layer
ETM	electro transport material
eV	electron volt
Hz	Hertz
HOMO	highest occupied molecular orbital
HRMS	high resolution mass spectrometry
HTM	hole transport material
ISC	intersystem crossing

J	coupling constant
K	Kelvin
L	liter, luminance
LC	ligand centered
LUMO	lowest unoccupied molecular orbital
m	meter, multiplet
M	Molar
mes	Mesityl
mg	Milligram
MHz	Megahertz
mL	Milliliter
MLCT	metal to ligand charge transfer
mmol	Millimole
MO	molecular orbital
mol	Mole
nm	Nanometers
NMR	nuclear magnetic resonance
OLED	organic light emitting diode
ph	Phenyl
ppy	2-phenylpyridine
py	Pyridine
r.t.	room temperature
s	Seconds
S_0	singlet ground state
S_1	singlet excited state

SWV	square wave voltammetry
t	Triplet
TBAF	tetra-*n*-butylammonium fluoride
td	triplet of doublets
THF	Tetrahydrofuran
UV	Ultraviolet
UV-vis	ultraviolet-visible
δ	chemical shift
μs	Microsecond
λ	Wavelength
Φ	quantum yield
τ	Lifetime

Chapter 1

Introduction

Conjugated organic compounds based on triarylboranes have been the focus of much recent research activity. These compounds have been developed into a wide range of functional materials, including highly efficient luminescent and electron-transport materials for organic light-emitting diodes (OLEDs),[1] nonlinear optical materials,[2] as well as highly sensitive and selective chemical sensors for fluoride and cyanide.[3] In the past few decades, significant efforts have been devoted to develop a number of fascinating π-conjugated frameworks, most of which involve extensive synthetic effort. Nevertheless, the electron-accepting nature of the boron center endows organoboron compounds with rich chemical reactivities that often lead to fascinating transformations. This aspect has been exploited for achieving new types of boron-containing π-conjugated materials possessing remarkable photophysical and electronic properties.[4]

This chapter will begin with a general introduction on luminescence, charge transport in OLEDs and organoboron compounds. As charge transport efficiency is a limiting factor in designing high-efficiency OLEDs, the role of boron will be discussed as a potential strategy for enhancing charge transport efficiencies in OLEDs. The majority of this chapter will be dedicated to literature reviews on the reactivity of organoboron compounds, particularly the unique reactivities promoted by the Lewis acidity of the boron center. Finally, this chapter will conclude by outlining the motivation and scope of this thesis.

1.1 Luminescence

When sufficient energy is provided to a molecule, its electrons can overcome the energy barrier required to move from their ground state to a higher energy level. An excited electron may return back to the ground state by dissipating its energy radiatively through fluorescence or phosphorescence, or through non-radiative decay, where the energy is lost through molecular vibrations or chemical reactions. In fluorescence, the excess energy is released as a photon; in phosphorescence, the emission of a photon occurs following the conversion of a singlet excited state to a triplet excited state. Although there are various methods of inducing excitation and subsequent emission (e.g. solvoluminescence[5] and mechanoluminescence[6]), the two methods relevant to the present discussion are photo- and electroluminescence.

1.1.1 Photoluminescence

In photoluminescence (PL), electrons in the molecular ground state are promoted to the excited state by irradiation with light. Excitation with photons of specific energies determine which excited state the excited electrons reach. Within each energy level there are several closely spaced vibrational states, and excited electrons will undergo internal conversion (IC) – rapid decay to the lowest vibrational energy level of the excited state (S_1) – before returning to the ground state (S_0). As a result, the re-emitted light has lower energy than that absorbed, and the emission wavelength is longer than the excitation wavelength. The difference between the positions of the band maxima in absorption and emission spectra is known as the Stokes shift.

As illustrated in the Jablonski diagram (Figure 1.1), fluorescence and phosphorescence are two pathways of photoluminescence. While excitation to and relaxation from a singlet state is typical of fluorescence, phosphorescence involves an intersystem crossing (ISC) – a forbidden transition where an electron from a singlet state crosses to a triplet state before relaxation to the

ground state. Due to its forbidden nature, phosphorescence is quite rare in organic materials, with a lifetime (the average time the molecule stays in its excited state before radiative relaxation) in the range of 10^{-3}-10^{-6} s, much longer than that of fluorescence (10^{-9} s).[7] Nevertheless, phosphorescence is commonly observed in metal complexes due to spin-orbital coupling.[8]

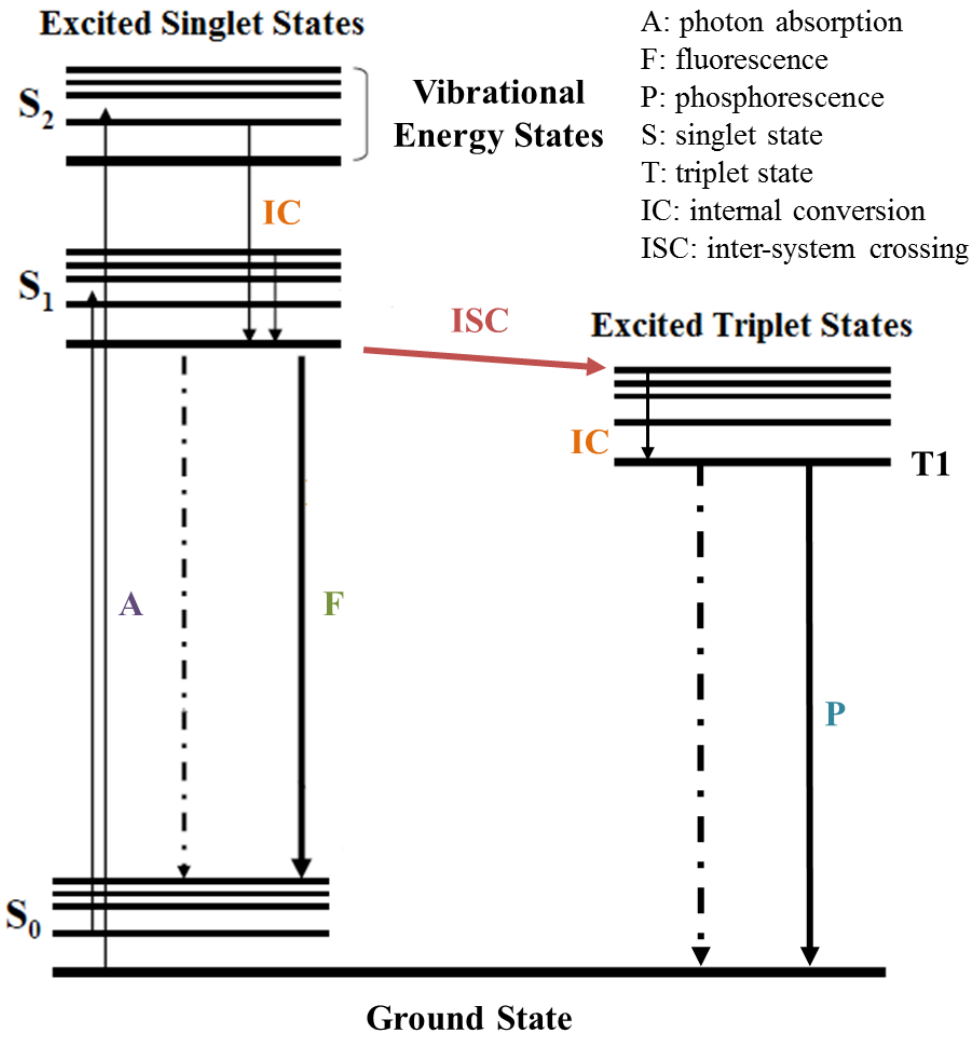

Figure 1.1 Jablonski energy diagram.[7]

1.1.2 Quantum yield

Due to the various radiative and non-radiative pathways an excited electron may take to return to its ground state, an important molecular characteristic is the quantum yield. This property is defined as the ratio of the number of photons emitted to the number of photons absorbed. Thus, a perfectly efficient molecule will have a quantum yield of 1.0. Determination of quantum yield can be achieved through a calibrated integrating sphere system, or the use of an accurate luminescence standard sample whose emission spectral properties closely match the unknown sample.[9] In the latter method, the quantum efficiency of an unknown sample is related to that of a standard by equation 1,[9] where Φ is quantum yield, and the subscripts *x* and *s* denote the unknown and standard samples, respectively. A is the absorbance at the excitation wavelength, F is the integrated emission intensity and n is the refractive index of the solvent used.

$$\Phi_x = \Phi_s \left(\frac{A_s}{A_x}\right)\left(\frac{F_x}{F_s}\right)\left(\frac{{n_x}^2}{{n_s}^2}\right) \qquad (1)$$

In order to achieve accurate quantum yield measurements, the absorbance at the intersection between the absorption peaks of the standard and the unknown compound, which will be used as the excitation wavelength, should be below 0.1.

1.1.3 Electroluminescence

Electroluminescence (EL) is a phenomenon observed in the operation of light emitting diodes (LEDs) and organic LEDs (OLEDs). In its simplest form, a LED consists of a layer of luminescent material sandwiched between two electrodes, and light is generated by passing an electric current through the diode.[8]

While photo-excitation directly generates singlet excited states, excited states generated in OLEDs contain both triplet and singlet excited states in 3:1 ratio. This is due to the triplet excited state (total spin of S = 1) having a multiplicity of three, while a singlet excited state (total

spin of S = 0) has a multiplicity of one. This implies that only one singlet excited state is created during excitation for every triplet excited state. Since the transition from the triplet excited state to singlet ground state is forbidden in most organic materials, only 25% of the input energy can be theoretically harvested as fluorescence. As such, the maximum internal quantum efficiency (IQE) of most metal-free OLEDs is 25%. During the past decade, however, extensive research efforts in metal-containing luminescent compounds have led to the development of emissive materials that can harvest both fluorescence and phosphorescence, thus allowing the IQE to approach 100%.[10]

1.2 Organic Light Emitting Diodes

Considerable progress has been made in the field of OLED-based flat-panel displays and lighting, as evidenced by the emergence of commercial products such as cell phones, digital cameras and white OLED light sources. OLEDs are electroluminescent devices that emit light in response to an electric current. As well, OLEDs are double charge injection devices, requiring the simultaneous supply of electrons from the cathode to the EL material and the removal of electrons from the EL material to the anode (Figure 1.2a). The process of removing electrons leaves behind positive charges called “holes”, and each electron-hole pair is an “exciton” bound together by electrostatic attraction. Upon recombination, energy is released in the form of visible light that results in the luminescence observed from OLEDs.

In theory, a functional OLED can be achieved by sandwiching a layer of emissive material between a transparent anode and a metallic cathode.[11] However, to achieve an efficient device with this single-layer configuration, the EL material would ideally have a high luminescent quantum yield, as well as be able to facilitate injection and transport of charges. This demand of multifunctional capabilities from a single material is very difficult to meet by current standards. Consequently, the simplest single-layer OLED configuration shown in Figure 1.2b

gives very poor efficiency and brightness.[12] On the other hand, the use of two or more different materials to perform efficient light emission, electron- and hole-injection and transport has resulted in significant improvement in OLED performance, albeit with more complex device architectures as seen in Figure 1.2c.[13,14]

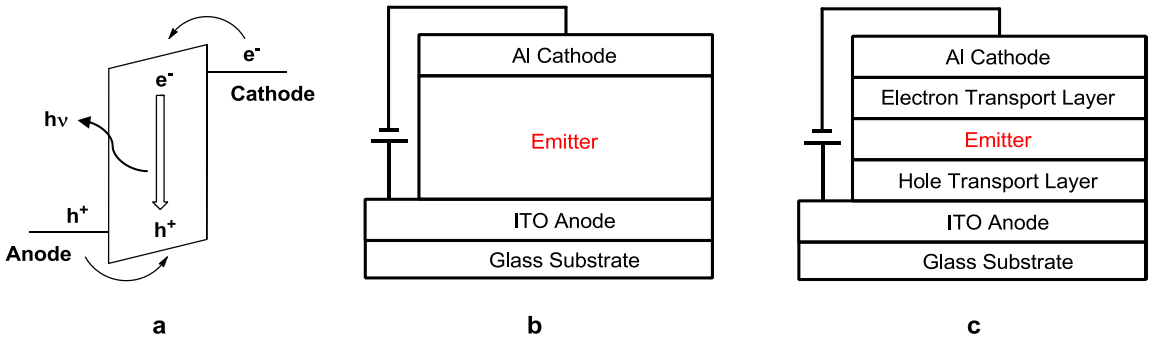

Figure 1.2 a) Charge injection into the emissive layer of an OLED. b) Architecture of a single-layer OLED and c) a three-layer OLED consisting of the emitter layer (EML) sandwiched between an electron-transport layer (ETL) and a hole-transport layer (HTL).

1.2.1 OLED Efficiency

The efficiency of an OLED is determined by measuring its external quantum efficiency (EQE), which is the number of photons emitted through the glass substrate versus the number of injected electrons. As shown in equation 2, the EQE is the product of the OLED's internal quantum efficiency (IQE) and out-coupling efficiency, η_{out}.

$$EQE = IQE(\eta_{out}) \qquad (2)$$

IQE is a term that incorporates the intrinsic quantum efficiency of the emitter material, the fraction of excitons that creates photons (maximum 0.25 for fluorescence and 1 for phosphorescence), as well as the ratio of electrons and holes injected from the electrode (electron-

hole balance). In standard OLED architecture, the out-coupling efficiency is approximately 20% due to the mismatch of refractive indices between the emissive layer (EML), HTL, indium-tin oxide (ITO) anode and the glass substrate.[15,16] As such, the ITO, along with the materials inside the device, traps the remaining 80% of the photons. In comparison, an OLED can theoretically have perfect IQE if the emitter material consists of a 100% quantum efficient phosphorescence compound, and if there is balanced charge injection from the electrode. As a result, one effective strategy to enhance the efficiency of OLEDs would be to improve charge injection and transport.

1.2.2 Charge transport

The energy level diagrams in Figure 1.3a define some of the electronic structure parameters relevant to designing organic materials for OLEDs. In a single-layer OLED, the electron affinity (EA) or LUMO level relative to the cathode work function (Φ_c), and the ionization potential (IP) or HOMO level relative to the anode work function (Φ_a), determine the charge injection into the diode. Large mismatches, thus large barriers for hole-injection at the anode (equation 3) and electron injection at the cathode (equation 4) lead to poor OLED performance.

$$\Delta E_h = \Phi_a - IP \qquad (3)$$

$$\Delta E_e = \Phi_c - EA \qquad (4)$$

For the commonly used ITO anode (Φ_c = 4.7-4.8 eV[11]) and air-stable cathodes such as aluminum (Φ_a = 4.3 eV[11]), most emissive organic materials have some barrier for hole injection and a particularly large barrier for electron injection. The barrier to charge injection leads to low external quantum efficiencies and brightness in the fabricated OLED.[11-12] As such, the introduction of one or more charge transport materials would provide a powerful means to controlling charge injection, transport and recombination in OLEDs.[13-15] The presence of an ETL in the three-layer OLED configuration (Figure 1.3b) not only lowers the barrier for electron

injection ($\Delta E_{e2} < \Delta E_{e1}$), but also serves to block holes since the ionization potential of electron-transport materials are generally large. Since hole mobility is orders of magnitude larger than electron mobility in most emissive organic materials,[17] the presence of an ETL can facilitate electron current and reduce hole current, thereby leading to improved charge balance in the device. Similarly, an HTL can significantly improve OLED performance by lowering the barrier for hole injection ($\Delta E_{h2} < \Delta E_{h1}$) and block electrons.[18]

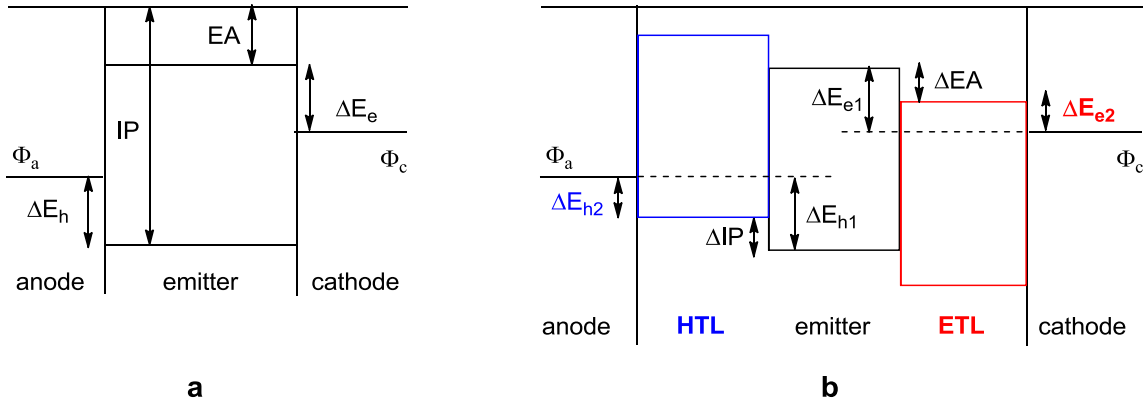

Figure 1.3 Energy-level diagram of a) a single-layer OLED and b) a three-layer OLED. Note the decrease in electron- and hole-injection barrier in diagram b (ΔE_{e2} and ΔE_{h2}).

1.2.3 Hole transport materials

As previously discussed, the hole-transport layer in an OLED is tasked with facilitating hole-injection and transport from the ITO anode into the emissive layer, as well as blocking electrons from escaping the EML. As such, successful hole-transport materials (HTMs) typically have low electron affinities and ionization potentials to promote electron removal, as well as a reversible anode oxidation that yields a stable cationic radical.[19] Furthermore, it is crucial that potential HTMs have a high glass transition temperature (T_g) so that the amorphous material remains morphologically stable at the high operating temperatures of an OLED.[20]

One class of compounds consisting of biphenyl diamine cores have shown promise as HTMs (Figure 1.4), with the most widely used being N,N'-diphenyl-N,N'-bis(3-methylphenyl)-(1,1'-biphenyl)-4,4'-diamine (TPD, **1.1**) and 4,4'-bis(N-(1-naphthyl)-N-phenylamino)-biphenyl (NPD, **1.4**).[20] These compounds offer attractive properties such as high charge carrier mobility and ease of sublimation, though the drawbacks are low T_g, ease of crystallization and unsatisfactory morphological stability.[21,22] Fortunately, the thermal and electrochemical stability of this class of molecules can be drastically improved by introducing structural rigidity using moieties such as carbazoles and fluorene.[23] This has been demonstrated recently using OFC-G2.[23] Alternatively, the T_g can be elevated by simply increasing the overall size and weight of the molecule as in the case of TPTE – an oligomer of TPD.[24] Nevertheless, such modifications often compromise the solubility and processibility of these materials.

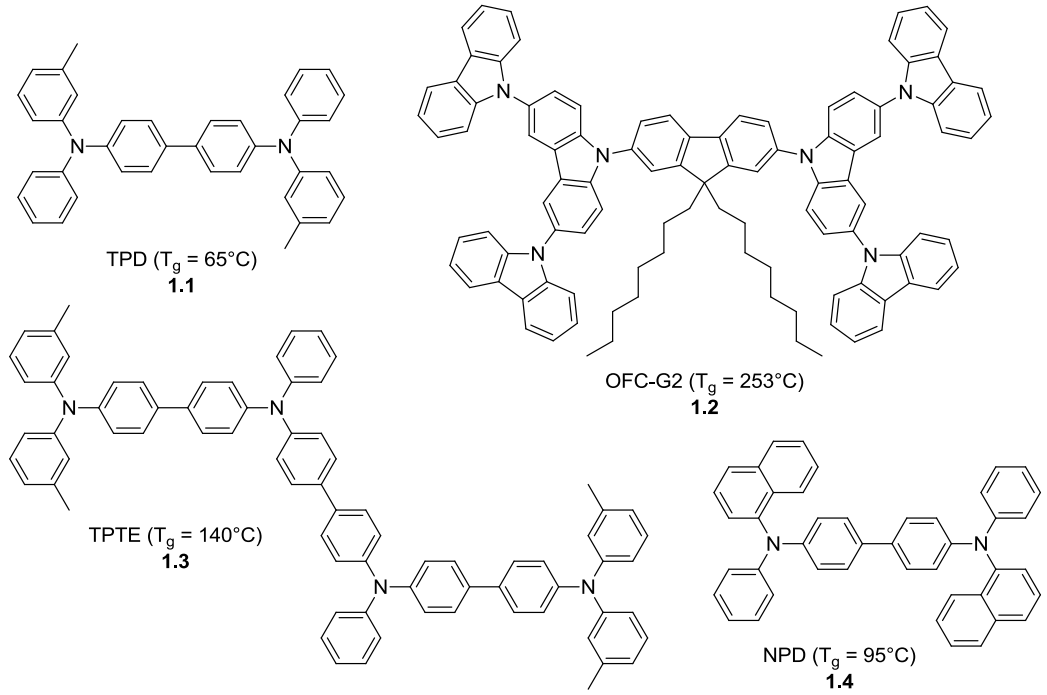

Figure 1.4 Selected hole transport material with diphenyl diamine core.

Another class of commonly used HTMs includes molecules with a triphenylamine core, such as 4,4',4"-tris(N,-3(3-methylphenyl)-N-phenylamino)triphenylamine (*m*-MTDATA, **1.5**) (Figure 1.5). Not only do these materials readily form stable amorphous glasses, they also have low IP values that are typically around 5.1 eV.[19] In addition, these compounds demonstrate relatively high T_g values and greater thermal stability than many other classes of HTMs. [25,26]

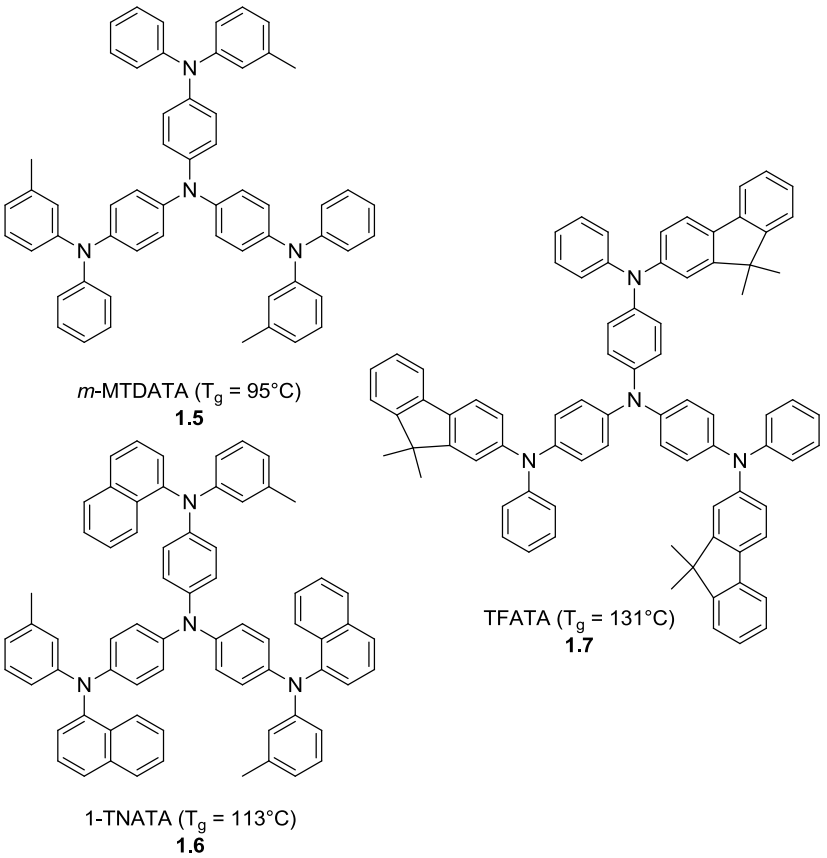

Figure 1.5 Selected hole transport materials with a triphenylamine core.

To date, the most impressive class of HTMs are those with a truxene core consisting of three fluorenyl moieties fused together. This configuration substantially enhances the overall rigidity of the molecule, resulting in compounds such as 2,7,12-tris(5,5,10,10,15,15-hexamethyltruxen-2-yl)-5,5,10,10,15,15-hexamethyltruxene (TTrTr, **1.8**) (Figure 1.6), which has

one of the highest T_g values of 358°C without compromise to solubility and processibility.[19,20,27] This is supported by dendrimer-like truxenes that have been synthesized more recently that exhibit decomposition at temperatures exceeding 400°C.[28]

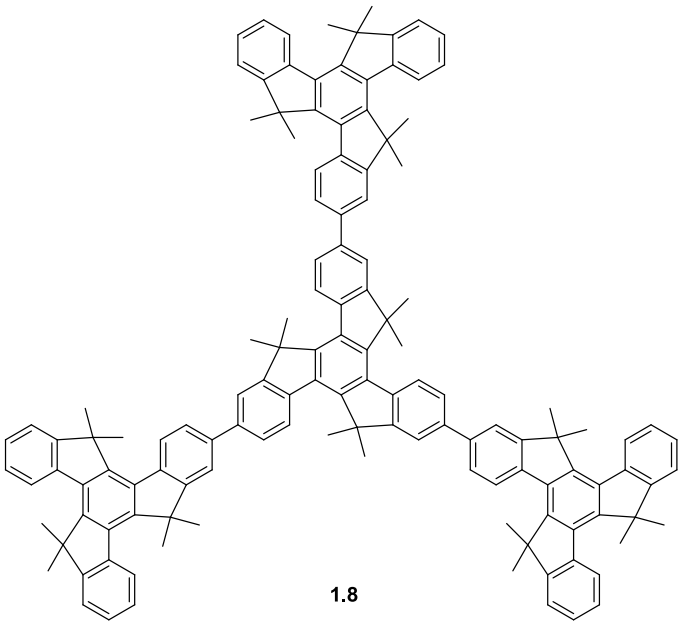

1.8

Figure 1.6 Structure of TTrTr.

1.2.4 Electron transport materials

Like the hole-transport layer, the electron-transport layer in OLEDs is used for achieving efficient electron injection from the metal cathode. In addition to accepting and transporting electrons, the ETL also plays a role in blocking holes. Thus, the material for use in the ETL should fulfill several requirements. It should have suitable EA and IP values relative to the emitter and the cathode to minimize electron injection barrier and to block holes effectively.[11] In order to serve as an efficient hole blocker, the material should have a wide band gap energy with high ionization potential. Moreover, the cathodic reduction processes of electron transport materials (ETMs)

should be reversible to form stable anion radicals.[29] Finally, the material should form homogeneous thin films with morphological and thermal stability.

ETMs contain electron-withdrawing functionalities in the molecule. Heteroaromatic rings such as pyridine, triazine, 1,3,4-oxadiazole, benzothiadiazole, triazole and silacyclopentadiene (silole) have all been applied as electron-withdrawing functionalities in ETMs.[19] Tris(8-quinolinolato)aluminum (Alq_3, **1.9**) is one of the earliest and most successful compounds used as an ETM. It has been widely used as an excellent electron transporter for green to red fluorescent-emitting OLEDs.[30,31] Other important classes of ETMs include phenanthrolines, polyquinolines, polymeric oxadiazoles (oxadiazole-containing oligoarylenes and oligo arylenevinylenes) and silacyclopentadiene (silole) derivatives.[11,19] Recent strategies in designing amorphous ETMs frequently incorporate electron-withdrawing groups at the *o*-, *m*-, or *p*-positions of a central triphenylbenzene core, or at the 2,4,6-positions of a triazine or triphenyltriazine core to form nonplanar molecules.[11]

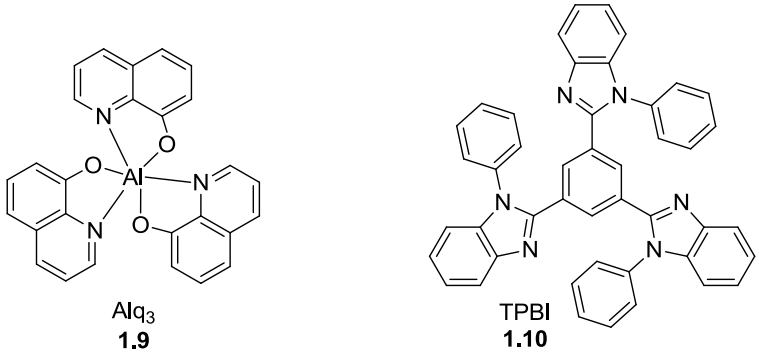

Figure 1.7 Structure of Alq_3 and the benzene-core-containing TPBI.

Among the successful ETMs that have been developed using that strategy, the most well-known molecule with a benzene core is the dentritic molecule 1,3,5-tris(*N*-phenylbenzimidizol-2-yl)benzene (TPBI, **1.10**). TPBI has been used as an ETM for OLEDs based on both fluorescent[30b,32] and phosphorescent[30c,33] emitters, including blue emitters due to its high optical

band gap (~3.0 eV). In addition, TPBI showed better hole blocking than Alq_3 due to its higher IP (6.2 eV), as well as higher device efficiency.[34] The central benzene core has also been replaced by a triazine core (Figure 1.8) to give 2,4,6-tris[di(2-pyridyl)amino]-1,3,5-triazine (**1.11**), 2,4,6-tricarbazole-1,3,5-triazine (TRZ2, **1.12**) and 2,4,6-tris(N-phenyl-2-naphthylamino)-1,3,5-triazine (TRZ3, **1.13**). Although the triazine-core-containing compounds demonstrate high thermal stability (T_g > 110°C) and good hole blocking characteristics due to their low HOMO levels (5.6-6.0 eV), their high LUMO levels (2.1-2.6 eV) result in overall poor performance.[35]

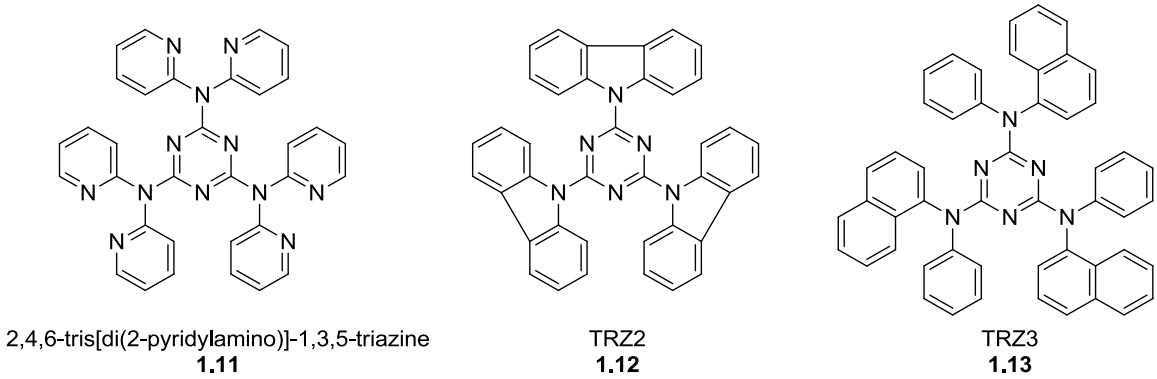

Figure 1.8 Structure of triazine-based ETMs.

In comparison, OLEDs that feature ETMs with a triphenylbenzene or a 2,4,6-triphenyl-1,3,5-triazine core have exhibited much better performance. In particular, the energy levels of both triphenylbenzene and triphenyltriazine-containing ETMs can be tuned by introducing pyridine rings in the periphery and by changing the orientation of nitrogen (Figure 1.9).[36,37] For example, 1,3,5-tri(*p*-pyrid-3-yl-phenyl)benzene (TpPyPB, **1.14**) and 1,3,5-tri(*m*-pyrid-3-yl-phenyl)benzene (TmPyPB, **1.15**) incorporates pyridine rings on either the *meta*- or *para*-positions of the triphenylbenzene core. Due to the low-lying LUMO levels of these two compounds (2.7 and 3.0 eV, respectively), their use as ETMs resulted in a substantial reduction in the operating voltage of the OLEDs.[36a] This design was further improved through the use of a

triphenyltriazine core in place of triphenylbenzene.[37] For compounds that contain a benzene core and pyridine periphery, the LUMO is mainly located at the pyridylphenyl arms. In comparison, the LUMO of compounds **1.16a-c** and **1.17a-c** is mainly located at the triphenyltriazine core, giving a lower-lying LUMO level (2.9-3.1 eV) due to stronger the electron affinity of triazine than pyridine.[37] Furthermore, changing the orientation of the pyridyl nitrogen can further reduce the LUMO level, giving an excellence electron injection and thus an extremely low device operating voltage.

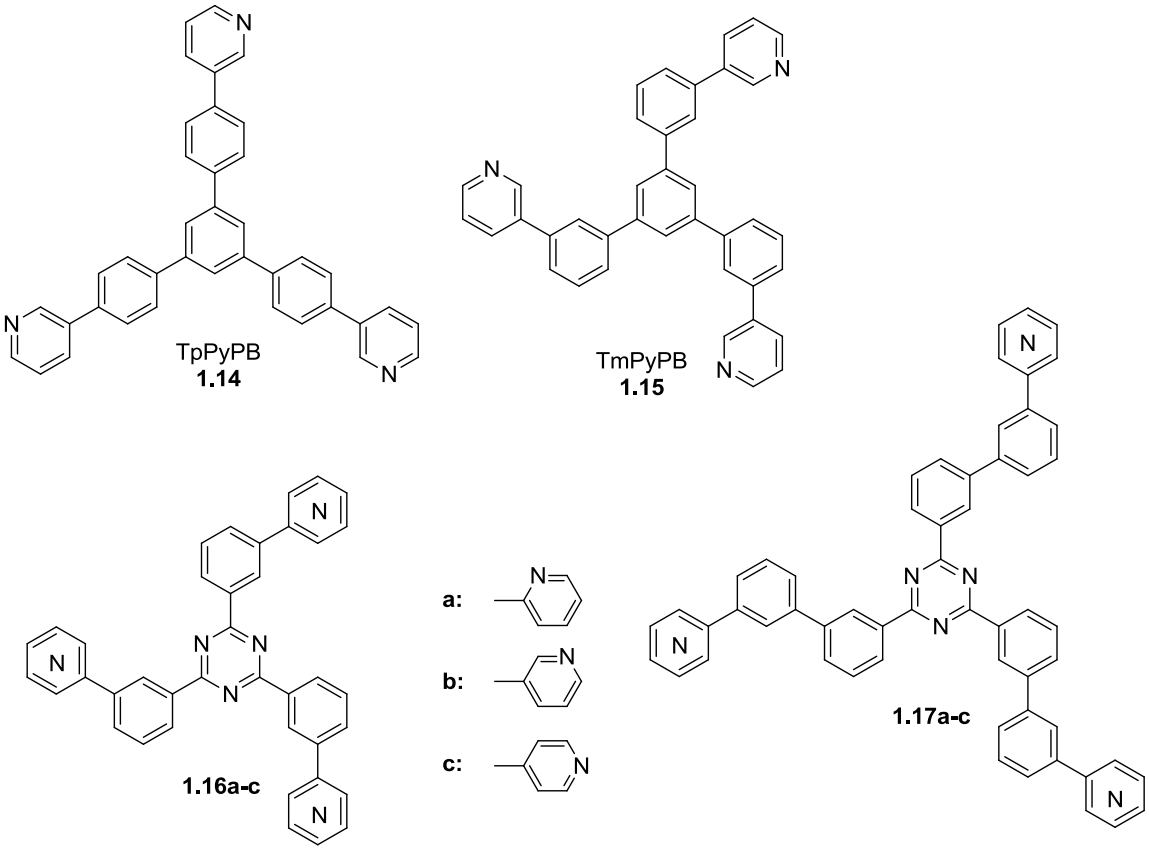

Figure 1.9 Structures of triphenylbenzene-core containing ETMs and triphenyltriazine-core containing ETMs with peripheral pyridine rings.

1.3 Organoboron Compounds

In the past decade, extensive investigations have been carried out on boron-containing organic molecules due to their fascinating photophysical properties and reactivities. As a result, organoboron compounds have been developed for a wide range of applications as fluorescent dyes, electron-transport materials, high-efficiency fluorescent emitters and anion sensors.[1-3] Moreover, the electron accepting nature of the boron center has played a strategic role in many unique molecular transformations, the details of which will be discussed in the following sections. Studies of these distinctive reactions have allowed boron chemists to make tremendous strides in understanding fundamental chemistry.

In general, organoboron compounds can be classified as either three-coordinate or four-coordinate. The geometry of the boron center is trigonal planar in three-coordinate organoboranes and tetrahedral in four-coordinate organoboron compounds. As expected, a three-coordinate organoboranes adopt a classic sp^2-hybridization with a vacant p_π orbital on the boron center (Figure 1.10). The boron center is inherently electron deficient and susceptible to attack by small molecules such as water (hydrolysis) and oxygen (oxidation).[37,38] Nevertheless, through the use of bulky aromatic substituents such as mesityl (mesityl = 2,4,6-trimethylphenyl), the steric crowding around the vacant p_π orbital can hinder most nucleophilic attack and produce many air-stable three-coordinate organoboron compounds.[37,38]

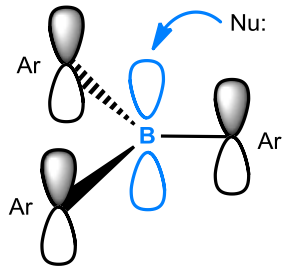

Figure 1.10 sp^2-Hybridized three-coordinate organoborane with vacant p_π orbital on boron.

In four-coordinate organoboron compounds, the boron center is sp^3 hybridized and adopts a tetrahedral geometry. The tetrahedral structure plays a role in constraining the chelating molecule in a planar fashion. Depending on the chelating ligand, there are three main types of chelation: N,N'-, N,O- or N,C-chelate (Figure 1.11). Compounds **1.18**[39] and **1.19**[40] are both excellent candidates as emitter material for OLEDs, and along with **1.21**,[41] have demonstrated electron-transporting capabilities. Boron-dipyrromethene (BODIPY, **1.20**)[42] and its analogues is a class of fluorescent dyes used in a variety of imaging applications.

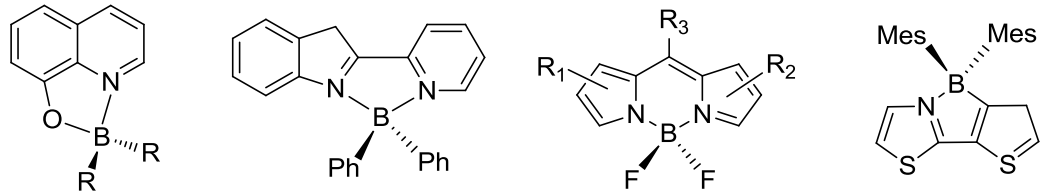

1.18 **1.19** **1.20** **1.21**

Figure 1.11 Examples of four-coordinate organoboron compounds.

1.3.1 Luminescence of organic triarylboranes

Organoboranes often have higher luminescent efficiency compared to traditional luminescent organic materials. This phenomenon can be attributed to the intramolecular charge transfer process with a large Stokes shift, which can leads to a decrease in intramolecular fluorescence self-quenching. Moreover, the bulky mesityl groups not only protect the boron center from moisture, they also prevent intermolecular stacking and interaction in the solid state, which results in intense solid-state emission.[43,44] In order to achieve high luminescent quantum efficiency, electron-rich groups such as thiophenyl or triarylamine are incorporated into the π-conjugated system, which can induce intramolecular charge transfer to the electron deficient

boron center (Figure 1.12). The emission color of triarylboron compounds may be easily tuned by varying the π-conjugated system or the Lewis acidity of the boron center.[37]

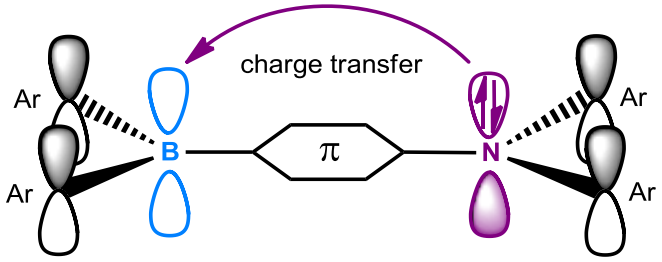

Figure 1.12 Intramolecular charge transfer from electron-rich triarylamine to the electron-deficient boron center.

1.3.2 Coordination to anions

For sterically protected triarylboron compounds, anions such as Cl^-, Br^- and I^- cannot access the boron center due to their size and relatively weak bond strength with boron. However, triarylboron compounds have a high selectivity toward fluoride,[3] cyanide[46] and even hydroxide[47] as these anions are relatively small in size. In triarylboron compounds, the vacant p_π orbital is conjugated with the π-system contributing to the overall LUMO level of the compound. Upon binding to anions, the p_π orbital is occupied and the conjugation is disrupted, resulting in changes to the emission pathway that can be monitored by emission or absorption spectroscopic methods. The selective recognition of anions, particularly fluoride, has raised much research interest in using triarylboron compounds as anion sensors.

1.4 Reactions of Organoboranes

1.4.1 Small molecule activation

Three-coordinate boron compounds are Lewis acids whose low-lying LUMOs can interact with the lone electron-pair in the high-lying HOMO of a Lewis base. Although most combinations of Lewis acids and bases form classical Lewis adducts, bulky Lewis pairs do not react. For example, it is observed that lutidine (2,6-dimethylpyridine) forms a stable adduct with BF_3 but does not react with $BMes_3$, which is attributed to the steric conflict of the *ortho*-methyl groups of lutidine with the methyl groups of the borane.[48] In systems in which such Lewis pair is incorporated into the same molecule ("ambiphilic" molecules), adduct formation is not observed. Such non-quenching Lewis pairs are described as frustrated Lewis pairs (FLPs) and are very reactive; the proximity of the of Lewis pair permits cooperative activation of CO_2, alkenes and alkynes.[49]

In studies of FLP reactivities carried out by the Stephan group, it was found that the zwitterionic salt **1.22** can eliminate H_2 at high temperature (150°C) to generate the phosphine-borane complex **1.23**.[50a] Lewis bases, including various phosphines or amines, polarize H_2 through donation of the lone pair electrons on the base into the σ* orbital of H_2.[50b] Moreover, it is well known that $B(C_6F_5)_3$ is a strong enough Lewis acid to abstract a hydride ion. As such, the cooperative action of the Lewis pair in Figure 1.13 could cleave H_2 by a concerted pathway.

Even more remarkable, however, is that the addition of H_2 to **1.23** at 25°C resulted in rapid regeneration of the zwitterionic salt. In general, this pairing of Lewis acidity and basicity allows for facile heterolytic activation of H_2, and is currently being exploited for metal-free catalytic hydrogenation,[51-52] where proton and hydride transfer from a phosphonium hydridoborate to a substrate must occur with regeneration of the Lewis acid-base pair. This pair would then reactivate H_2 and be available for subsequent substrate reduction (Figure 1.13).

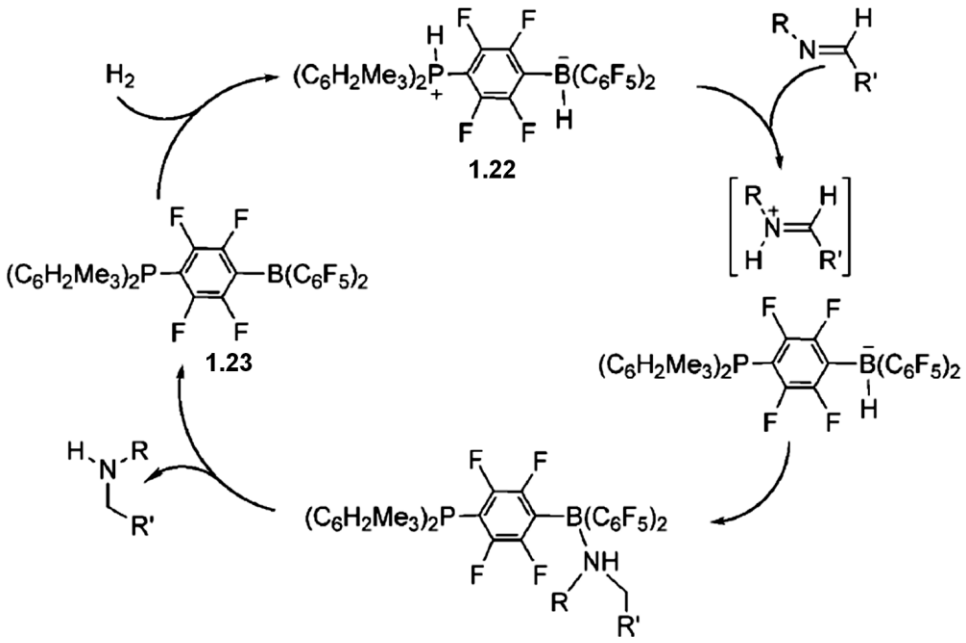

Figure 1.13 Proposed mechanism for metal-free catalytic hydrogenation using **1.22** and **1.23**.[52]

Recently, the reactivity of alkynes with bulky phosphine-borane Lewis pairs has also been demonstrated via reactions with terminal alkynes.[53] Combination of $B(C_6F_5)_3$ with (*o*-$C_6H_4Me)_3P$ generated a FLP that reacts with phenylacetylene through two reaction pathways to give the zwitterionic species **1.24** and **1.25**. Depending on the nature of the phosphine Lewis base, either alkynylborate salt will form through terminal C-H activation or olefinic phosphonium borate will form via addition to the alkyne.[53,54] The subsequent reactivity and properties of both classes of alkyne derivatives are subjects of continuing interest.

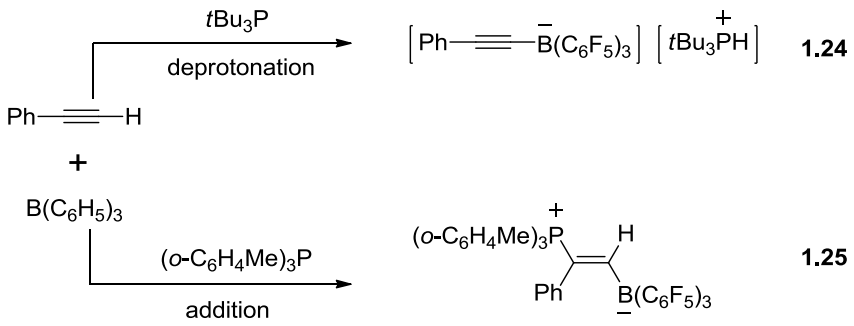

Figure 1.14 Reactions of phosphine-borane pairs with phenylacetylene.

1.4.2 Intramolecular cascade cyclization

One important direction in the advancement of organic electronics, such as OLEDs and photovoltaic devices, is the development of new, highly luminescent and efficient π-conjugated compounds. Among the various types of π-conjugated compounds, the ladder π-electron systems, which have fully ring-fused polycyclic skeletons, are a particularly promising class of materials. In π-conjugated skeletons embedded with two different main-group elements, the synergistic effect of the elements allows the electronic structure to be modulated to a significant extent.[4a] In particular, the combination of Lewis acidic boron and Lewis basic phosphorus endows unique reactivities and properties to these molecules. By taking advantage of the complementary features of the phosphine-borane pair, Yamaguchi and coworkers have successfully synthesized a series of highly emissive phosphonium and borate-bridged zwitterionic stilbenes (Figure 1.15 and 1.16).[55] In this synthesis, once **1.26** is produced, it undergoes the spontaneous intramolecular nucleophilic cascade cyclization if the phosphanyl group has sufficient nucleophilicity.

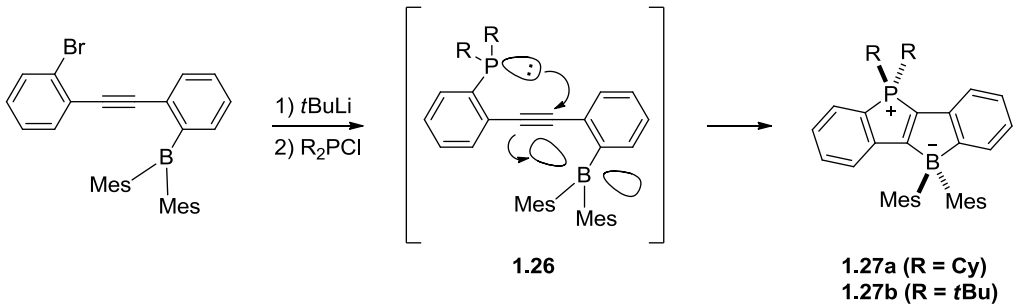

Figure 1.15 Synthesis of phosphonium- and borate-bridged stilbenes.[4d]

Systematic studies on the mechanism of this reaction confirm that this process is mainly promoted by the nucleophilic attack of the phosphanyl group, while the electrophilic boryl group also contributes to lowering the activation energy.[56] The more σ-donating dialkylphosphanyl derivatives favour the production of the cyclized products. In contrast, in the case where the less nucleophilic diphenylphosphanyl derivatives were made, heating at high temperature only produced a trace amount of the corresponding cyclized product.[56] This cyclization method is also applicable to the preparation of more extended homologues, and a thiophene fused analogue (Figure 1.16).[55] The simplicity of this method is an advantage over the conventional synthesis of zwitterionic π-conjugated compounds.

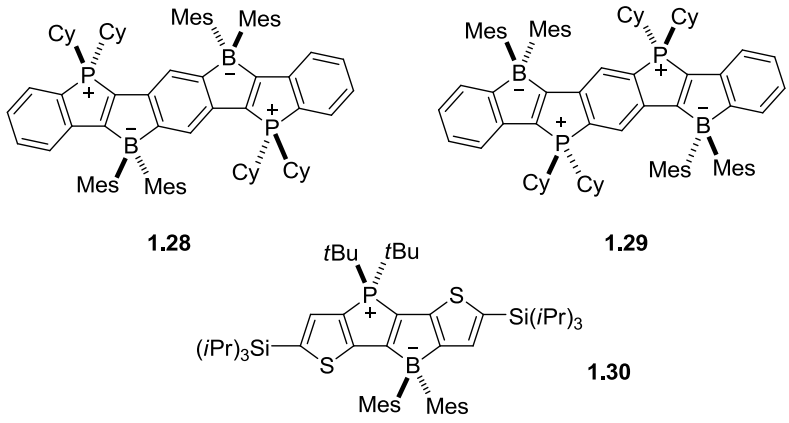

Figure 1.16 A series of phophonium- and borate-bridged ladder π-electron systems.

1.4.3 Alkynyltriarylborate rearrangements

Recently, a class of amine-borane compounds has become an intriguing synthetic target for novel π-conjugated materials. The nitrogen-containing π-conjugated skeleton is designed to form a complex with an internal triarylborane moiety, thereby constraining the skeleton into a planar structure and lowering the LUMO level considerably. Murakami and coworkers have recently reported palladium-catalyzed reactions of alkynyltriarylborates to stereoselectively synthesize intramolecular amine-borane complexes.[57]

This reaction proceeds by treating the zwitterionic alkynyltriarylborate (**1.31a**) with a catalytic amount of Pd_2dba_3•$CHCl_3$ and P(*o*-tol)$_3$ in refluxing THF. A rearrangement reaction takes place and the cyclic alkenylborane product (**1.32a**), in which the amino group is coordinated to boron, can be isolated after one hour. In this product (Figure 1.17), the ammonium proton on nitrogen migrates onto the alkynyl carbon β to boron, and the phenyl group on boron migrates to the α alkynyl carbon. The hydrogen atom and phenyl group migrate across the carbon-carbon triple bond in a *cis* fashion to give the *E*-isomer selectively. Furthermore, this palladium-catalyzed rearrangement can be extended to a variety of substrates in excellent yields. Substrates **1.31b** and **1.31c** undergoes analogous reactions to form a five-membered ring pyridine-borane complex (**1.32b**) and a six-membered ring aniline-borane complex (**1.32c**), respectively.

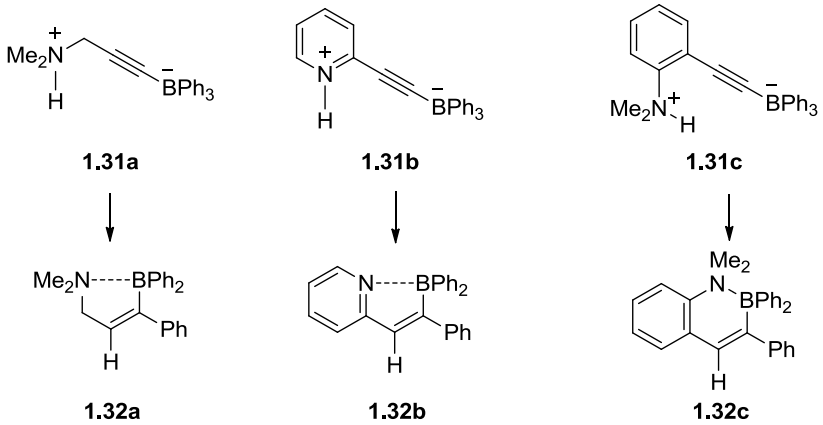

Figure 1.17 Palladium-catalyzed alkynyltriarylborate rearrangement.

A possible mechanism of this rearrangement reaction is shown in Figure 1.18. Transfer of the proton from the ammonium to Pd(0) takes place initially to give cationic palladium intermediate **A**, followed by regioselective *cis*-hydropalladation across the carbon-carbon triple bond to afford intermediate **B**. One of the phenyl groups migrates from boron to palladium, and the resulting three-coordinated boron atom can spontaneously form a Lewis acid-base complex with the tertiary amino group to give intermediate **C**. Finally, the cyclic amine-borane adduct **1.32a** is released through reductive elimination with the regeneration of Pd(0).

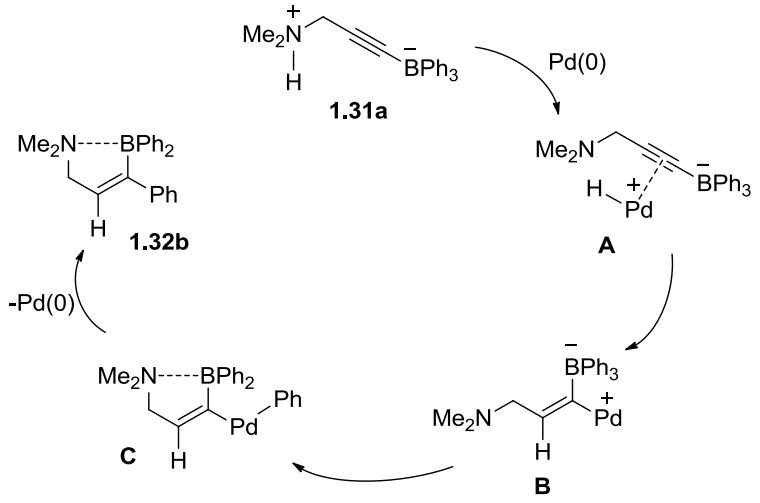

Figure 1.18 Possible rearrangement mechanism.

Lastly, in a remarkable modification to this alkynylborate rearrangement reaction, Murakami and coworkers used pyridine-N-oxides to form complexes with organoboranes through donation of the oxygen lone pair electron.[58] However, such complexes have been limited to intermolecular interactions as substrates containing both pyridine-N-oxide and triarylborate are difficult to synthesize. In this study (Figure 1.19), the reaction of 2-bromopyridine-N-oxide hydrochloride (**1.33**) with ethynyltriphenylborate and diisopropylamine in the presence of catalytic amounts of $[Pd(\pi\text{-allyl})Cl]_2$ and bis-[2-(diphenylphosphino)phenyl]ether (DPEPhos)

generated an air-stable pyridine-N-oxide-borane complex (**1.34**). The stability of the product can be attributed to the intramolecular coordination of oxygen to boron.

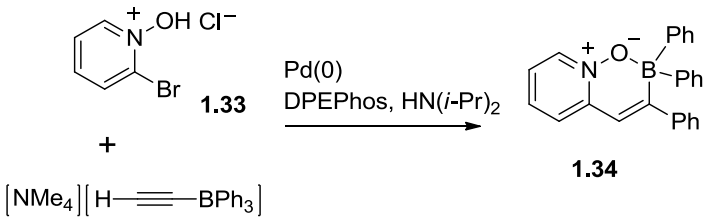

Figure 1.19 Palladium-catalyzed reaction of 2-bromopyridine-N-oxide with alkynylborate.

One plausible reaction mechanism is depicted in Figure 1.20. Oxidative addition of **1.33** to Pd(0) gives arylpalladium bromide **A**, which then undergoes carbopalladation across the alkyne carbons of ethynyltriphenylborate in a *cis* fashion to afford **B**. Then, the phenyl group on boron migrates onto the α-carbon, leaving a three-coordinated boron center. The Pd(0) species is released and the oxygen atom on the pyridine-N-oxide coordinates to boron to form the pyridine-N-oxide-borane complex (**1.34**).

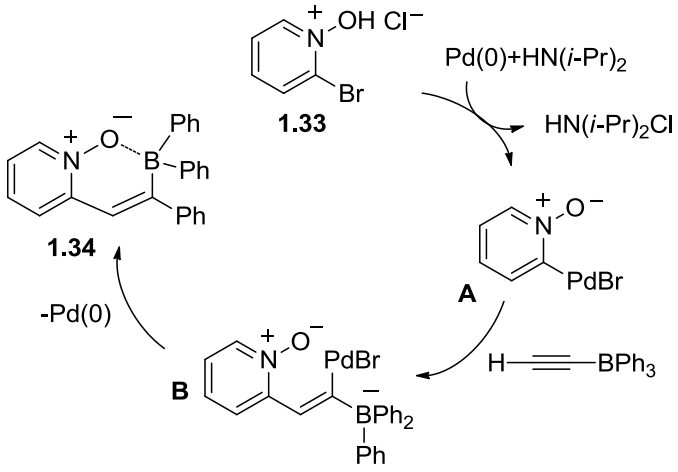

Figure 1.20 Possible reaction mechanism.

1.5 Motivation and Scope of Thesis

At this time, electron transport in organic materials remains poorly understood and research into new electron-transport materials has been less prolific compared to hole-transport materials. Moreover, there are few examples of ETMs that would be suitable for blue emitters due to the high energy band-gap required in the ETMs. Therefore, the aim of Chapter 2 is to synthesize a new ETM with improved electron affinity and a large band-gap. We planned to achieve this by synthesizing a triazine-core-containing molecule that would be functionalized by electron-deficient dimesitylboryl ($BMes_2$) groups. OLEDs based on the new boron-containing ETM were fabricated and their performance was evaluated.

In Chapter 3, a luminescent boron enol compound was discovered serendipitously through the hydration of 2-(2'-(dimesitylboryl)phenylethynyl)pyridine. The simultaneous presence of a Lewis acidic triarylboryl group and a Lewis basic pyridyl group not only facilitated the addition of H_2O across the carbon-carbon triple bond, but also stabilized the enol product through the formation of a six-membered ring. This intriguing reaction initiated our investigation into the cooperative effect of Lewis acid and base, as well as the reactions promoted by this effect. One such reaction is the intramolecular cascade cyclization described in section **1.4.2**, where the cyclization proceeds spontaneously as the result of the Lewis acid-base synergy. Inspired by that work, we replaced the main-group donor group with a transition metal donor to obtain phosphorescent π-conjugated materials. In Chapter 4, a series of platinum(II)-containing alkynyltriarylboranes were synthesized. We reasoned that the electron-rich Pt(II) centers on these compounds, coupled with the electron-deficient $BMes_2$ groups, would activate the alkyne bond in concert and initiate a cascade cyclization reaction. However, rather than forming the transition metal analogues of **1.27**, these compounds underwent a remarkable transformation. The mechanism of this reaction was studied in detail.

1.6 References

(1) (a) Entwistle, C. D.; Marder, T. B. *Angew. Chem., Int. Ed*. **2002**, *41*, 2927. (b) Entwistle, C. D.; Marder, T. B. *Chem. Mater*. **2004**, *16*, 4574. (c) Noda, T.; Shirota, Y. *J. Am. Chem. Soc*. **1998**, *120*, 9714. (d) Noda, T.; Ogawa, H.; Shirota, Y. *Adv. Mater*. **1999**, *11*, 283. (e) Kinoshita, H.; Okumoto, K.; Shirota, Y. *Chem. Mater*. **2003**, *15*, 1080. (f) Shirota, Y. *J. Mater. Chem*. **2000**, *10*, 1.

(2) (a) Porres, L.; Charlot, M.; Entwistle, C. D.; Beeby, A.; Marder, T. B.; Blanchard-Desce, M. *Proc. SPIE* **2005**, 59340F. (b) Yuan, Z.; Collings, J. C.; Taylor, N. J.; Marder, T. B.; Jardin, C.; Halet, J.-F. *J. Solid State Chem*. **2000**, *154*, 5.

(3) For recent reviews see (a) Hudnall, T. W.; Chiu, C. W.; Gabbaï, F. P. *Acc. Chem. Res.* **2009**, *42*, 388. (b) Wade, C. R.; Broomsgrove, A. E. J.; Aldridge, S.; Gabbaï, F. P. *Chem. Rev*. **2010**, *110*, 3958. (c) Jäkle, F. *Coord. Chem. Rev*. **2006**, *250*, 1107 and references therein.

(4) (a) Fukazawa, A.; Yamaguchi, S. *Chem. Asian. J.* **2009**, *4*, 1386 and references therein. (b) Iida, A.; Yamaguchi, S. *J. Am. Chem. Soc.* **2011**, *133*, 6952.

(5) Taylor, M. B.; Barrera, G. D.; Allan, N. L.; Barron, T. H. K.; Mackrodt, W. C.; Fung, E. Y.; Olmstead, M. M.; Vickery, J. C.; Balch, A. L. *Coord. Chem. Rev*. **1998**, *171*, 151 and references therein.

(6) Eddingsaas, N. C.; Suslick, K. S. *J. Am. Chem. Soc.* **2007**, *129*, 6718.

(7) Lakowicz, J. R. *Principles of Fluorescence Spectroscopy*, 2nd ed.; Springer: New York, **1999**.

(8) Yersin, H.; Finkenzeller, W. J. Triplet Emitters for Organic Light-Emitting Diodes: Basic Properties. In *Highly Efficient OLEDs with Phosphorescent Materials*; Yersin, H., Ed.; Wiley-VCH: Weinheim, **2008**; p 1.

(9) Eaton, D. F. *Pure & Appl. Chem.* **1988**, *60*, 1107.

(10) (a) Thompson, M. E. *MRS Bull.* **2007**, *32*, 694 and references there in. (b) Baldo, M. A.; Forrest, S. R.; Thompson, M. E. Organic Electrophosphorescence. In *Organic Electrophosphorescence*; Kafafi, Z. H., Ed.; Taylor & Frances: Boca Raton, **2005**; p 267. (c) Zhou, G. J.; Ho, C. L.; Wong, W. Y.; Wang, Q.; Ma, D. G.; Wang, L. X.; Lin, Z. Y.; Marder, T. B.; Beeby, A. *Adv. Func. Mater.* **2008**, *18*, 499.

(11) Jenekhe, S. A. *Chem. Mater*. **2004**, *16*, 4556.

(12) (a) Tang, C. W.; VanSlyke, S. A.; Chen, C. H. *J. Appl. Phys.* **1989**, *65*, 3610. (b) Burroughes, J. H.; Bradley, D. D. C.; Brown, A. R.; Marks, R. N.; Mackay, K.; Friend, R. H.; Burns, P. L.; Holmes, A. B. *Nature* **1990**, *347*, 539. (c) Braun, D.; Heeger, A. J. *Appl. Phys. Lett.* **1991**, *58*, 1982.

(13) (a) Kraft, A.; Grimsdale, A. C.; Holmes, A. B. *Angew. Chem., Int. Ed.* **1998**, *37*, 402. (b) Mitschke, U.; Bauerle, P. *J. Mater. Chem.* **2000**, *10*, 1471. (c) Bernius, M. T.; Inbasekaran, M.; O'Brien, J.; Wu, W. *Adv. Mater*. **2000**, *12*, 1737.

(14) (a) Friend, R. H.; Gymer, R. W.; Holmes, A. B.; Burroughes, J. H.; Marks, R. N.; Taliani, C.; Bradley, D. D. C.; Dos Santos, D. A.; Bredas, J. L.; Logdlund, M.; Salaneck, W. R. *Nature* **1999**, *397*, 121. (b) Sheats, J. R.; Antoniadis, H.; Huesche, M.; Leonard, W.; Miller, J.; Moon, R.; Roitman, D.; Stocking, A. *Science* **1996**, *273*, 884.

(15) Adachi, C.; Baldo, M. A.; Thompson, M. E.; Forrest, S. R. *J. Appl. Phys*. **2001**, *90*, 5048.

(16) Greenham, N. C.; Friend, R. H.; Bradley, D. D. C. *Adv. Mater.* **1994**, *6*, 491.

(17) Antoniadis, H.; Abkowitz, M. A.; Hsieh, B. R. *Appl. Phys. Lett.* **1994**, *65*, 2030.

(18) Zhang, X.; Jenekhe, S. A. *Macromolecules* **2000**, *33*, 2069.

(19) Shirota, Y; Kageyama, H. *Chem. Rev.* **2007**, *107*, 953 and references therein.

(20) Shirota, Y. *J. Mater. Chem*. **2005**, *15*. 75.

(21) Han, E.-M.; Do, L.-M.; Nidome, Y.; Fujihira, M. *Chem. Lett.* **1994**, 969.

(22) Fenter, P.; Schreiber, F.; Bulovic, V.; Forrest, S. R. *Chem. Phys. Lett*. **1997**, *277*, 521.

(23) Usluer, O.; Serafettin, D.; Egbe, D. A. M.; Birckner, E.; Tozlu, C.; Pivrikas, A.; Ramil, A. M.; Sariciftci, N. S. *Adv. Funct. Mater*. **2010**, *20*, 4152.

(24) Tanaka, H.; Tokito, S.; Taga, Y.; Okada, A. *Chem. Commun*. **1996**, 2175.

(25) Murata, H.; Merritt, C. D.; Inada, H.; Shirota, Y.; Kafafi, Z. H. *Appl. Phys. Lett*. **1999**, *75*, 3252.

(26) Okumoto, K.; Shirota, Y. *Chem. Lett*. **2000**, 1034.

(27) Shirota, Y.; Okumoto, K. *Jpn. Kokai Tokkyo Koho*. **2003**, 261473.

(28) Yang, Z.; Xu, B.; He, J.; Xue, L.; Guo, Q.; Xia, H.; Tian, W. *Org. Electron*. **2009**, *10*, 954.

(29) Babel, A.; Jenekhe, S. A. *J. Am. Chem. Soc.* **2003**, *125*, 13656.

(30) (a) Kim, K.; Lee, D. W.; Jin, J.-L. *Synth. Met*. **2000**, *114*, 49. (b) Thomas, K. R. J.; Lin, J. T.; Tao, Y.-T.; Chuen, C.-H. *Chem. Mater*. **2002**, *14*, 3852. (c) Duan, J.-P.; Sun, P.-P.; Cheng, C.-H. *Adv. Mater.* **2003**, *15*, 224.

(31) Anderson, J. D.; McDonald, E. M.; Lee, P. A.; Anderson, M. L.; Ritchie, E. L.; Hall, H. K.; Hopkins, T.; Mash, E. A.; Wang, J.; Padias, A.; Thayumanavan, S.; Barlow, S.; Marder, S. R.; Jabbour, G. E.; Shaheen, S.; Kippelen, B.; Peyghambarian, N; Wightman, R. M.; Armstrong, N. R. *J. Am. Chem. Soc*. **1998**, *120*, 9646.

(32) Shih, H.-T.; Lin, C.-H.; Shih, H.-H.; Cheng, C.-H. *Adv. Mater*. **2002**, *14*, 1409.

(33) Anthopoulos, T. D.; Markham, J. P. J.; Namdas, E. B.; Samuel, I. D. W.; Lo, S.-C.; Burn, P. L. *Appl. Phys. Lett*. **2003**, *82*, 4824.

(34) Gao, Z.; Lee, C. S.; Bello, I.; Lee, S. T.; Chen, R.-M.; Luh, T.-Y.; Shi, J.; Tang, C. W. *Appl. Phys. Lett*. **1999**, *74*, 865.

(35) Inomata, H.; Goushi, K.; Masuko, T.; Konno, T.; Imai, T.; Sasabe, H.; Brown, J. J.; Adachi, C. *Chem. Mater*. **2004**, *16*, 1285.

(36) (b) Su, S.-J.; Chiba, T.; Takeda, T.; Kido, J. *Adv. Mater*. **2008**, *20*, 2125. (b) Su, S.-J.; Takahashi, Y.; Chiba, T.; Takeda, T.; Kido, J. *Adv. Funct. Mater*. **2009**, *19*, 1260.

(37) Hudson, Z. M.; Wang, S. *Acc. Chem. Res*. **2009**, *42*, 1584.

(38) Jäkle, F. *Chem. Rev*. **2010**, *110*, 3985.

(39) Wu, Q.; Esteghamatian, M.; Hu, N. X.; Popovic, Z.; Enright, G.; Tao, Y.; D'Iorio, M.; Wang, S. *Chem. Mater*. **2000**, *12*, 79.

(40) Liu, Q.; Mudadu, M. S.; Schnider, H.; Thummel, R.; Tao, Y.; Wang, S. *Organometallics* **2002**, *21*, 4743.

(41) Wakamiya, A.; Taniguchi, T.; Yamaguchi, S. *Angew. Chem. Int. Ed*. **2006**, *45*, 3170.

(42) Speiser, S. *Chem. Rev*. **1996**, *96*, 1953.

(43) Zhao, C. H.; Wakamiya, A.; Lnukai, Y.; Yamaguchi, S. *J. Am. Chem. Soc*. **2006**, *128*, 15934.

(44) Li, H.; Sundararaman, A.; Venkatasubbaiah, K.; Jäkle, F. *J. Am. Chem. Soc*. **2007**, *129*, 5792.

(45) Elbing, M.; Bazan, G. C. *Angew. Chem.; Int. Ed*. **2008**, 4I7, 834.

(46) (a) Hudnall, T. W.; Gabbaï, F.P. *J Am. Chem. Soc.* **2007**, *129*, 11978. (b) Chiu, C.-W.; Gabbaï, F. P. *Dalton Trans*. **2008**, 814.

(47) Kim, Y.; Gabbaï, F. P. *J. Am. Chem. Soc*. **2009**, *42*, 756.

(48) (a) Brown, H. C.; Schlesinger, H. I.; Cardon, S. Z. *J. Am. Chem. Soc*. **1942**, *64*, 325. (b) Brown, H. C.; Kanner, B. *J. Am. Chem. Soc*. **1966**, *88*, 986.

(49) For recent reviews see: (a) Stephan, D. W. *Dalton Trans*. **2009**, 3129. (b) Stephan, D. W.; Erker, G. *Angew. Chem., Int. Ed*. **2010**, *49*, 46 and references therein.

(50) (a) Welch, G. C.; Juan, R. R. S.; Masuda, J. D.; Stephan, D. W. *Science* **2006**, *5*, 351. (b) Sumerin, V.; Schulz, F.; Nieger, M.; Leskela, M.; Repo, T.; Rieger, B. An*gew. Chem., Int. Ed*. **2008**, *47*, 6001.

(51) Chase, P. A.; Welch, G. C.; Jurca, T.; Stephan, D. W. *Angew. Chem., Int. Ed*. **2007**, *46*, 8050.

(52) (a) Axenov, K. V.; Kehr, G.; Fröhlich, R.; Erker, G. *J. Am. Chem. Soc*. **2009**, *694*, 2654. (b) Spies, P.; Schwendemann, S.; Lange, S.; Kehr, G.; Fröhlich, R.; Erker, G. *Angew. Chem., Int. Ed*. **2008**, *47*, 7543.

(53) Dureen, M. A.; Stephan, D. W. *J. Am. Chem. Soc*. **2009**, *131*, 8396.

(54) Dureen, M.A.; Brown, C. C.; Stephan, D. W. *Organometallics* **2010**, *29*, 6594.

(55) Fukazawa, A.; Yamada, H.; Yamaguchi, S. *Angew. Chem., Int. Ed.* **2008**, *47*, 5582.

(56) Fukazawa, A.; Yamaguchi, E.; Ito, E.; Yamada, H.; Wang, J.; Irle, S.; Yamaguchi, S. *Organometallics* **2011**, *30*, 3870.

(57) Ishida, N.; Narumi, M.; Murakami, M. *Org. Lett*. **2008**, *10*, 1279.

(58) Ishida, N.; Ikemoto, W.; Narumi, M.; Murakami, M. *Org. Lett*. **2011**, *13*, 3008.

Chapter 2

A Polyboryl-Functionalized Triazine as an Electron Transport Material for Organic Light-Emitting Diodes

2.1 Introduction

Triarylboron-containing compounds have tremendous potential for applications in electronic materials such as organic light-emitting diodes (OLEDs) due to the electron-accepting nature of the empty p_π orbital on boron.[1] Although remarkable progress has been made in the development of OLEDs for applications in displays and solid-state lighting, efficient electron-transport materials (ETMs) are still in high demand.[2]

Among the desired properties of an effective electron-transport material are a high electron affinity, a high chemical and thermal stability, and the ability to form amorphous films.[2,3] When sufficient steric bulk is introduced, triarylboron compounds can undergo reversible reduction while maintaining a high chemical and thermal stability.[1] In addition, the incorporation of a bulky triarylboron functionality such as $BMes_2Ph$ often facilitates the formation of amorphous films.[1b] As such, this class of compounds are very promising as ETMs in OLEDs and has been explored previously in 1,2,3-tris[5-dimesitylboryl)thiophen-2-yl]benzene (**TMB-TB**, Figure 2.1)[1i] and in tris[3-(3-pyridyl)mesityl]borane (**3TPYMB**, Figure 2.1).[1j]

On the other hand, 2,4,6-triaryl substituted triazine compounds are known to be effective electron transport materials for OLEDs due to the high electron affinity of the triazine and the thermal stability of the π-skeleton.[4] Thus, combining a triarylboron group with a triazine core is an attractive approach to achieve new and perhaps better electron transport materials.

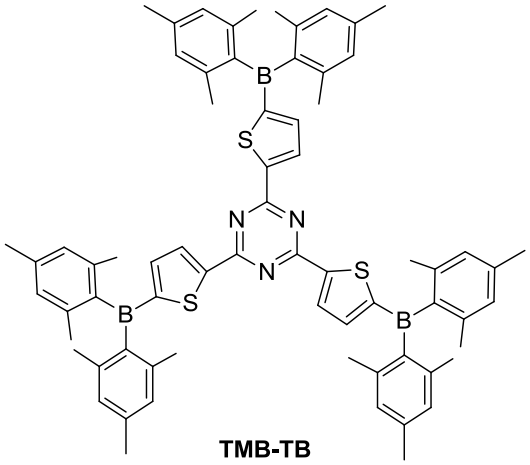

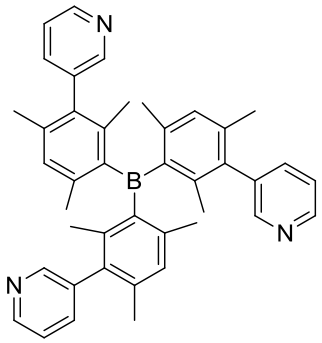

Figure 2.1 Structure of **TMB-TB** and **3-TPYMB**.

With this in mind, we have designed and synthesized a new molecule 2,4,6-tris(*m*-dimesitylborylphenyl)-1,3,5-triazine (**2.1**) shown in Figure 2.2. Compound **2.1** incorporates the low-lying LUMO of a triphenyltriazine core, as well as the electron-accepting ability of the triarylboron moiety. In addition, the use of a triazine core is expected to confer a deep HOMO level, allowing this material to function also as a hole-blocking layer in organic electronic devices. By functionalizing the *meta* position of the pendant phenyl rings of the core rather than the *para* position, the π-conjugation of the pendant groups with the central core is partially disrupted due to steric interactions, ensuring a large HOMO-LUMO gap and high triplet level[3c] that is highly desired for use in phosphorescent OLEDs.

2.2 Results and Discussion

2.2.1 Synthesis of compound 2.1

The synthesis of **2.1** was achieved in two steps from commercially available starting materials, as shown in Figure 2.2. Trimerization of 3-bromobenzonitrile in the presence of trifluroacetic acid

(TfOH) readily affords 2,4,6-tris(3'-bromophenyl)triazine[4a] in good yield. Subsequent metal-halogen exchange with *n*-butyllithium and reaction with $FBMes_2$ gives the final product, which contains three $BMes_2$ pendant groups to ensure that a single product is formed, rather than a mixture of *mono*- and *di*-borylated compounds. Compound **2.1** is stable under air in both solution and in the solid state, and has been fully characterized by NMR and elemental analyses.

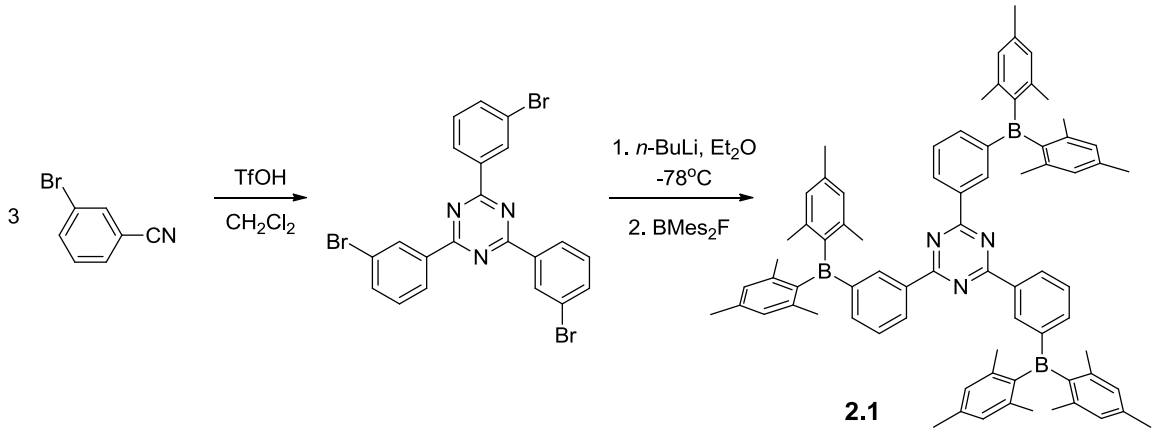

Figure 2.2 Synthetic scheme for compound **2.1**.

2.2.2 Structure of 2.1

^{1}H NMR spectrum shows that the three pendant arms of compound **2.1** are equivalent due to the free rotation of the phenyl group at ambient temperature in solution. While the compound forms amorphous glassy films on evaporation from many common organic solvents, small crystals were obtained from a mixture of toluene and CH_2Cl_2 by slow solvent evaporation. The key structural features were established by single-crystal X-ray diffraction, although the quality of data is poor.[5] In the crystal lattice, the molecule of **2.1** does not have the anticipated pinwheel structure with a C_3 symmetry as shown in Figure 2.3, which may be attributed to the extended intermolecular interactions and the presence of solvent molecules in the crystal lattice. In the amorphous films, compound **2.1** likely exists as a mixture of different conformers.

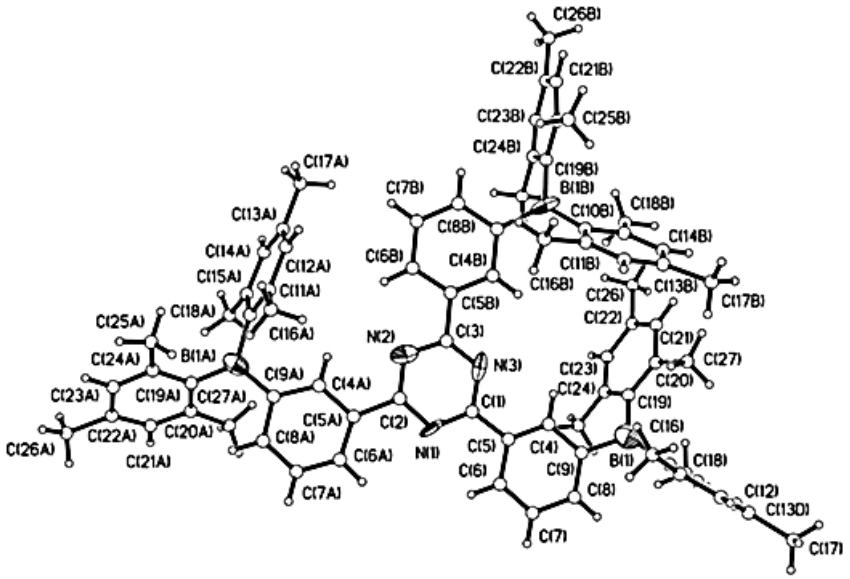

Figure 2.3 Crystal structure of **2.1** viewed from the top

2.2.3 Electrochemical and photoelectrochemical properties of 2.1

Cyclic and square-wave voltammetry diagrams of compound **2.1** show multiple but not well resolved reduction peaks that may be attributed to the boryl groups and the central triazine as well (Figure 2.4). Based on electrochemical data, the LUMO level of **2.1** is approximately at -2.70 eV, considerably lower than those of triphenyltriazine and derivatives,[4] supporting the improved electron accepting ability provided by the $BMes_2$ groups.

UV photoelectron spectroscopic (UPS) measurements for the **2.1** solid revealed that it has an exceptionally low HOMO energy level of -6.73 eV in the solid state, consistent with previous triazine-based electron transport materials.[4a] Using the HOMO value determined by UPS and the absorption edge of the solid state absorption spectrum (Figure 2.5), the LUMO energy of **2.1** in the solid state was determined to be -3.25 eV, significantly lower than those of simpler triphenyltriazines.[4a,6a,6b] The discrepancy between the LUMO value estimated from CV data and

the one obtained using UPS and solid state absorption spectrum has been noted previously for certain triarylboron-derivative compounds.[7]

The value obtained from UPS and the solid state UV absorption spectrum is clearly more realistic and meaningful. The exceptionally low LUMO and the deep HOMO level of **2.1** are reminiscent of a well-known triarylboron electron transport molecule tris-[3-(3-pyridyl)mesityl]borane (**3TPYMB**), reported by Kido and coworkers.[1c,1d]

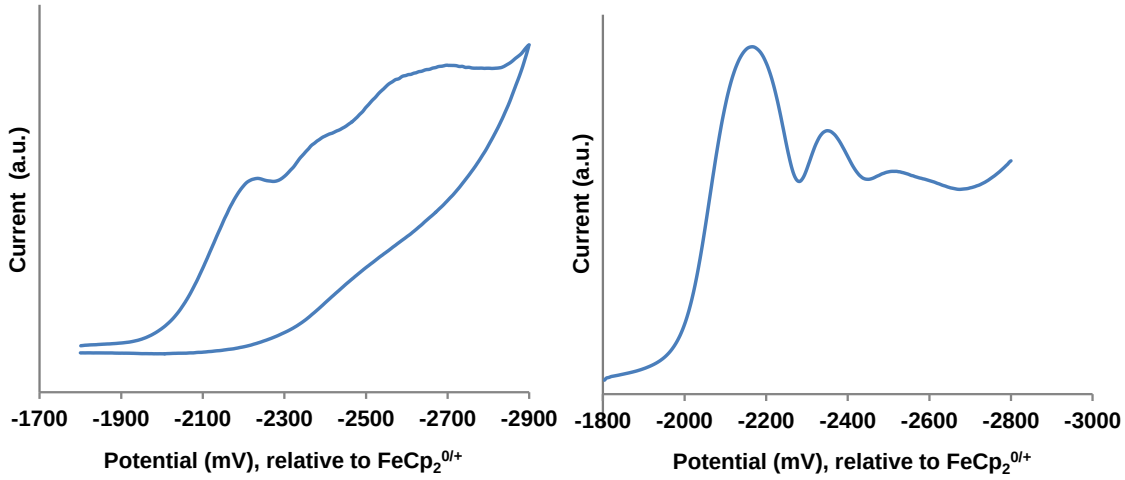

Figure 2.4 Cyclic voltammetry (CV, left) and square-wave voltammetry (SWV, right) diagram of **2.1** in THF. Note: a peak value in SWV corresponds to the half-potential of an ideal CV wave.

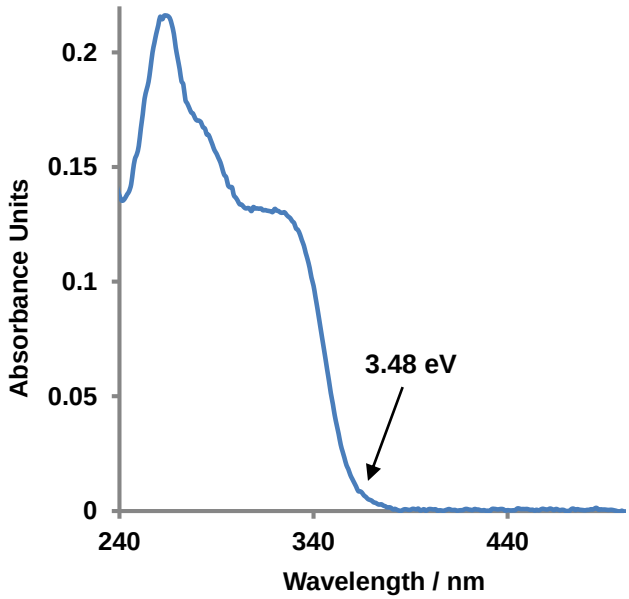

Figure 2.5 Solid-state absorption spectrum of **2.1** film. The arrow indicates the energy gap, E_g.

2.2.4 Experimental and computational photochemical properties of 2.1

Compound **2.1** shows three strong and broad absorption bands in the UV-vis spectrum (Figure 2.6) due to charge-transfer from the mesityl π orbitals to the empty p_π orbitals on boron and the π* orbitals of the triazine. Molecular orbital and molecular geometry calculations were performed using the Gaussian 03 program suite using a computational model as the starting point for geometry optimization. Time-dependent density functional theory (TD-DFT) calculations[8] carried out at the B3LYP level of theory with 6-31G* as the basis set support these assignments. As show in Figure 2.7, the top three occupied orbitals have contributions almost entirely on the mesityl groups, and LUMO and LUMO+1 have contributions mainly from the empty p orbitals on boron and the electron-deficient core. The TD-DFT results are also summarized in Table 2.1.

At room temperature, compound **2.1** shows a purple fluorescent emission at 395 nm (Φ = 0.13 in CH_2Cl_2). The compound has a remarkably high triplet energy level (E_T) of 3.07 eV determined from its low-temperature phosphorescence spectrum at 77K (Figure 2.6), which is considerably higher than common green phosphorescent emitters (e.g. $Ir(ppy)_3$[9] and

$Ir(ppy)_2(acac)$[10]) and blue phosphorescent emitters (e.g. FIrpic[11]). As such, this material also shows promise as an electron-transporting host material for triplet emitters as triplet excitons should be readily transferred from the host to phosphorescent dopants.[6]

Table 2.1 TD-DFT Results

Excited State	Transition	Energy (eV)	*F*
1	HOMO-1 → LUMO	3.55	0.0431
2	HOMO-2 → LUMO	3.55	0.0828
3	HOMO → LUMO+1	3.55	0.0823
	HOMO → LUMO+2		

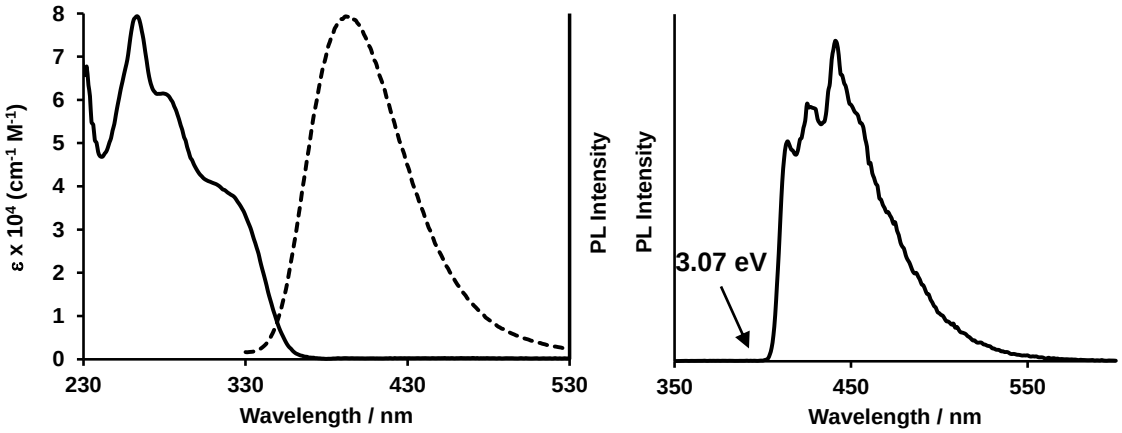

Figure 2.6 Left: 298 K absorption (solid line) and emission (dashed line) spectrum of **2.1** (10^{-5} M in CH_2Cl_2). Right: 77 K phosphorescence spectrum of **2.1** in 2-MeTHF. The arrow indicates the triplet energy level.

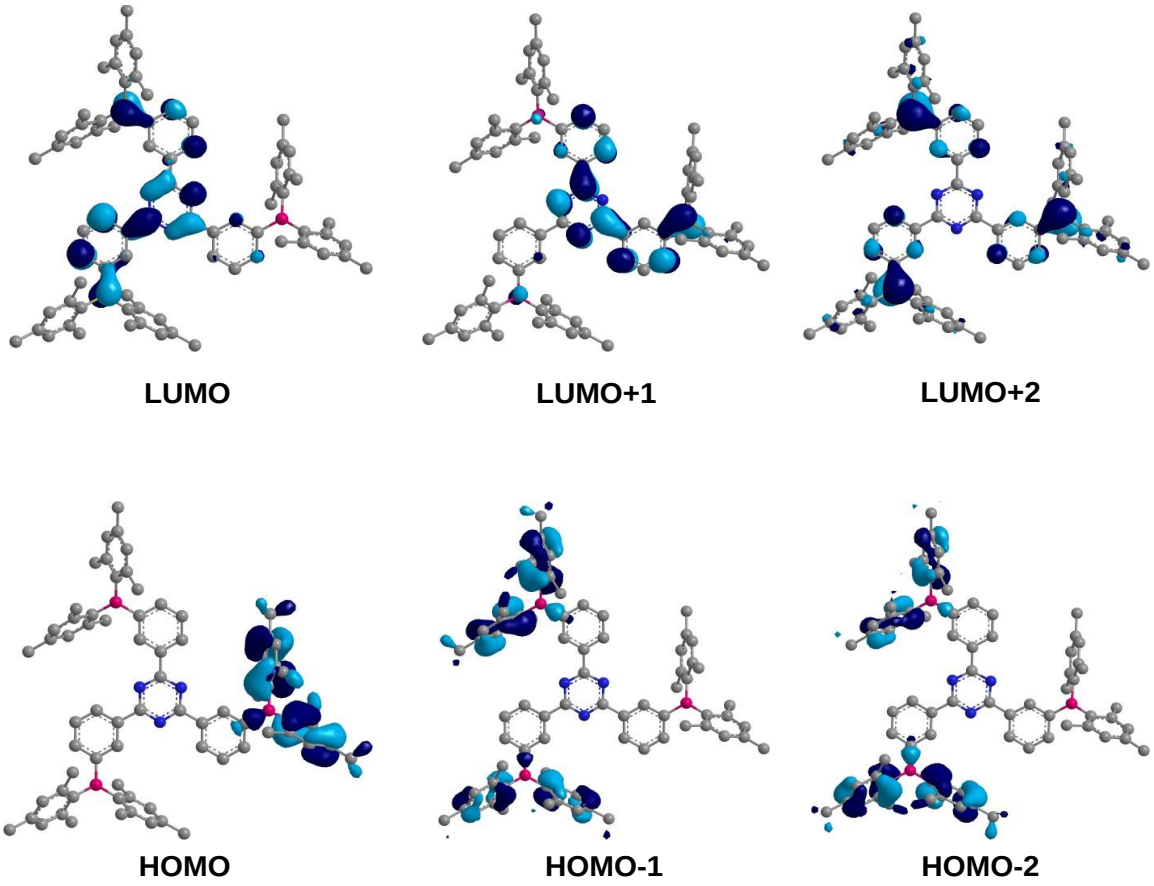

Figure 2.7 Frontier molecular orbitals of **2.1** plotted with an isocontour value of 0.03.

2.2.5 Device fabrication and performance

To evaluate the potential use of compound **2.1** in OLEDs, green phosphorescent OLEDs were fabricated using $Ir(ppy)_2(acac)$ as the emitter and **2.1** as the undoped electron transport layer (the complete device structure is shown in Figure 2.8). The use of the MoO_3 layer sufficiently raises the anodic work function to allow direct charge injection into the host material, thus permitting the use of CBP (4,4'-*N,N'*-dicarbazolylbiphenyl) as a hole transport and hosting layer and eliminating the need for a discrete HTL.[12] Three devices with varied thickness of the electron transport layer were fabricated to examine the performance of **2.1** as an electron transport material. All devices produced a characteristic green emission of $Ir(ppy)_2(acac)$ shown in Figure 2.9d and the performance data are summarized in Table 2.2.

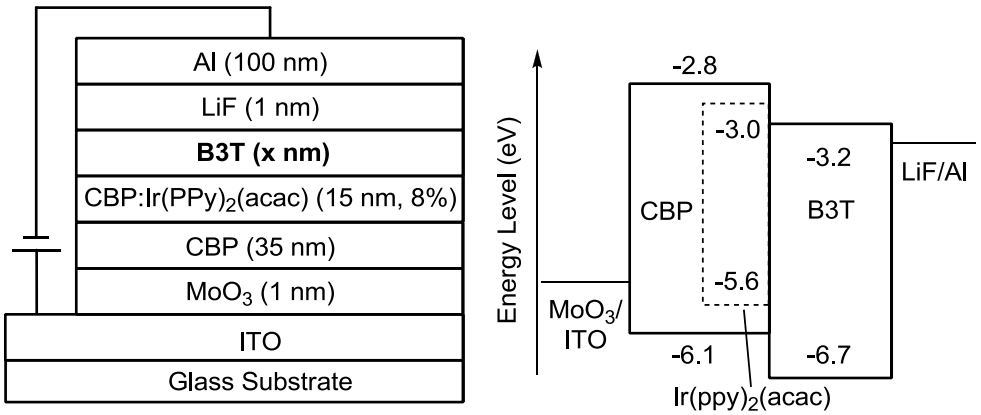

Figure 2.8 Device structure and energy level diagram of OLEDs fabricated using $Ir(ppy)_2(acac)$ as the emitter at a doping concentration of 8% and **2.1** as the electron transport material.

It was found that the efficiency of the OLEDs increased in proportion to the thickness of the ETL; the most efficient device was obtained using a 60 nm-thick layer of **2.1** as the ETL (device C). At a display-relevant luminescence of 100 cd/m^2, device C displays a high current efficiency of 68.9 cd/A, with an impressive external quantum efficiency of 19.4%, as shown in Figure 2.9. These devices do however show notably higher turn-on voltages than those demonstrated in previous reports using triazine-based electron transport materials,[4a] likely due to inefficient charge injection from the LiF/Al cathode.

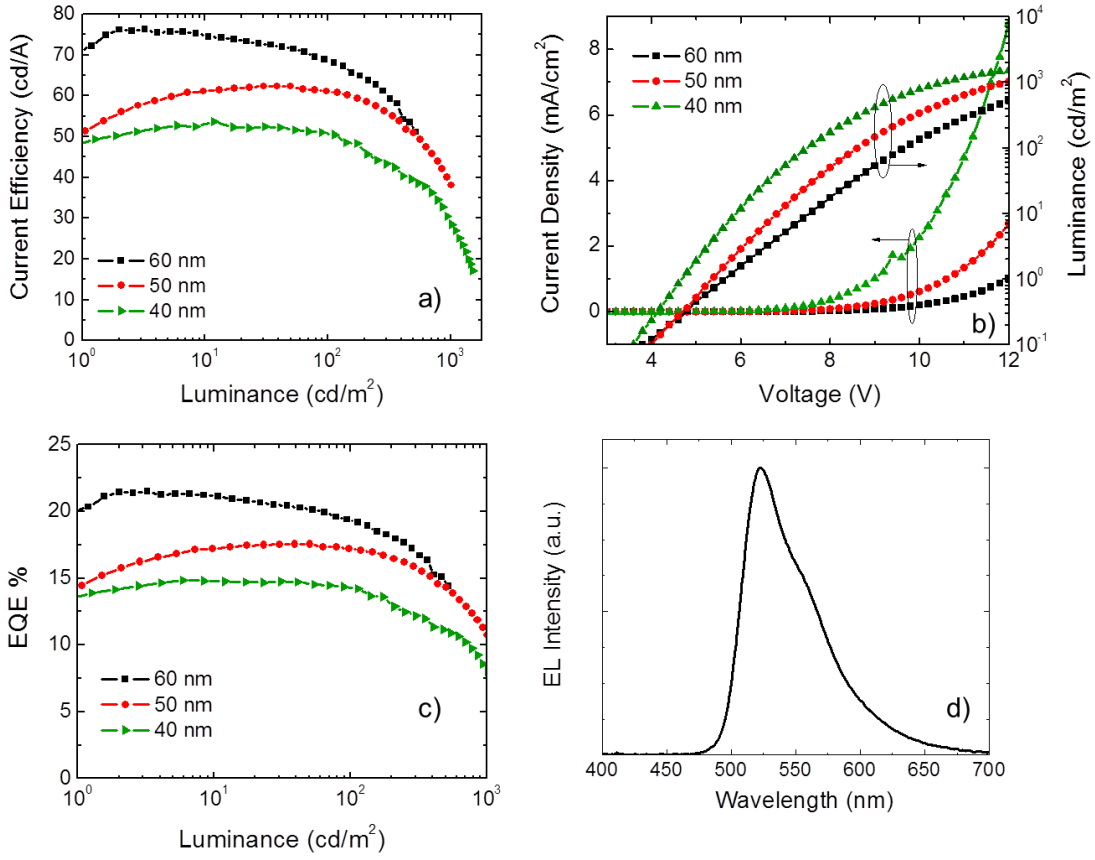

Figure 2.9 Diagrams of a) current efficiencies, b) *L-J-V* characteristics and c) external quantum efficiencies for devices A-C. d) Electroluminescence spectrum of OLEDs using $Ir(ppy)_2(acac)$ as emitter.

Table 2.2 OLED performance data

Device	Luminance[a] / cd m^{-2}	$\eta_{ext,max}$ [%]	η_L[b] / cd/A
A	1510	14.8	50.5
B	1019	17.6	61.1
C	521	21.5	68.9

[a] Values obtained at 12.0 V. [b] Values obtained at 100 cd/m^2.

2.3 Conclusions

A new triarylboron-based electron transport material with a triazine core has been achieved. This compound exhibits a remarkably high triplet energy level with low-lying HOMO and LUMO energy levels due to the presence of three electron-accepting boron centers. Preliminary experiments incorporating this material into phosphorescent OLEDs as an electron transport layer gave devices with high current and external quantum efficiencies at brightness levels appropriate for display applications. Future work will focus on optimizing the device structure and the use of this material as an electron-transporting host material for high triplet energy blue electrophosphorescent devices.

2.4 Experimental

2.4.1 General considerations

All experiments were performed under a nitrogen atmosphere by standard Schlenk techniques unless otherwise noted. Methylene chloride was dried and distilled over P_2O_5 as solvent for photophysical measurements. Thin-layer and flash chromatography were performed on silica gel. ^{1}H and ^{13}C NMR spectra were recorded on a 400 MHz Bruker Avance spectrometer, and deuterated solvents were purchased from Cambridge Isotopes and used without further drying. The high resolution mass spectrum (HRMS) was obtained from an Applied Biosystems QStar XL spectrometer. Elemental analysis was obtained from Laboratoire d'Analyse Élémentaire de l'Université de Montréal, Montréal, Québec, Canada. 2,4,6-tris(*m*-bromophenyl}triazine was synthesized according to a literature procedure.[13]

2.4.2 Synthesis of 2,4,6-tris(*m*-dimesitylborylphenyl)-1,3,5-triazine (2.1)

In a dropwise manner, *n*-butyllithium in hexane (1.6 M, 3.02 mL, 4.83 mmol) was added to a solution of 2,4,6-tris(*m*-bromophenyl}triazine (0.80 g, 1.45 mmol) in 100 mL THF at -78°C. After stirring at -78°C for 1 h, a solution of trimesitylboron fluoride (1.3 g, 4.83 mmol) in 30 mL THF was added dropwise to this mixture. Stirring was continued for 3 h at -78°C and for 2 h at room temperature. THF was evaporated *in vacuo* and the residue was extracted using CH_2Cl_2/sat. NH_4Cl. The organic layer was dried over $MgSO_4$, concentrated, and the residue purified by column chromatography on silica (4:1 hexanes:EtOAc) to afford **2.1** as a white solid (0.35 g, 23%). ^{1}H NMR (400 MHz, $CDCl_3$): 8.80 (s, 3H, phenyl), 8.52 (d, J = 7.8 Hz, 3H, phenyl), 7.75 (d, J = 7.3 Hz, 3H, phenyl), 7.48 (t, 7.6 Hz, 3H, phenyl), 6.88 (s, 12H, mesityl), 2.36 (s, 18H, mesityl), 2.06 (s, 36H, mesityl) ppm. ^{13}C NMR (100 MHz, $CDCl_3$): 171.7, 145.6, 141.6, 140.9, 140.4, 138.8, 137.5, 135.8, 132.4, 129.1, 128.2, 23.6, 21.3 ppm. HRMS calc'd for $C_{75}H_{78}B_3N_3$ [M^+] 1053.6493, found 1053.6475. CHN calc'd for $C_{75}H_{78}B_3N_3$: C 84.75, H 7.14, N 3.78 %, found C 85.48, H 7.46, N 3.99 %.

2.4.3 Electrochemical and photophysical measurements

Cyclic voltammetry experiments were performed using a BAS CV-50W analyzer with a scan rate of 0.1-0.2 V/sec using 2 mg sample in 0.5 mL dry THF. The electrochemical cell was a standard three-compartment cell composed of a Pt working electrode, a Pt auxiliary electrode, and an Ag/AgCl reference electrode. CV measurements were carried out at room temperature with 0.1 M tetrabutylammonium hexafluorophosphate (TBAP) as the supporting electrolyte. The LUMO of **2.1** was determined using square-wave voltammetry relative to $FeCp_2^{0/+}$. Excitation and emission spectra were recorded using a Photon Technologies International QuantaMaster Model 2 spectrometer (CH_2Cl_2 at 1×10^{-5} M). UV/Visible spectra were recorded using a Varian Cary 50Bio UV-vis spectrophotometer. Photoluminescent quantum yields were measured using optically dilute method (1×10^{-5} M, A ≈ 0.1) at room temperature in CH_2Cl_2 relative to anthracene (Φr =

0.27 in EtOH). The fluorescence quantum yields were calculated using reported procedures.[2] UPS measurements were performed using a PHI 5500 MultiTechnique system, with attached organic deposition chamber with a base pressure of 10^{-10} Torr.

2.4.4 Electroluminescent device fabrication

Devices were fabricated in a Kurt J. Lesker LUMINOS® cluster tool with a base pressure of ~10^{-8} Torr without breaking vacuum. The ITO anode is commercially patterned and coated on glass substrates 50 x 50 mm^2 with a sheet resistance less than 15 Ω. Substrates were ultrasonically cleaned with a standard regiment of Alconox®, acetone, and methanol followed by UV ozone treatment for 15 min. The active area for all devices was 2 mm^{14}. The film thicknesses were monitored by a calibrated quartz crystal microbalance and were further verified for single-carrier devices using using capacitance-voltage measurements (Agilent 4294A). I-V characteristics were measured using a HP4140B picoammeter in ambient air. Luminance measurements and EL spectra were taken using a Minolta LS-110 luminance meter and an Ocean Optics USB200 spectrometer with bare fiber, respectively. The external quantum efficiency of EL devices was calculated following the standard procedure.[15]

2.4.5 X-ray diffraction analysis

Single crystals of **2.1** were obtained from a mixed solvent solution of CH_2Cl_2 and toluene and mounted on glass fibers for data collection. Data were collected on a Bruker Apex II single-crystal X-ray diffractometer with graphite-monochromated Mo K_α radiation, operating at 50 kV and 30 mA and at 180 K. Data were processed on a PC with the aid of the Bruker SHELXTL software package (version 5.10) and corrected for absorption effects. Exposure time is 60s per frame. The detector to crystal distance is 62 mm. All non-hydrogen atoms except C(3) were

refined anisotropically. Due to the lack of sufficient data, C(3) could not be refined anisotropically (became non-positively defined). Compound **2.1** co-crystallizes with CH_2Cl_2 and toluene solvent molecules in the crystal lattice, which were removed by the Platon Squeeze routine. The crystal of **2.1** diffracts weakly with only 16% of the data having intensity > 2σ, despite the long exposure time we used (60s per frame). The crystal of **2.1** possesses a very long axis (72.08(3) Å), which along with the low parameters versus data ratio certainly contributed to the relatively poor quality of the refinement. The crystal data of **2.1** have been deposited at Cambridge Crystallographic Data Center (CCDC 841441).

Table 2.3 Crystallographic data for compound **2.1**

Compound	**2.1**
Formula	$C_{75}H_{78}B_3N_3$
FW	1053.83
Space Group	C2/c
a, Å	72.08(3)
b, Å	8.563(4)
c, Å	23.406(10)
α, °	90
β, °	105.001(4)°
γ, °	90
V, Å^3	13954(11)
Z	8
D_{calc}, g cm^{-1}	1.003
T, K	180(2)
μ, mm^{-1}	0.057
$2\theta_{max}$, °	56.82
Reflns measured	69526
Reflns used (R_{int})	13735(0.3317)
Parameters	743
Final R Values [I > 2σ(I)]:	
R_1[a]	0.1124
wR_2[b]	0.2433
R values (all data):	
R_1[a]	0.03825
wR_2[b]	0.3341
Goodness-of-fit on F^2	0.782

[a] $R_1 = \Sigma[(|F_0| - |F_c|) / \Sigma |F_0|$

[b] $wR2 = [\Sigma w[(F_0^2-F_c^2)^2] / \Sigma[w(F_0^2)^2]]^{1/2}$

$w = 1 / [\sigma^2(F_0^2) + (0.075P)^2]$, where $P = [Max (F_0^2, 0) + 2F_c^2] / 3$

Table 2.4 Selected bond lengths (Å) and angles (°) for compound **2.1**

C(1)-C(5)	1.430(10)	N(1)-C(1)-C(5)	120.8(8)
C(2)-C(5A)	1.504(10)	N(3)-C(1)-C(5)	118.6(8)
C(3)-C(5B)	1.479(10)	N(2)-C(2)-C(5A)	117.3(8)
C(9)-B(1)	1.591(13)	N(1)-C(2)-C(5A)	115.8(9)
C(9A)-B(1A)	1.591(12)	N(3)-C(3)-C(5B)	123.5(8)
C(9B)-B(1B)	1.622(12)	N(2)-C(3)-C(5B)	112.4(8)
C(10)-B(1)	1.562(13)	C(10)-B(1)-C(9)	119.7(9)
C(10A)-B(1A)	1.582(12)	C(10)-B(1)-C(19)	124.1(9)
C(10B)-B(1B)	1.519(11)	C(9)-B(1)-C(19)	116.0(9)
		C(19A)-B(1A)-C(10A)	126.1(9)
		C(19A)-B(1A)-C(9A)	119.5(8)
		C(10A)-B(1A)-C(9A)	114.4(8)
		C(10B)-B(1B)-C(19B)	125.7(9)
		C(10B)-B(1B)-C(9B)	120.2(8)
		C(19B)-B(1B)-C(9B)	114.1(8)

2.5 References

(1) (a) Noda, T.; Shirota, Y. *J. Am. Chem. Soc*. **1998**, *120*, 9714. (b) Shirota, Y. *J. Chem. Mater*. **2005**, *15*, 75. (c) Tanaka, D.; Takeda, T.; Chiba, T.; Watanabe, S.; Kido, J. *Chem. Lett*. **2007**, *36*, 262. (d) Tanaka, D.; Agata, Y.; Takeda, T.; Watanabe, S.; Kido, *J. Jpn. J. Appl. Phys*. **2007**, *46*, L117. (e) Hudson, Z. M.; Wang, S. *Acc. Chem. Res*. **2009**, *42*, 1584. (f) Hudson, Z. M.; Sun, C; Helander, M. G; Amarne, H.; Lu, Z. H.; Wang, S. *Adv. Funct. Mater*. **2010**, *20*, 3426. (g) Jäkle, F. *Coord. Chem. Rev*. **2006**, *250*, 1107. (h) Jäkle, F., *Chem. Rev.* **2010,** *110*, 3985. (i) Kinoshita, M.; Shirota, Y. *Chem. Lett*. **2001**, *30*, 614. (j) Tanaka, D.; Takeda, T.; Chiba, T.; Watanabe, S.; Kido, J. *Chem. Lett*. **2007**, *36*, 262.

(2) (a) Kulkarni, A. P.; Tonzola, C. J.; Babel, A.; Jenekhe, S. A. *Chem. Mater*. **2004**, *16*, 4556. (b) Hughes, G.; Bryce, M. R. *J. Mater. Chem*. **2005**, *15*, 94. (c) Sasabe, H.; Kido, J. *Chem. Mater*. **2011**, *23*, 621.

(3) (a) Shirota, Y.; Kageyama, H. *Chem. Rev*. **2007**, *107*, 953. (b) Walzer, K.; Maennig, B.; Pfeiffer, M.; Leo, K. *Chem. Rev*. **2007**, *107*, 1233. (c) Sasabe, H.; Gonmori, E.; Chiba, T.; Li, Y. -J.; Tanaka, D.; Su, S. -J.; Takeda, T.; Pu, Y. -J.; Nakayama, K.; Kido, J. *Chem. Mater*. **2008**, *20*, 5951.

(4) (a) Su, S. –J.; Sasabe, H.; Pu, Y. –J.; Nakayama, K.; Kido, *J. Adv. Mater*. **2010**, *22*, 3311. (b) White, W.; Hudson, Z. M.; Feng, X.; Han, S.; Lu, Z. H.; Wang, S. *Dalton Trans*. **2010**, *39*, 892. (c) Fink, R.; Heischkel, Y.; Thelakkat, M.; Schmidt, H. W. *Chem. Mater*. **1998**, *10*, 3620.

(5) The crystals of **2.1** contain disordered solvent molecules and have one very long axis (monoclinic, C2/c, a = 72.08(3) Å) that contribute to the poor data quality and weak diffraction of the crystal (with only 16% reflections having intensity > 2σ.

(6) (a) Zeng, L.; Lee, T. Y. –H.; Merkel, P. B.; Chen, S. H. *J. Mater. Chem*. **2009**, *19*, 8772. (b) Chen, H. –F.; Yang, S. –J.; Tsai, Z. –H.; Hung, W. –Y.; Wang, T. –C.; Wong, K. –T. *J. Mater. Chem.* **2009**, *19*, 8112. (c) Xiao, L.; Chen, Z.; Qu, B.; Luo, J.; Kong, S.; Gong, Q.; Kido, J. *Adv. Mater.* **2011**, *23*, 926. (d) Chi, Y.; Chou, P. T. *Chem. Soc. Rev*. **2010**, *39*, 638.

(7) For example, according to CV data recorded in DMF, the LUMO level of **3TPYMB** is at ~ -2.6 eV, much higher than the value (-3.32 eV) obtained from UPS and solid state absorption spectra reported in reference 1c.

(8) Frisch, M. J. et al, *Gaussian 03* , Revision C.02, Gaussian, Inc. , Wallingford, CT **2004** .

(9) (a) Baldo, M. A.; Lamansky, S.; Burrows, P. E.; Thompson, M. E.; Forrest, S. R. *Appl. Phys. Lett.* **1999**, *75*, 4. (b) Baldo, M. A.; Thompson, M. E.; Forrest, S. R. *Nature* **2000**, *403*, 750.

(10) (a) Lamansky, S.; Djurovich, P.; Murphy, D.; Abdel-Razzaq, F.; Lee, H. E.; Adachi, C.; Burrows, P. E.; Forrest, S. R,; Thompson, M. E. *J. Am. Chem. Soc*. **2001**, *123*, 4304. (b) Wang, Z. B; Helander, M. G.; Qiu, J.; Puzzo, D. P.; Greiner, M. T.; Liu, Z. W.; Lu, Z. H. *Appl. Phys. Lett.* **2011**, *98*, 073310.

(11) Adachi, C.; Kwong, R. C.; Djurovich, P.; Adamovich, V.; Baldo, M. A.; Thompson, M. E.; Forrest, S. R. *Appl. Phys. Lett*. **2001**, *79*, 2082.

(12) (a) Wang, Z. B.; Helander, M. G.; Qiu, J.; Liu, Z. W.; Greiner, M. T.; Lu, Z. H. *J. Appl. Phys.* **2010**, *108*, 024510. (b) Wang, Z. B.; Helander, M. G.; Hudson, Z. M.; Qiu, J.; Wang, S.; Lu, Z. H. *Appl. Phys. Lett.* **2011**, *98*, 213301.

(13) Chen, H.-F.; Yang, S.-J.; Tsai, Z.-H.; Hung, W.-Y.; Wang, T.-C.; Wong, K.-T. *J. Mater. Chem*. **2009**, *19*, 8112.

(14) Demas, N. J.; Crosby, G. A. *J. Am. Chem. Soc.*, **1970**, *29*, 7262.

(15) Helander, M. G.; Greiner, M. T.; Wang, Z. B; Lu, Z. H. *Appl. Surf. Sci.* **2010**, *256*, 2602.

Chapter 3

Donor-Acceptor Assisted Alkyne Hydration for Formation of a Luminescent Boron-Stabilized Enol

3.1 Introduction

Triarylboron compounds have excellent electron-accepting properties due to the Lewis-acidic nature of the boron centre.[1] Although *ortho*-substituted aryl groups are often used to protect the boron center from nucleophilic attack, it has been well established that small anions (e.g. F^- and CN^-) can still access sterically protected triarylboron centers such as $BMes_2Ar$.[2] Gabbaï and coworkers have also shown that OH^- can bind to sterically congested boron centers to form hydroxo adducts.[3] In addition, the presence of both a triarylborane and an appropriate Lewis donor group such as amine or phosphine is known to promote unusual reactivities, including the activation of hydrogen, alkenes or alkynes.[4] Recent review of aminoboronic acids show that these bifunctional compounds have potential as catalysts for direct amide formation and catalytic asymmetric transformation.[5] Furthermore, Yamaguchi and coworkers have demonstrated that alkyne molecules functionalized by a triarylboron group and a phosphine or pyridine can undergo cascade double cycliczation, extending π-conjugation of the molecule.[6]

Compound **3.1** was designed to be a ligand for intramolecular cyclization with platinum, a process detailed in Chapter 4. During our investigation of this compound, we have observed that the presence of an internal Lewis base along with the boryl group can greatly facilitate alkyne hydration reaction under ambient conditions. Hydration of internal alkynes typically occurs at high temperatures and requires the use of either toxic[7] (e.g. mercury(II) salts) or costly metal catalysts[7] (e.g. platinum or gold). As such, the ability of intramolecular Lewis donor and acceptor groups to activate small molecules plays a key role in promoting alkyne hydration reactivity.

3.2 Results and Discussion

3.2.1 Synthesis of compounds 3.1-3.3

Compound **3.1**, 2-(2'-dimesitylphenylethynyl)pyridine, was initially obtained in 18% yield by Sonogashira coupling between *o*-(dimesitylboryl)ethynylbenzene and 2-bromopyridine in refluxing wet THF/Et_3N using $Pd(PPh_3)_2Cl_2$ and CuI as catalysts (Figure 3.1). From the same reaction, a yellow precipitate, compound **3.2**, with bright yellow-green fluorescence was isolated in 22% yield. When freshly dried THF was used in the synthesis, the yield of **3.1** was improved to 35% and no compound **3.2** was obtained. The control compound, 2-(2'-dimesitylphenylethynyl)benzene (**3.3**) was obtained by a similar procedure in 45% yield. All three compounds are air stable in solution and in the solid state. They were fully characterized by NMR, HRMS and single-crystal X-ray diffraction analyses.

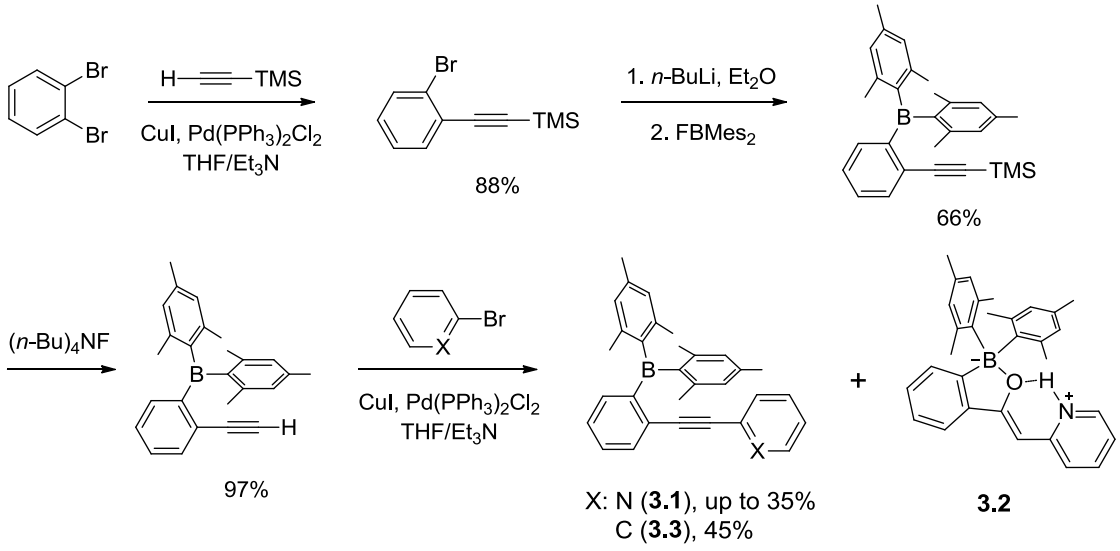

Figure 3.1 Synthetic scheme for compounds **3.1**, **3.2** and **3.3**.

3.2.2 Structure of 3.1-3.3

Both **3.1** and **3.2** crystallize in the monoclinic space group $P2_1/c$ while compound **3.3** crystallizes in the triclinic P-1 space group. The structures of **3.1** and **3.3** are shown in Figure 3.2 for comparison. The B-C bond lengths in both molecules span the range of 1.55(1) Å to 1.58(1) Å, which are typical of triarylboron compounds. In **3.1**, one mesityl group is parallel and directly above the pyridylalkyne group with a dihedral angle of 16.4° and short separation distances (e.g. 3.00 Å, 3.48 Å). Such π-stacking interaction may be faciliated by the attraction between the electron rich mesityl ring and the electron deficient pyridylalkynyl group. In contrast, the mesityl ring in **3.3** is nearly perpendicular to the phenylakynyl group with a dihedral angle of 106.4°. This conformation of **3.3** may be attributed to the dimer formation via intermolecular C-H (methyl)···π (alkynylphenyl) interactions in the solid state (Figure 3.2).

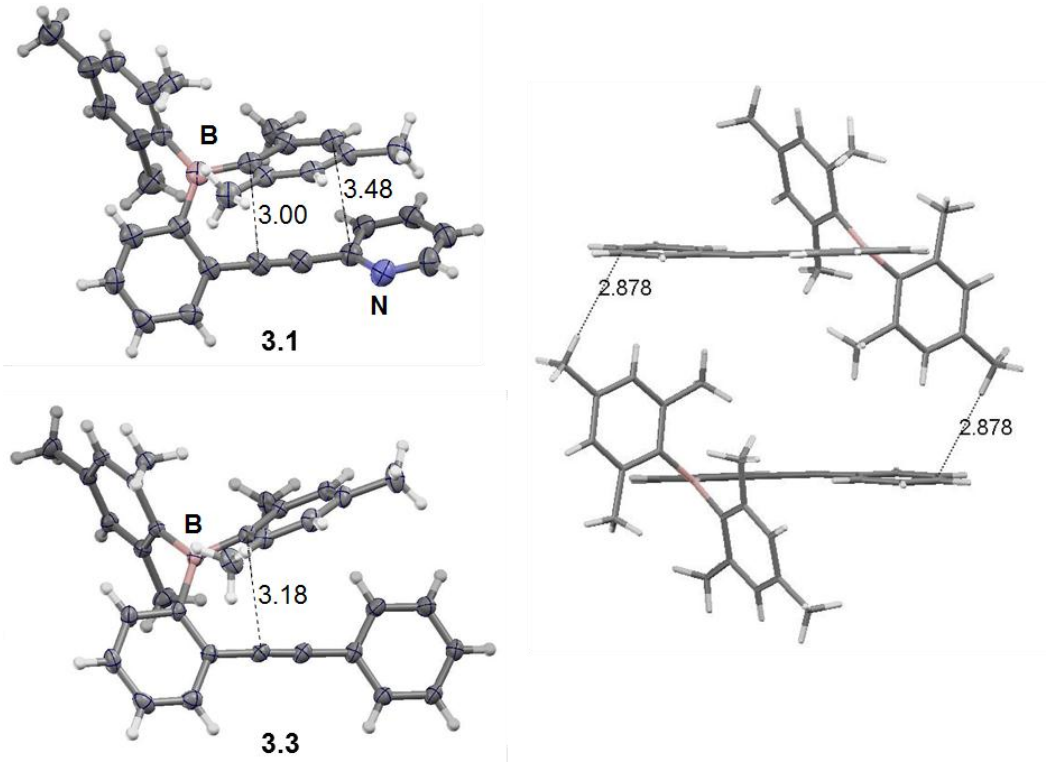

Figure 3.2 Left: crystal structure of **3.1** and **3.3** with 35% thermal ellipsoids. Right: structure of a **3.3** dimer showing intermolecular H-π interaction.

Compound **3.2** is stable in solution and the solid state under air with an unusual structure. As shown in Figure 3.3, it has a rare C,O-chelate around the four-coordinate boron atom. The B-C bonds are much longer (1.610(9) to 1.642(9) Å) than those of **3.1** and **3.3**, but similar to those of previously reported four-coordinate $BMes_2$ compounds.[8] The B-O bond is 1.603(7) Å, somewhat longer than those observed in non-congested four-coordinate boron compounds (e.g. $BPh_2(q)$, q = 8-hydroxyquinolato).[9] The alkyne bond has been transformed to an olefin bond with a typical double bond distance, 1.352(8) Å and an *E*-geometry with respect to the pyridyl and phenyl groups. A proton bound to the *py* nitrogen atom was located and refined successfully in X-ray analysis. This proton forms a hydrogen bond with the oxygen atom (N-H = 1.03(6) Å, O···H = 1.78(6) Å), holding the *py* ring in plane with the phenyl ring. The C-O bond length is 1.322(7) Å, typical of conjugated C-O bonds.[10]

Thus, based on the crystal structure, compound **3.2** can be described as a zwitterionic $BMes_2$ enolate. Between the *enol* and *keto* tautomers, the *keto* form is usually much more stable, thus more commonly observed than the enol tautomer.[11] Clearly, binding to the $BMes_2$ unit by the oxygen atom stabilizes the otherwise unstable *enol* tautomer.

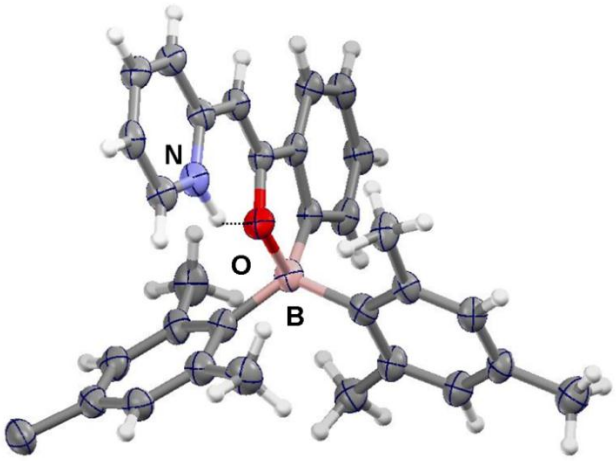

Figure 3.3 Crystal structure of **3.2** with 35% thermal ellipsoids.

3.2.3 Experimental and computational photophysical properties of compound 3.1-3.3

In solution, compounds **3.1** and **3.3** are colorless with little absorption in the visible region. In contrast, compound **3.2** has a distinct yellow color in solution due to an intense and broad absorption band between 360 – 470 nm (λ_{max} = 435 nm, ε = 27,000 $M^{-1}cm^{-1}$) in the absorption spectrum (Figure 3.4). The photophysical properties of all three compounds are summarized in Table 3.1. Based on TD-DFT calculation results, the strong absorption band observed in **3.2** can be attributed to a π to π* transition on the chelate backbone with a small charge transfer contribution from the mesityl to the π* orbital of the backbone.

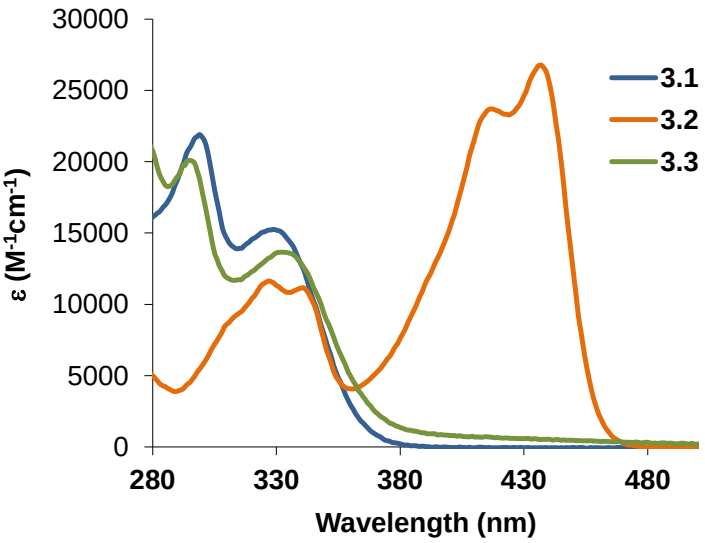

Figure 3.4 Absorption spectra of compounds **3.1-3.3** in CH_2Cl_2 (10^{-5} M).

Table 3.1 Photophysical and Electrochemical Properties of **3.1-3.3**.

Complex	Absorption, λ_{max} ε (10^4 cm^{-1} M^{-1})	Solution Emission, 298K		
		λ_{max} (nm)	Φ_P	$E_{1/2}^{red}$ (V) (vs. $FeCp_2^{+/0}$)
3.1	297 (2.2), 326 (1.5)	455	0.04	-2.22
3.2	331 (1.1), 435 (2.7)	464	0.04	--
3.3	298 (1.9), 340 (1.3)	455	0.04	-2.29

3.2.4 Monitoring the conversion of 3.1 to 3.2 by ^{1}H NMR

The formation of **3.2** from the synthesis of compound **3.1** clearly involved adventitious water molecules in the reaction solvent since when dry THF was used, no compound **2** was observed and the yield of **3.1** was doubled. To determine if compound **3.1** is a precursor for **3.2**, several control reactions were performed and monitored by ^{1}H NMR spectroscopy. The resulting NMR spectra are shown in Figures 3.5 to 3.7. In each of the control reactions, H_2O and **3.1** were mixed in a 10:1 molar ratio in THF under nitrogen at ambient temperature with varied amounts of CuI, $Pd(PPh_3)_2Cl_2$ and Et_3N. Based on the results of these studies, we concluded that the Pd(II) catalyst is not required for the formation of **3.2**. The presence of a catalytic amount of CuI (10%) is however necessary to enable the transformation of **3.1** to **3.2** as the reaction does not occur in the presence of Et_3N/H_2O only. In fact, the conversion of **3.1** to **3.2** occurs within minutes of the addition of CuI and is readily observable due to a distinct solution color change from colorless to bright yellow.

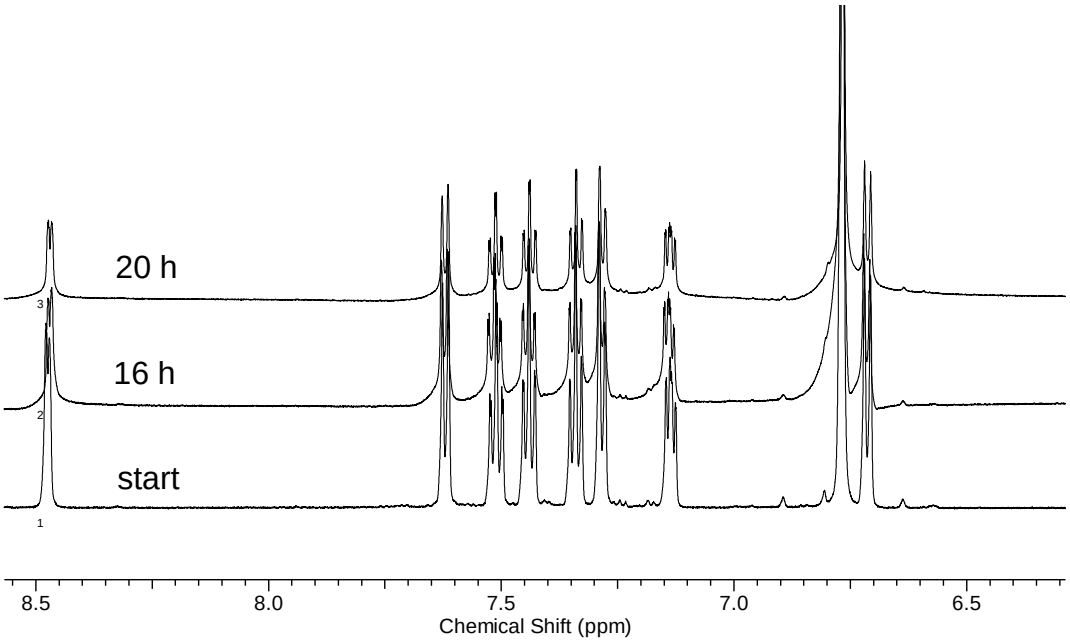

Figure 3.5 ^{1}H NMR spectra of **3.1** in CD_2Cl_2 showing that no reaction occurred after the addition of 10 equiv. H_2O for 16 hours and after the subsequent addition of 1.5 equiv. Et_3N for 4 hours (16 h to 20 h) at ambient temperature.

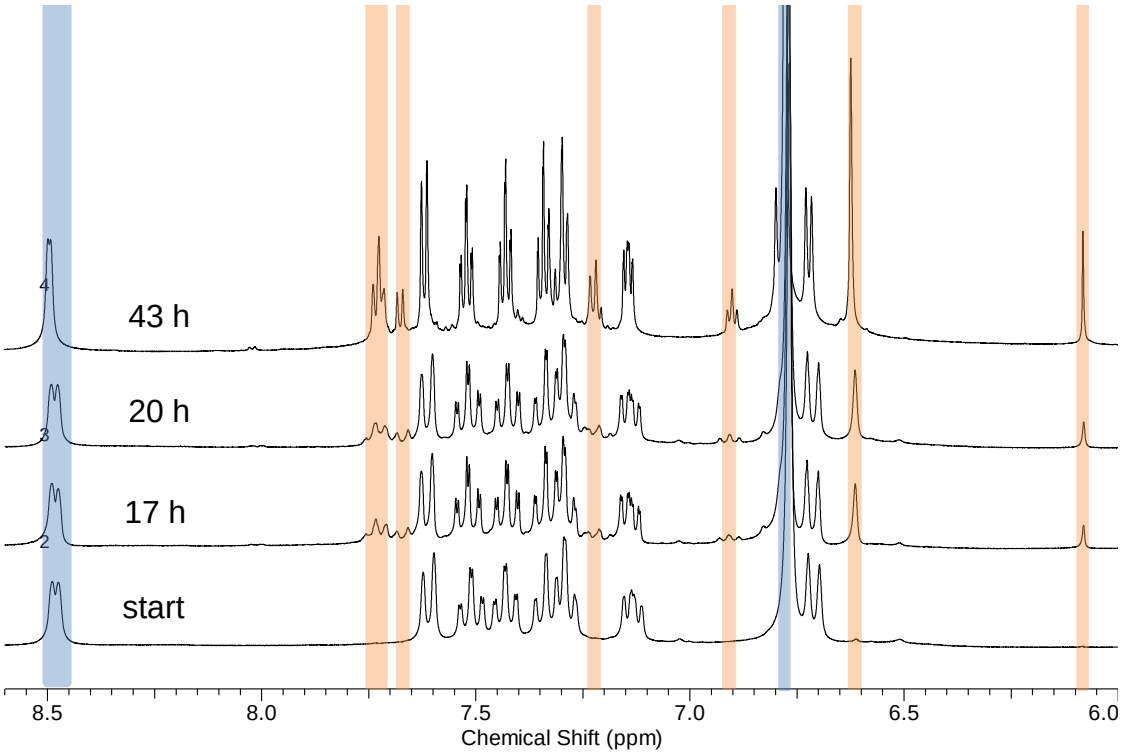

Figure 3.6 ^{1}H NMR spectra of **3.1** in CD_2Cl_2 showing conversion to **3.2** after the addition of 10 equiv. H_2O and 10 mol% CuI.

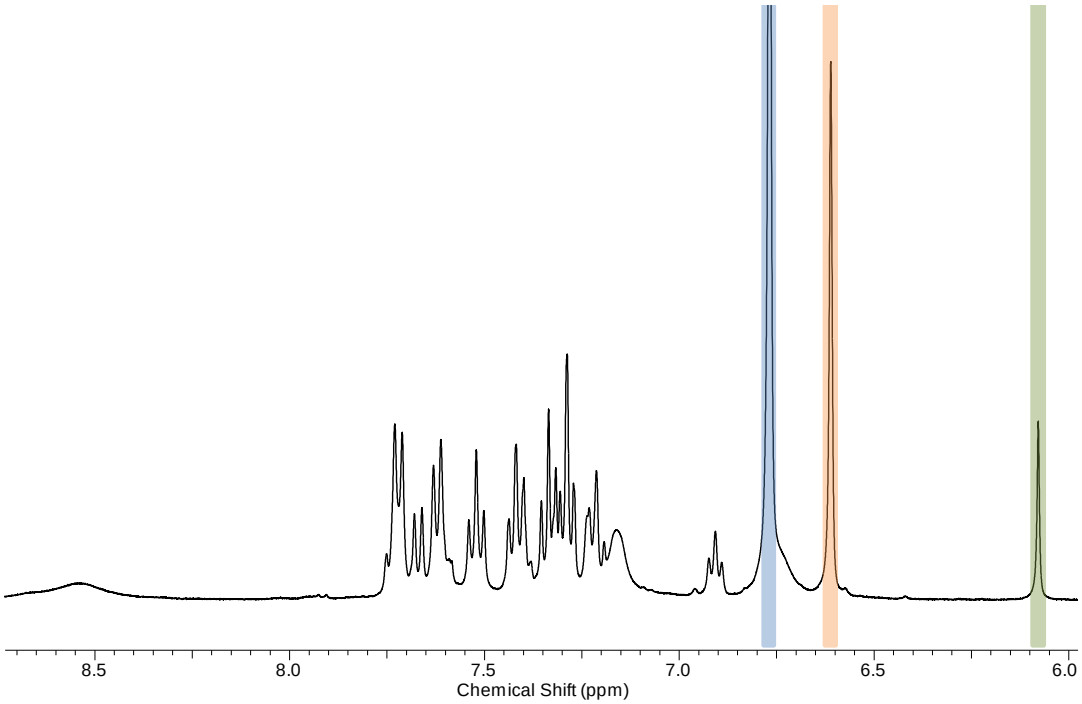

Figure 3.7 ^{1}H NMR spectrum showing 40% conversion of **3.1** (peak highlighted in blue) to **3.2** (peak highlighted in orange). Note the vinyl proton of **3.2** at 6.1 ppm (green).

3.2.5 Mechanism of alkyne hydration

The proposed catalytic cycle for the hydration of **3.1** and the formation of **3.2** is shown in Figure 3.8. In this cycle, the pyridyl group on **3.1** facilitates the dissociation of a proton from H_2O to generate OH^-, which can then coordinate to the boron site. Despite the comparatively high pKa of water, this step is likely promoted by the synergistic effect of the Lewis basic pyridine nitrogen acting in concert with the Lewis acidic boron and the result is consistent with the well-known binding ability of sterically congested boron to hydroxide.[3] Coordination of CuI activates the triple bond and allows the facile addition of the bound hydroxo group. Finally, replacement of CuI by a proton leads to the regeneration of CuI and the formation of **3.2**.

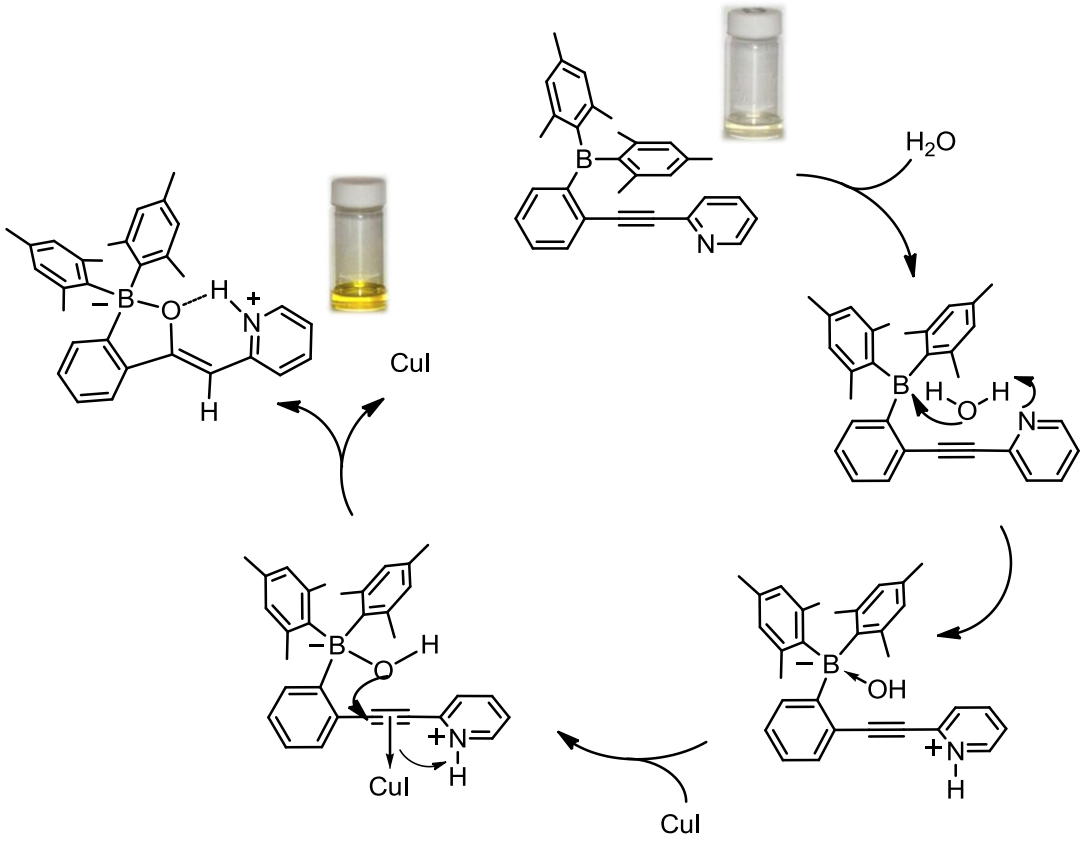

Figure 3.8 A proposed mechanism for the conversion of **3.1** to **3.2**.

3.2.6 Control reactions using compound 3.3

Although metal-catalyzed hydration of alkynes are known previously,[7,8] CuI catalyzed hydration of internal alkynes under ambient temperature is rare. The only related example is a Cu(I) catalyzed intramolecular cyclization reaction.[12] The facile hydration of **3.1** to form **3.2** is believed to be the consequence of cooperative action by the $BMes_2$ group and the pyridyl group. This is confirmed by the fact that the boron center in both compounds has a similar electrophilicity as evidenced by their similar reduction potential ($E_{1/2}^{red}$ = -2.22 V for **3.1** and 2.29 V for **3.3**, vs. $FeCp_2^{+/0}$, Figure 3.9) and similar affinity to fluoride ions (Figure 3.10), but no hydration reaction occurred at all for compound **3.3** when subjected to the same reaction conditions as monitored by ^{1}H NMR (Figure 3.11). The pyridyl group in **3.1** likely acts as an internal base that helps to trap the OH^- anion, enhances its nucleophilicity and stabilizes the transition state/intermediate in the hydration process via the formation of an internal H-bond with OH^-.

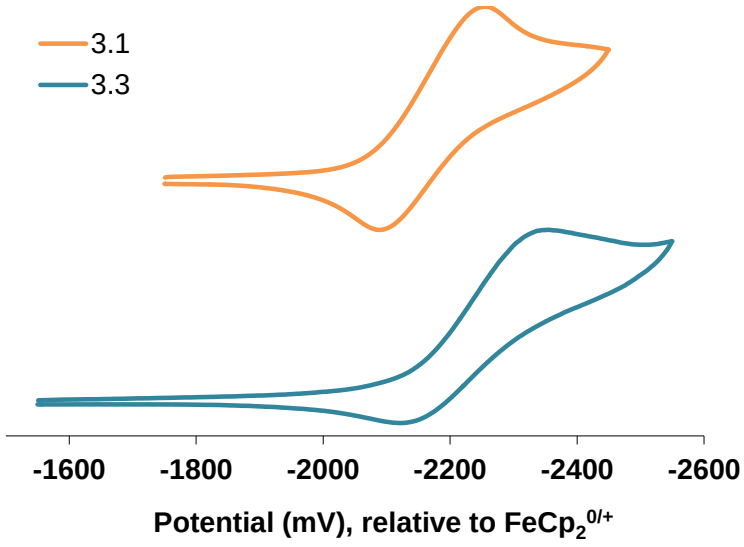

Figure 3.9 Cyclic voltammetry diagram of compounds **3.1** and **3.3** in DMF.

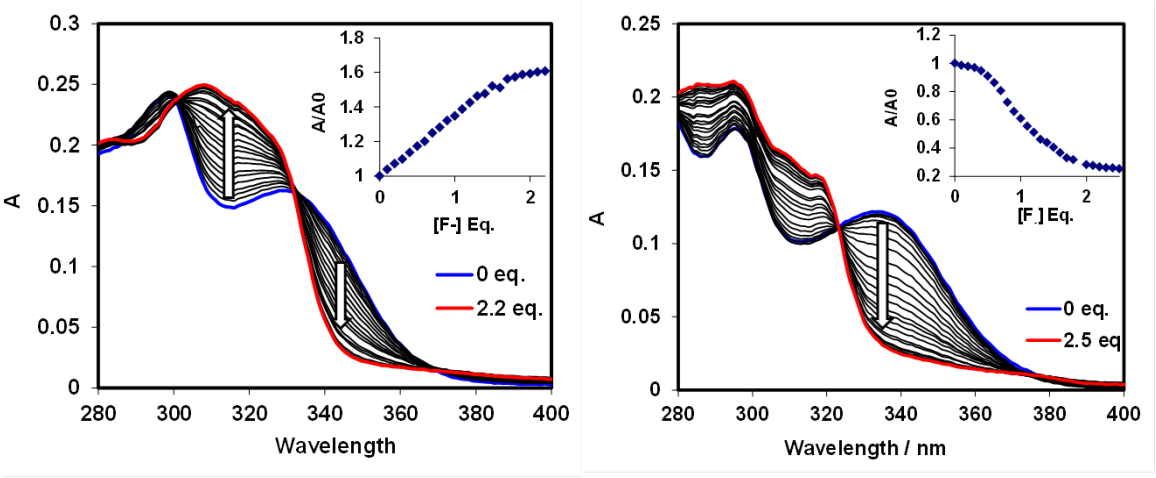

Figure 3.10 UV-vis titration of **3.1** (left) and **3.3** (right) by NBu_4F in CH_2Cl_2 (1×10^{-5} M). Inset: Stern-Volmer plot at 312 nm (**3.1**, left) and at 335 nm (**3.3**, right).

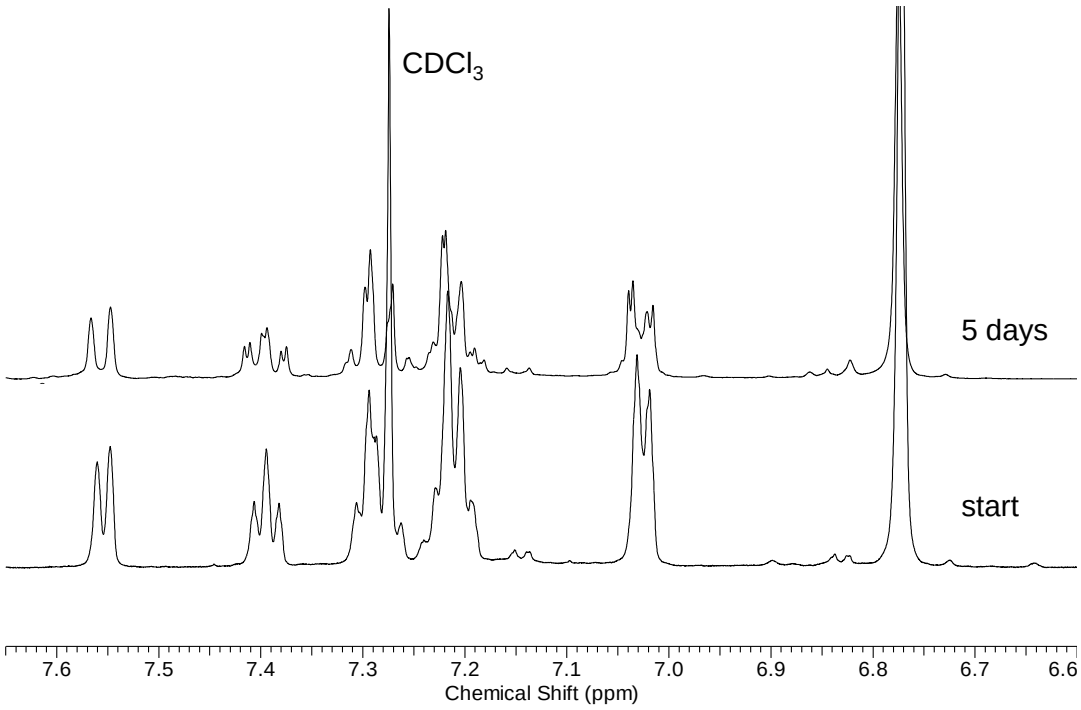

Figure 3.11 ^1H NMR spectra of **3.3** after 5 days in $CDCl_3$ in the presence of 10% CuI, 10 equiv. H_2O, and 10 equiv. Et_3N at ambient temperature. The top and bottom spectra were recorded using the 600 and 300 MHz NMR spectrometer, respectively.

The formation of **3.2** is related to the double-cyclization phenomenon reported recently by Yamaguchi and coworkers where a six-membered N,O-chelate borole species was generated by hydration of a bis(pyridyl)acetylene with two internally coordinated bromobenzoborole groups.[13] Although this reaction mechanism was not well understood, it was suggested that the high Lewis acidity and reactivity of the bromobenzoborole group may have played a key role in the observed transformation.[13]

3.2.7 Response of compound 3.2 to base

To determine the role of the H-bond in stabilizing the boron enol ester structure in **3.2**, we examined the response of **3.2** toward base. Titration experiments in both absorption and fluorescence modes using NaOMe/CH_3OH were performed. The addition of base caused a change in solution color from yellow to colorless. As shown in Figure 3.12, the fluorescence intensity of **3.2** decreases gradually with increasing concentrations of NaOMe; the absorption peak at λ_{max} = 435 nm is quenched and replaced with a new absorption band at 350 nm. This can be attributed to the formation of the anionic boron enol ester [**3.2**]$^-$ and the diminished charge-transfer to pyridine due to the removal of the H-bond proton. This is supported by the TD-DFT calculation results that show an increase of about 0.90 eV in the HOMO-LUMO gap from **3.2** to its anion, as well as by the calculated molecular orbital surfaces of **3.2** and **[3.2]**$^-$ (Figure 3.13). The addition of two equivalence of HBF_4 to the NaOMe-titrated solution of **3.2** restores the yellow color, and the absorption and fluorescence spectra (Figure 3.12), supporting that the anion [**3.2**]$^-$ is a stable species in solution. Thus, the stability of **3.2** can be mostly attributed to chelation to the boron center. However, we have observed that the addition of a large excess HBF_4 causes irreversible spectral changes to **3.2**, indicating that compound **3.2** is not stable under acidic conditions.

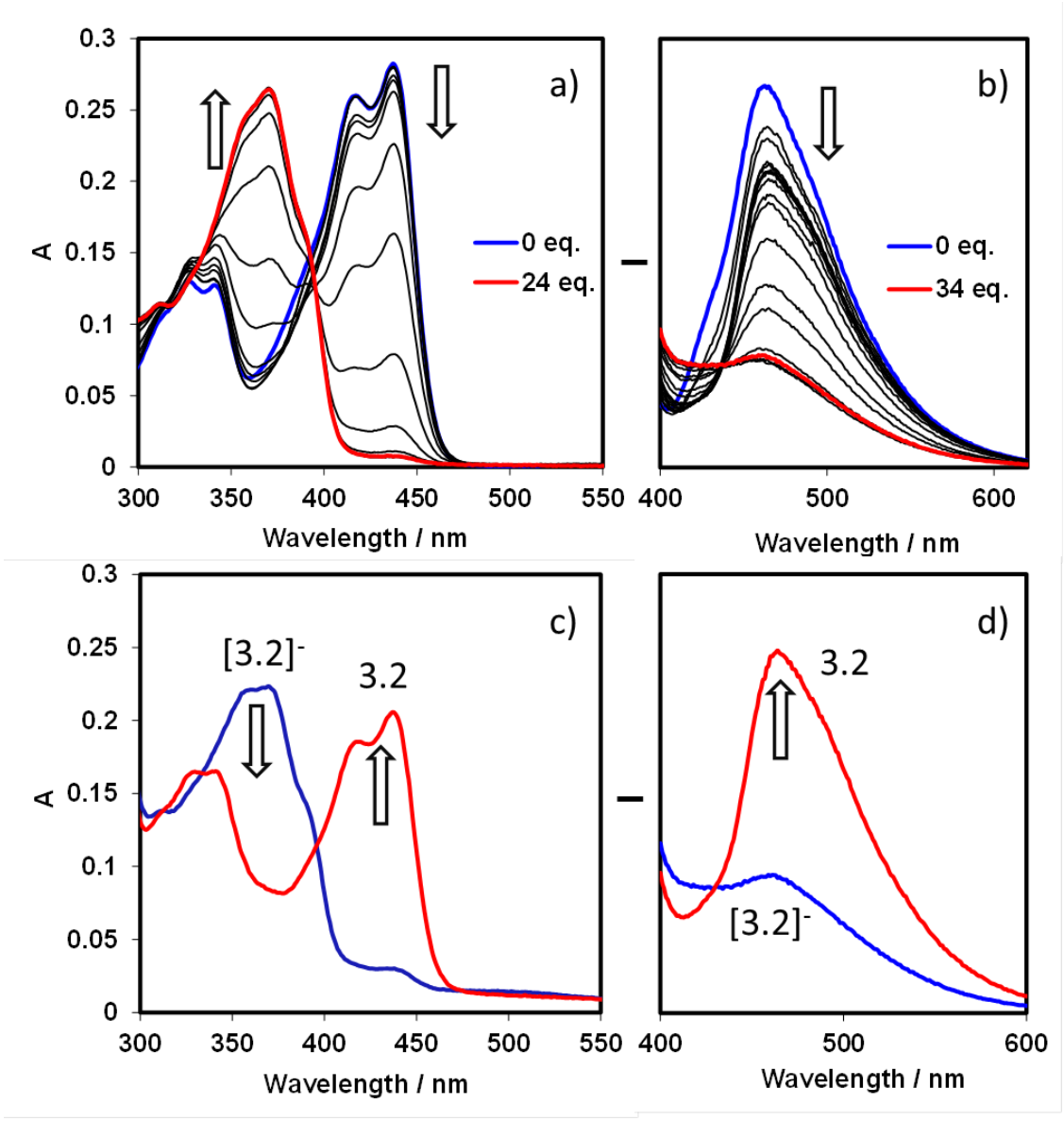

Figure 3.12 Top: titration of **3.2** in CH_2Cl_2 (1.0×10^{-5} M) by NaOMe/CH_3OH: UV-Vis (a) and fluorescent (b) spectral change. Bottom: UV-Vis (c) and fluorescence (d) spectral change after the addition of 2 equiv. HBF_4 (vs. amount of NaOMe added) to the NaOMe titrated solution of **3.2**.

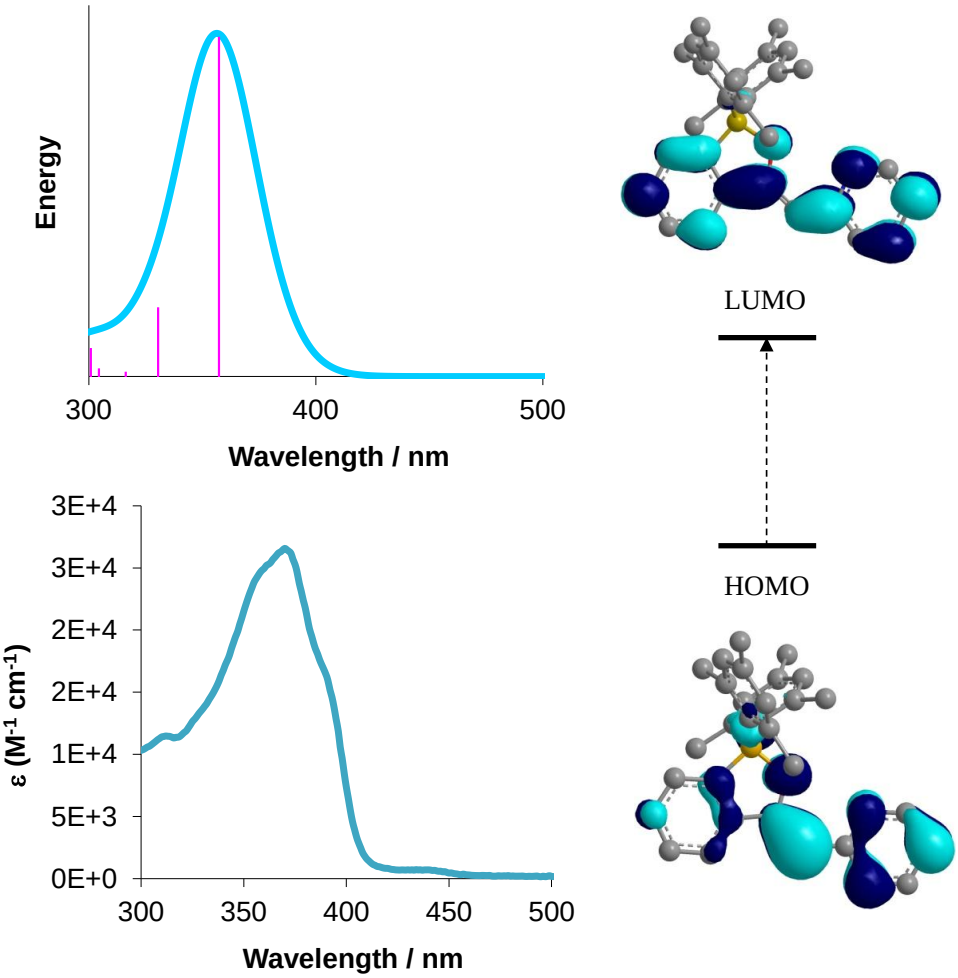

Figure 3.13 Left: energy spectrum calculated using TD-DFT for **[3.2]**$^-$ (top) and absorbance spectrum of **3.2** at the endpoint of NaOMe titration (bottom). Right: the MOs responsible for the lowest energy transition band in the UV-Vis spectrum (HOMO-LUMO gap calculated from TD-DFT is 3.42 eV).

3.3 Conclusions

In summary, a dimesitylboryl and pyridyl-functionalized acetylene has been found to undergo a facile hydration reaction in the presence of CuI and Et_3N. The cooperativity between the Lewis acidic and basic groups has been demontrated to play a key role in promoting the hydration process and in stabilizing the enol structure of the product.

3.4 Experimental

3.4.1 General considerations

All experiments were performed under a nitrogen atmosphere in a Vacuum Atmospheres drybox or by standard Schlenk technique unless otherwise noted. THF was dried and distilled over sodium benzophenone ketyl prior to use; CH_2Cl_2 was dried and distilled over P_2O_5 as solvent for photophysical measurements. Thin-layer and flash chromatography were performed on silica gel. ^1H and ^{13}C NMR spectra were recorded on Bruker Avance spectrometers, and deuterated solvents were purchased from Cambridge Isotopes and used without further drying. High resolution mass spectra (HRMS) were obtained from an Applied Biosystems QStar XL spectrometer. 1-Dimesitylboryl-2-ethynylbenzene was synthesized according to a literature procedure.[6a]

3.4.2 Synthesis and characterization

2-(2'-(dimesitylboryl)phenylethynyl)pyridine (3.1): 1-dimesitylboryl-2-ethynylbenzene (0.326 g, 0.93 mmol), 2-bromopyridine (0.176 g, 1.12 mmol), $Pd(PPh_3)_2Cl_2$ (0.039 g, 0.056 mmol) and CuI (0.009 g, 0.046 mmol) in 15 mL THF/2 mL Et_3N were reacted overnight at 70°C under N_2. THF was evaporated *in vacuo* and the residue was extracted using CH_2Cl_2/5% aq. NH_4Cl. The organic layer was dried over $MgSO_4$, concentrated, and the residue purified by column chromatography on silica (15:1 hexanes:EtOAc) to afford **3.1** as a white solid (0.141 g, 35%). ^1H NMR (400 MHz, $CDCl_3$): δ 8.50 (d, J = 4.3 Hz, 1H, pyridine), 7.66 (d, J = 7.6 Hz, 1H, phenyl), 7.48 (dt, J = 7.8 Hz, J = 1.5 Hz, 1H, pyridine), 7.40 (dt, J = 7.6 Hz, J = 1.8 Hz, 1H, pyridine), 7.30 (m, 2H, phenyl), 7.10 (dt, J = 6.7 Hz, J = 1.6 Hz, 1H, phenyl), 6.76 (s, 4H, mesityl), 6.68 (d, J = 7.8 Hz, 1H, pyridine), 2.24 (s, 6H, mesityl), 2.02 (s, 12H, mesityl). ^{13}C NMR (75 MHz, $CDCl_3$): δ 149.1, 143.3, 142.8, 140.9, 139.0, 135.7, 134.5, 133.5, 130.4, 128.6, 128.3, 127.4, 126.0, 122.2, 91.0, 90.5, 23.2, 21.2 ppm. HRMS calc'd for $C_{31}H_{30}BN$ [M^+] 427.2471, found 427.2482.

3.2: 1-dimesitylboryl-2-ethynylbenzene (0.630 g, 1.80 mmol), 2-bromopyridine (0.341 g, 2.16 mmol), $Pd(PPh_3)_2Cl_2$ (0.076 g, 0.108 mmol) and CuI (0.017 g, 0.090 mmol) in THF/Et_3N (5:1) were reacted overnight at 70°C under N_2. THF was evaporated *in vacuo* and the residue was extracted using CH_2Cl_2/5% aq. NH_4Cl. The resulting precipitate was separated from the liquid organic layer and purified by column chromatography on silica (1:1 hexanes:CH_2Cl_2) to afford **3.2** as a yellow solid (0.180 g, 22%). ^{1}H NMR (C_6D_6, 400 MHz): δ 14.1 (s, br, pyridinium), 8.13 (d, J = 7.5 Hz, 1H, pyridine), 7.58 (d, J = 7.7 Hz, 1H, pyridine), 7.24 (t, J = 7.5 Hz, 1H, pyridine), 7.14, (t, J = 7.7 Hz, 1H, pyridine), 6.92 (s, 4H, mesityl), 6.32 (t, J = 8.6 Hz, 1H, phenyl), 6.14 (t, J = 6.0, 1H, phenyl), 5.96 (d, J = 8.9 Hz, 1H, phenyl), 5.57 (s, 1H, vinyl), 5.42 (t, J = 6.7 Hz, 1H, phenyl), 2.42 (s, 12H, mesityl), 2.29 (s, 6H, mesityl) ppm; ^{13}C NMR (CD_2Cl_2, 75 MHz): δ 179.8, 155.3, 141.8, 140.6, 137.9, 135.4, 133.8, 132.2, 131.2, 129.6, 125.6, 124.7, 124.1, 122.2, 116.4, 85.0, 24.9, 21.0 ppm. HRMS calc'd for $C_{31}H_{32}BNO$ [M^+] 445.2577, found 445.2570.

NMR-scale reaction: degassed CD_2Cl_2 (5 mL) was added to a vial containing **3.1** (0.010 g, 0.023 mmol) and CuI (0.447 mg, 0.002 mmol) under N_2. The starting materials were mixed by gently agitating the vial, followed by the addition of 10 equiv. H_2O (4.0 μL, 0.233 mmol). The mixture was stirred under inert atmosphere at room temperature and monitored by ^{1}H NMR. The conversion yield was determined by integrating the aromatic dimesityl proton peak of **3.2** in reference to that of **3.1**. After three days, ^{1}H NMR spectra showed 40% conversion of **3.1** to **3.2**.

2-(2'-(dimesitylboryl)phenylethynyl)benzene (3.3): prepared in analogy to **3.1**, 1-dimesitylboryl-2-ethynylbenzene (0.080 g, 0.23 mmol), iodobenzene (0.056 g, 0.27 mmol), $Pd(PPh_3)_2Cl_2$ (0.010 g, 0.014 mmol) and CuI (0.002 g, 0.011 mmol) in THF (10 mL) and Et_3N (0.16 mL) was reacted overnight at 50°C under N_2. The crude product was purified by column chromatography on silica (50:1 hexanes:EtOAc) to afford **3.3** as a white solid (0.045 g, 45%). ^{1}H NMR (CD_2Cl_2, 400 MHz): δ 7.55 (d, J = 7.6 Hz, 1H, borylphenyl), 7.41, (dt, J = 7.4 Hz, J = 1.6

Hz, 1H, borylphenyl), 7.29 (dt, J = 7.3 Hz, J = 1.2 Hz, 1H, borylphenyl), 7.25, (d, J = 7.6 Hz, 2H, phenyl), 7.22 (m, 2H, phenyl), 7.02 (dd, J = 7.6 Hz, J = 1.9 Hz, 2H, phenyl), 6.78 (s, 4H, mesityl), 2.26 (s, 6H, mesityl), 2.00 (s, 12H, mesityl) ppm. ^{13}C NMR (CD_2Cl_2, 100 MHz): δ 143.4, 141.3, 139.7, 134.9, 133.4, 132.0, 130.8, 128.8, 128.3 128.4, 127.6, 123.9, 92.8, 90.6, 23.4, 21.5 ppm. HRMS calc'd for $C_{32}H_{31}B$ [M^+] 426.2519, found 426.2531.

3.4.3 Electrochemical and photophysical measurements

Cyclic voltammetry experiments were performed using a BAS CV-50W analyzer with a scan rate of 0.1-0.2 V/sec using 2 mg sample in 0.5 mL dry DMF. The electrochemical cell was a standard three-compartment cell composed of a Pt working electrode, a Pt auxiliary electrode, and an Ag/AgCl reference electrode. CV measurements were carried out at room temperature with 0.1 M tetrabutylammonium hexafluorophosphate as the supporting electrolyte. Emission spectra were recorded using a Photon Technologies International QuantaMaster Model 2 spectrometer (CH_2Cl_2 at 1×10^{-5} M). UV/Visible spectra were recorded using a Varian Cary 50Bio UV-vis spectrophotometer. Photoluminescent quantum yields were measured using optically dilute method (1×10^{-5} M, A ≈ 0.1) at room temperature in CH_2Cl_2 relative to anthracene (Φr = 0.36 in CH_2Cl_2). The fluorescence quantum yields were calculated using previously known procedures.[14]

3.4.4 Density functional theory calculations

Molecular orbital and molecular geometry calculations were performed using the Gaussian 03 program suite using crystal structures as the starting point for geometry optimizations where possible. Calculations were performed at the B3LYP level of theory using 6-31G* basis set.

3.4.5 X-ray diffraction analysis

Single crystals of **3.1**, **3.2** and **3.3** were mounted on glass fibers for data collection. Data were collected on a Bruker Apex II single-crystal X-ray diffractometer with graphite-monochromated Mo Kα radiation, operated at 50 kV and 30 mA and at 180 K. Data were processed on a PC with the aid of the Bruker SHELXTL software package (version 6.14)[15] and corrected for absorption effects. No significant decay was observed. Compound **3.2** co-crystallized with a disordered diethylether molecule (0.5 diethylether per molecule of **3.2**), which was removed using the Platon Squeeze routine[16] to improve the overall quality of the structure.

Table 3.2 Crystallographic data for compounds **3.1**-**3.3**.

Compound	**3.1**	**3.2**	**3.3**
Formula	$C_{31}H_{30}BN$	$C_{31}H_{29}BNO$	$C_{31}H_{29}B$
FW	427.37	442.36	426.38
Space Group	P2(1)/c	P2(1)/c	P-1
a, Å	8.148(12)	13.196(15)	9.3686(14)
b, Å	23.74(3)	13.291(15)	12.1651(18)
c, Å	12.404(18)	15.960(18)	12.2768(18)
α, °	90	90	65.465(2)
β, °	92.161(16)	98.526(13)	81.937(2)
γ, °	90	90	81.928(2)
V, $Å^3$	2398(6)	2768(5)	1255(3)
Z	4	4	2
D_{calc}, g cm^{-1}	1.184	1.061	1.128
T, K	180(2)	180(2)	180(2)
μ, mm^{-1}	0.067	0.063	0.063
$2\theta_{max}$, °	55.04	54.54	54.00
Reflns measured	17675	27117	13712
Reflns used (R_{int})	5198(0.1667)	6095(0.1958)	5366(0.0235)
Parameters	912	940	456
Final R Values [I > 2σ(I)]:			
R_1[a]	0.1339	0.1021	0.0462
wR_2[b]	0.3375	0.2249	0.1217
R values (all data):			
R_1[a]	0.2643	0.2476	0.0629
wR_2[b]	0.3971	0.2873	0.1352
Goodness-of-fit on F^2	1.074	0.892	1.037

[a] $R_1 = \Sigma[(|F_0| - |F_c|) / \Sigma |F_0|$

[b] $wR2 = [\Sigma w[(F_0^2-F_c^2)^2] / \Sigma[w(F_0^2)^2]]^{1/2}$

$w = 1 / [\sigma^2(F_0^2) + (0.075P)^2]$, where $P = [Max (F_0^2, 0) + 2F_c^2] / 3$

Table 3.3 Selected bond lengths (Å) and angles (°) for compounds **3.1**-**3.3**.

3.1			
B(1)-C(23)	1.549(10)	C(23)-B(1)-C(1)	117.1(6)
B(1)-C(14)	1.563(10)	C(23)-B(1)-C(14)	125.0(6)
B(1)-C(1)	1.587(10)	C(14)-B(1)-C(1)	117.8(6)
N(1)-C(13)	1.324(9)	C(13)-N(1)-C(9)	114.9(6)
N(1)-C(9)	1.340(9)		
C(6)-C(7)	1.431(10)		
C(7)-C(8)	1.178(9)		
C(8)-C(9)	1.452(10)		
3.2			
B(1)-O(1)	1.609(6)	O(1)-B(1)-C(23)	100.2(3)
B(1)-C(23)	1.616(7)	O(1)-B(1)-C(1)	96.0(4)
B(1)-C(1)	1.623(7)	O(1)-B(1)-C(14)	110.3(4)
B(1)-C(14)	1.638(7)	C(7)-O(1)-B(1)	113.8(3)
O(1)-C(7)	1.317(5)	C(23)-B(1)-C(14)	119.2(4)
N(1)-C(9)	1.346(6)	C(9)-N(1)-C(13)	124.1(4)
N(1)-C(13)	1.382(6)	C(9)-N(1)-H(1A)	126(3)
N(1)-H(1A)	0.90(5)	C(13)-N(1)-H(1A)	109(3)
C(6)-C(7)	1.490(6)		
C(7)-C(8)	1.353(6)		
C(8)-C(9)	1.436(6)		
3.3			
C(15)-B(1)	1.574(2)	C(15)-B(1)-C(24)	123.20(12)
C(1)-B(1)	1.571(2)	C(1)-B(1)-C(24)	116.09(12)
C(24)-B(1)	1.574(2)	C(1)-B(1)-C(15)	120.67(12)
C(6)-C(7)	1.436(2)		
C(7)-C(8)	1.196(2)		
C(8)-C(9)	1.433(2)		

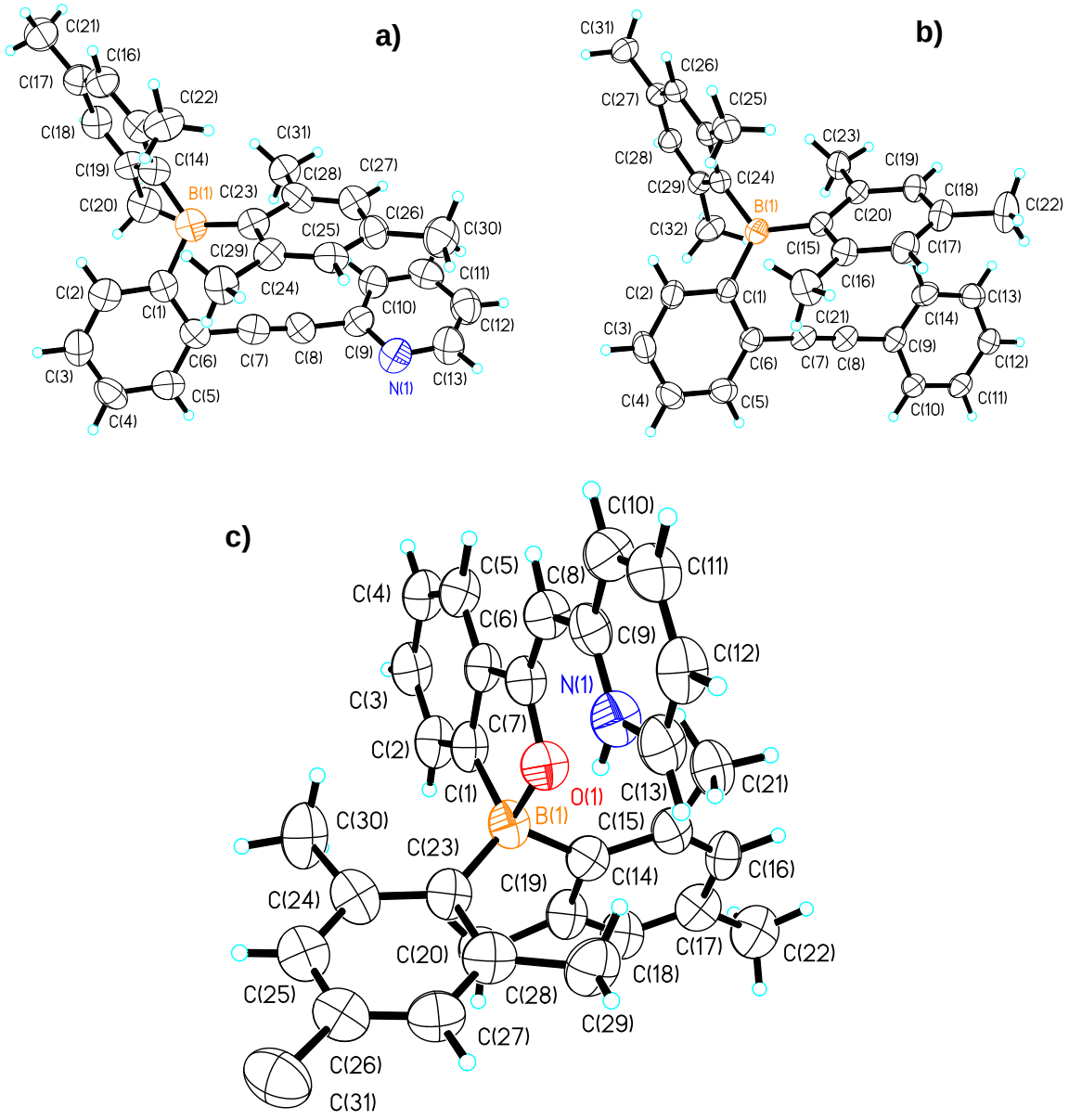

Figure 3.14 Crystal structures of compound **3.1** (a), **3.3** (b) and **3.2** (c) with labeling schemes and 50% thermal ellipsoids.

3.5 References

(1) For recent reviews see: (a) Hudson, Z. M.; Wang, S. *Acc. Chem. Res.* **2009**, *42*, 1584. (b) Yamaguchi, S.; Wakamiya, A. *Pure Appl. Chem.* **2006**, *78*, 1413. (c) Entwistle, C. D.; Marder, T. B. *Chem. Mater.* **2004**, *16*, 4574. (d) Jäkle, F. *Chem. Rev.*, **2010,** *110*, 3985 and references therein.

(2) (a) Yamaguchi, S.; Shirasaka, T.; Akiyama, S.; Tamao, K. *J. Am. Chem. Soc*. **2002**, *124*, 8816. (b) Wade, C. R.; Broomsgrove, A. E. J.; Aldridge, S.; Gabbai, F. P. *Chem. Rev.* **2010**, *110*, 3958.

(3) Kim, Y.; Gabbai, F. P. *J. Am. Chem. Soc*. **2009**, *131*, 3363.

(4) (a) Stephan, D. W.; Erker, G. *Angew. Chem. Int. Ed*. **2010**, *49*, 46. (b) Voss, T.; Chen, C.; Kehr, G.; Nauha, E.; Erker, G.; Stephan, D. W. *Chem. Eur. J*. **2010**, *16*, 3005.

(5) Georgiou, I.; Ilyashenko, G.; Whiting, A. *Acc. Chem. Res.* **2009**, *42*, 756.

(6) (a) Fukazawa, A.; Yamada, H.; Yamaguchi, S. *Angew. Chem. Int. Ed*. **2008**, *47*, 5582. (b) Fukazawa, A.; Yamaguchi, S. *Chem. Asian J.* **2009**, *4*, 1386.

(7) Alonso, F.; Beletskaya, I. P.; Yus, M. *Chem. Rev*. **2004**, *104*, 3079. (b) Wakatsuki, Y.; Hou, Z.-M.; Tokunaga, M. *Chem. Rec.* **2003**, *3*, 144.

(8) (a) Baik, C.; Hudson, Z. M.; Amarne, H.; Wang, S. *J. Am. Chem. Soc.* **2009**, *131*, 14549. (b) Amarne, H.; Baik, C.; Murphy, S. K.; Wang, S. *Chem. Eur. J*. **2010**, *16*, 4750.

(9) Cui, Y.; Wang, S. *J. Org. Chem*. **2006**, *71*, 6485.

(10) Bond lengths in crystalline organic compounds. *CRC Handbook of Chemistry and Physics*, 91st ed.; CRC Press: Boca Raton, Fl., 2010; p 9-10.

(11) March, J. *Advanced Organic Chemistry: Reactions, Mechanisms, and Structures*, 4th ed.; John Wiley & Sons: New York, 1992; p 762.

(12) Chowdhury, C.; Chaudhuri, G.; Guha, S.; Mukherjee, A. K.; Kundu, N. G. *J. Org. Chem.* **1998**, *63*, 1863.

(13) Zhao, Q.; Zhang, H.; Wakamiya, A.; Yamaguchi, S. *Synthesis*. **2009**, 127.

(14) Demas, N.J.; Crosby, G. A. *J. Am. Chem. Soc.*, **1970**, *29*, 7262.

(15) SHELXTL Version 6.14, Bruker AXS, 2000-2003.

(16) Spek, A. L. *Acta Cryst*. **1990**, *A46*, C34.

Chapter 4

Organoboron and Diarylplatinum-Enabled Double Cascade Cyclization/Aryl Migration across an Alkyne Bond

4.1 Introduction

As discussed previously, organoboron compounds exhibit rich chemical reactivity that can lead to fascinating transformations and applications due to the electron-accepting nature of the boron center.[1-4] In particular, molecules that incorporate both Lewis acidic boranes and Lewis basic amines or phosphines are well known for their unusual ability to activate small molecules.[5-7] In a recent report, Yamaguchi and coworkers demonstrated that such a Lewis acid/base pair can act synergistically to promote the cascade intramolecular cyclization of π-conjugated systems across internal alkyne bonds involving a stable boryl group, $BMes_2$ (Figure 4.1).[5b] This reactivity has been exploited as a highly effective strategy for achieving a new class of zwitterionic π-conjugated materials that display unusual photonic and electronic properties.[5] Stephan and coworkers have shown that tandem addition by PR_3 and $B(C_6F_5)_3$ across an alkyne bond can also occur readily.[6a,d]

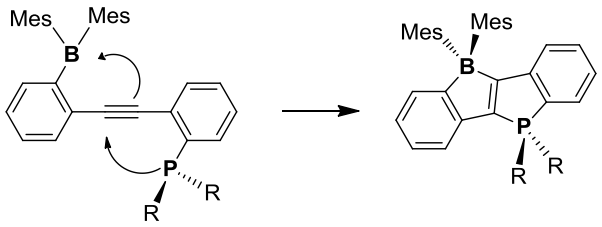

Figure 4.1 Cascade intramolecular cyclization of a π-conjugated system across an internal alkyne.

Inspired by this work, we sought to determine if similar co-operativity between an electron-rich metal center and a $BMes_2$ group could be used to construct cyclometallated π-skeletons using metal atoms such as Pt(II) as the donor. Our interest in boron-containing Pt(II) cyclometallated compounds is motivated by the fact that incorporation of a $BMes_2$ group can greatly enhance phosphorescence efficiency or anion sensing ability of the Pt(II) complexes.[8] We designed ligand **4.1** for this study, which allows for facile coordination of transition metal ions to the $BMes_2$-alkyne scaffold. Furthermore, **4.1** is known for its unusual reactivity, as it has been shown to undergo facile hydration of the internal alkyne at ambient temperature due to the synergistic action of the borane and pyridine groups.[9] Using **4.1**, we have found that coordination to an electron-rich Pt(II) centre readily promotes a spontaneous double cyclization of the π-system, accompanied by double aryl rearrangement and reduction of the internal alkyne to a C-C single bond (compound **4.3a** and **4.3b**, Figure 4.2). The details of this remarkable transformation are reported herein.

4.2 Results and Discussion

4.2.1 Synthesis of compounds 4.3a-c

The reaction of **4.1** with Pt(*p*-R-C_6H_4)$_2$(DMSO)$_2$[10] in a 1:1 ratio in either CH_2Cl_2 or toluene at ambient temperature led first to the formation of complexes **4.2a–c**, which can be isolated nearly quantitatively and have been fully characterized by ^{1}H NMR and elemental analyses. Compounds **4.2a–c** are air-stable light yellow solids under ambient conditions; however, upon prolonged standing in solution (CH_2Cl_2 or toluene) under N_2, **4.2a** and **4.2b** undergo gradual transformation to compounds **4.3a** and **4.3b**, respectively, while **4.2c** remains unchanged. Block yellow crystals were obtained for **4.3a**, which allowed the determination of its structure by single-crystal X-ray diffraction analysis.[11]

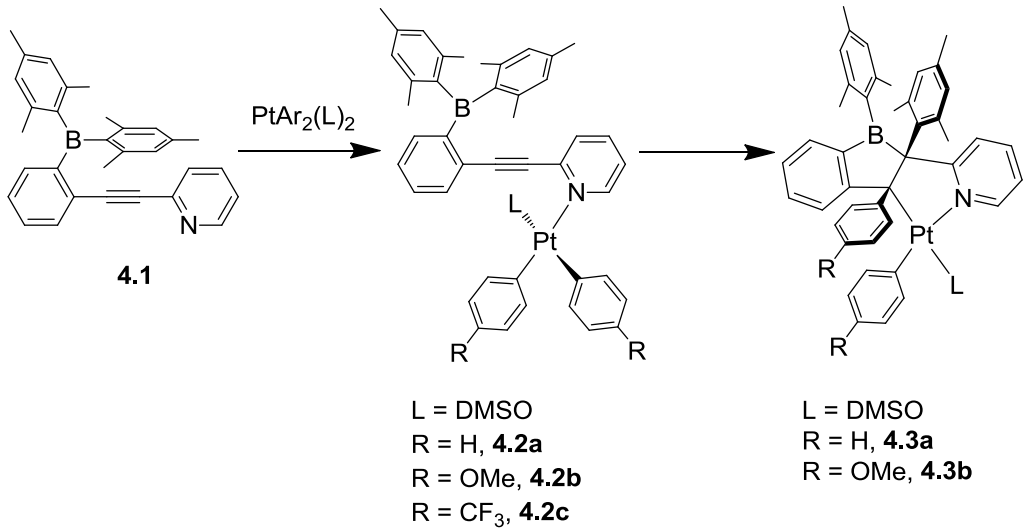

Figure 4.2 Spontaneous double cyclization of **4.2a-4.2b** and double aryl migration.

4.2.2 Structural determination of 4.3a and 4.3b

The crystal structure of **4.3a** reveals several important features of the transformation (Figure 4.3). First, one mesityl group from the boron centre and one phenyl group from the Pt centre have migrated to the C(2) and C(1) atoms, respectively. In addition, the boron and platinum atoms have each formed σ bonds with C(2) and C(1) of the internal alkyne, respectively. As a consequence of this bond formation and rearrangement, the C(1)-C(2) triple bond is transformed to a single bond, with a C-C distance of 1.627(4) Å.

Furthermore, the migrated aryl groups exclusively adopt a *syn* conformation in all crystals examined, facing each other with significant π-π interactions. Similar π-π interactions are also evident between the C(3) and the C(9) phenyl rings, as well as the pyridyl and the C(17) mesityl ring. The C(1) and C(2) atoms both exhibit distorted tetrahedral geometries, while the Pt centre has a square planar geometry with the two Pt-C bonds being *cis* to each other. The boron centre has a typical trigonal planar geometry, with considerable variation in B-C bond lengths that are attributable to the steric congestion of the molecule.

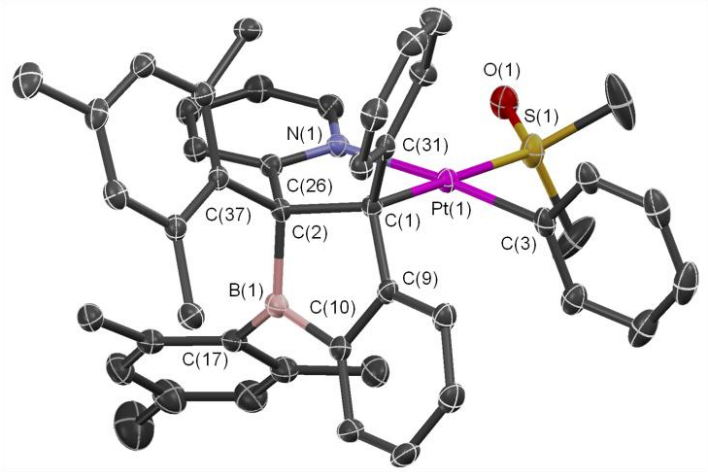

Figure 4.3 Crystal structure of compound **4.3a** with 50% thermal ellipsoids and labeling schemes. Hydrogen atoms are omitted for clarity.

The transformation of **4.2a** to **4.3a** converts internal alkyne carbons C(1) and C(2) into chiral centers, with both enantiomers of **4.3a** found in the unit cell (space group *P*-1). In agreement with the asymmetric structure of this molecule, the magnetically equivalent methyl groups of **4.2a** become diastereotopic in **4.3a**, resulting in six well-resolved methyl peaks in its ^{1}H NMR spectrum (see Figure 4.15 in section 4.4). Despite the presence of a three-coordinate boron centre with only a single sterically-protecting mesityl group, compound **4.3a** is air-stable in the solid state. NMR spectroscopic studies confirmed that compound **4.3b** is an analogue of **4.3a** (Figure 4.16) and is air-stable as a yellow powder. In non-halogenated solvents such as benzene or toluene, **4.3a** and **4.3b** are stable for days under air. However, in CH_2Cl_2, slow degradation of both compounds was observed after exposure to air for several days.

4.2.3 Monitoring the conversion of 4.2a-b to 4.3a-b by ^{1}H NMR

To establish whether compounds **4.3a** and **4.3b** are the major products from the transformation of the corresponding **4.2a** and **4.2b**, we monitored the reaction and the product conversion by ^{1}H NMR spectroscopy at ambient temperature. In all cases, compounds **4.2a** and **4.3b** are generated

in situ by mixing the ligand **4.1** and the corresponding $PtAr_2(DMSO)_2$ in 1:1 ratio. Conversion of **4.2a** to **4.3a** or **4.2b** to **4.3b** was observed within a few days in either CD_2Cl_2 or C_6D_6, although minor impurities due to either decomposition or side reactions were observed after prolonged standing of the solution.

NMR studies confirmed that for both **4.2a** and **4.2b**, the double-aryl migrated product **4.3a** or **4.3b** is the dominant product, and the results are summarized on figures 4.4 to 4.7. However, we have observed that the transformation of **4.2b** to **4.3b** proceeds much faster than from **4.2a** to **4.3a**. For example, in CD_2Cl_2, 37% conversion of **4.2b** to **4.3b** was observed after seven days while only 18% conversion of **4.2a** to **4.3a** was achieved under the same conditions. Longer reaction times did lead to higher conversion yields for both compounds; for example, up to 56% conversion of **4.2a** to **4.3a** can be observed after four weeks at ambient temperature. This conversion can be accelerated by mild heating, resulting in 50% conversion of **4.2a** to **4.3a** in one day at 45°C in C_6D_6.

In contrast to the facile transformation of **4.2a** and **4.3a**, compound **4.2c** did not show any change at all after being monitored for 17 days in CD_2Cl_2 at ambient temperature (Figure 4.8). These experiments established that compounds **4.2a** and **4.2b** are indeed the precursors of **4.3a** and **4.3b**, and the unusual transformation is favored by electron-rich $PtAr_2$ groups.

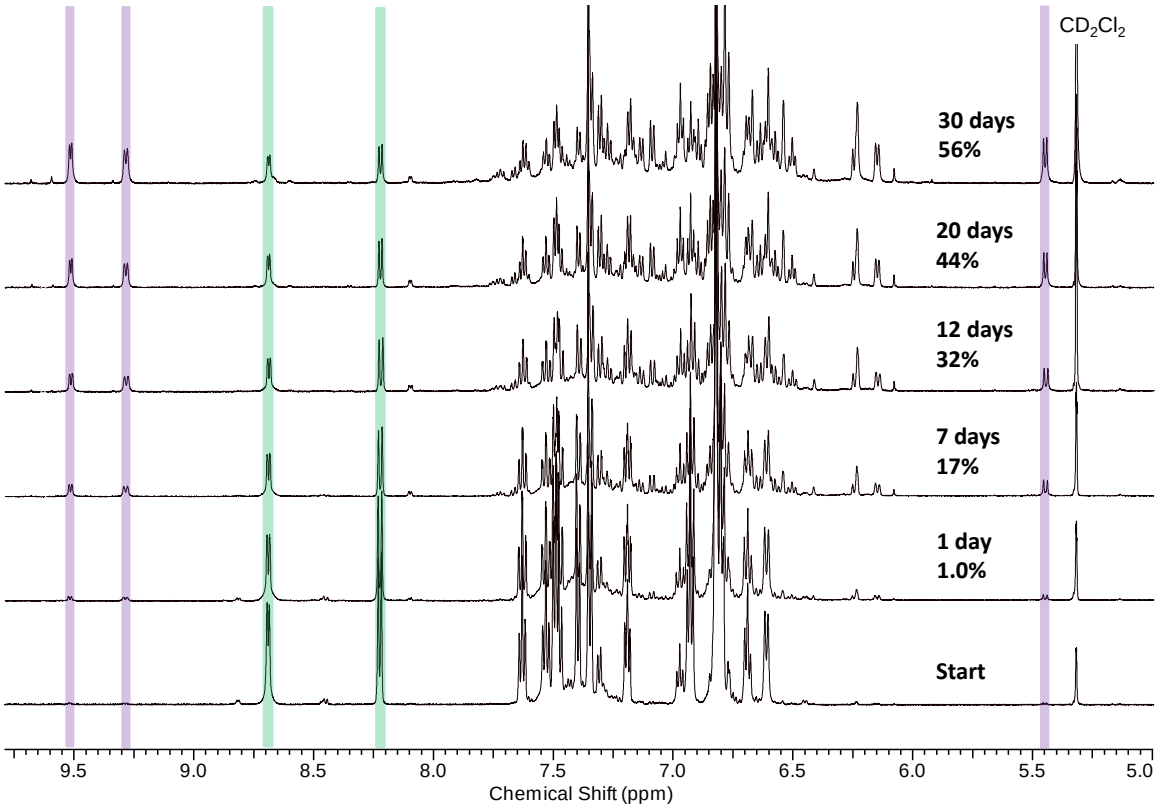

Figure 4.4 The aromatic region of ^{1}H NMR spectra (CD_2Cl_2, RT) showing the conversion of **4.2a** to **4.3a**. Peaks highlighted in green belong to **4.2a**; peaks highlighted in purple belong to **4.3a**.

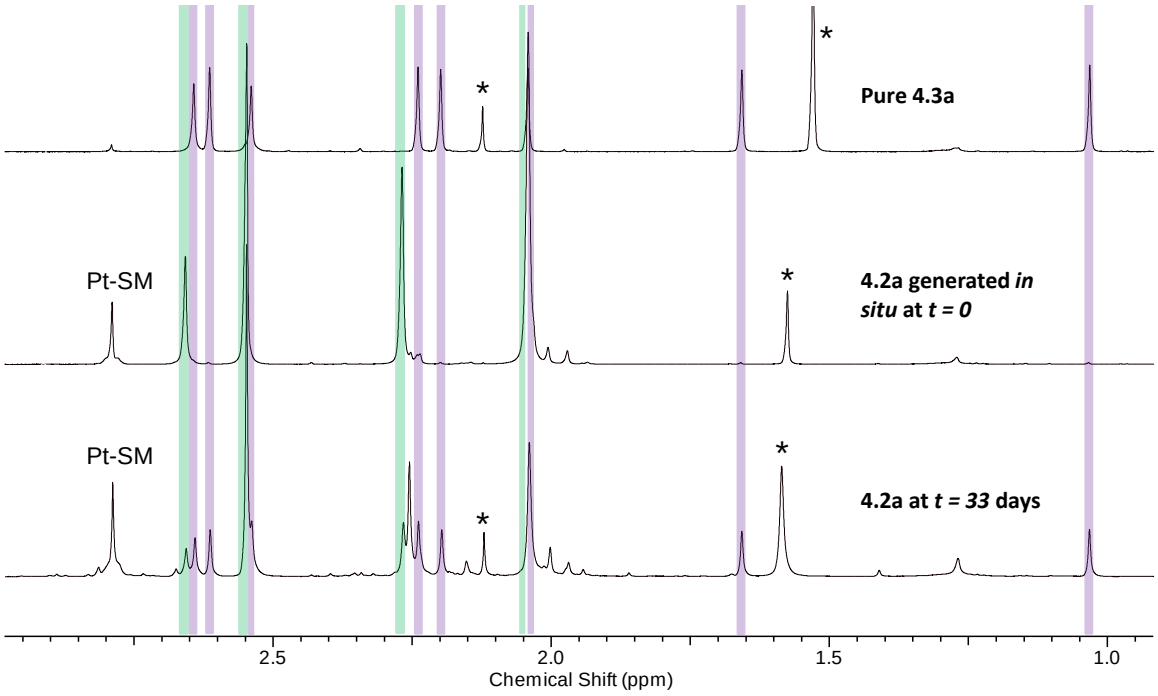

Figure 4.5 The aliphatic region of ^{1}H NMR spectra (CD_2Cl_2, RT) showing the clean conversion of **4.2a** to **4.3a**. The peak marked by "Pt-SM" is from the slight excess of $PtPh_2(DMSO)_2$. Impurity peaks from solvents are marked by "*". Peaks highlighted in green belong to **4.2a**; peaks highlighted in purple belong to **4.3a**.

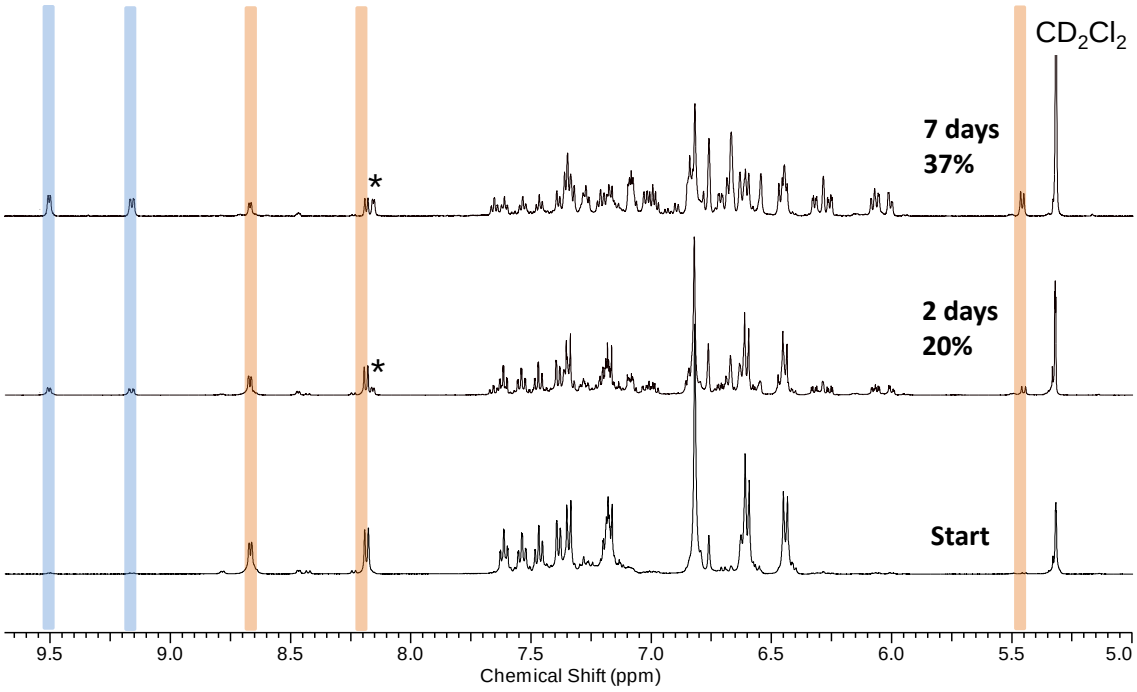

Figure 4.6 The aromatic region of ^{1}H NMR spectra (CD_2Cl_2, RT) showing the conversion of **4.2b** to **4.3b**. An impurity peak is marked by "*". Peaks highlighted in orange belong to **4.2b**; peaks highlighted in blue belong to **4.3b**.

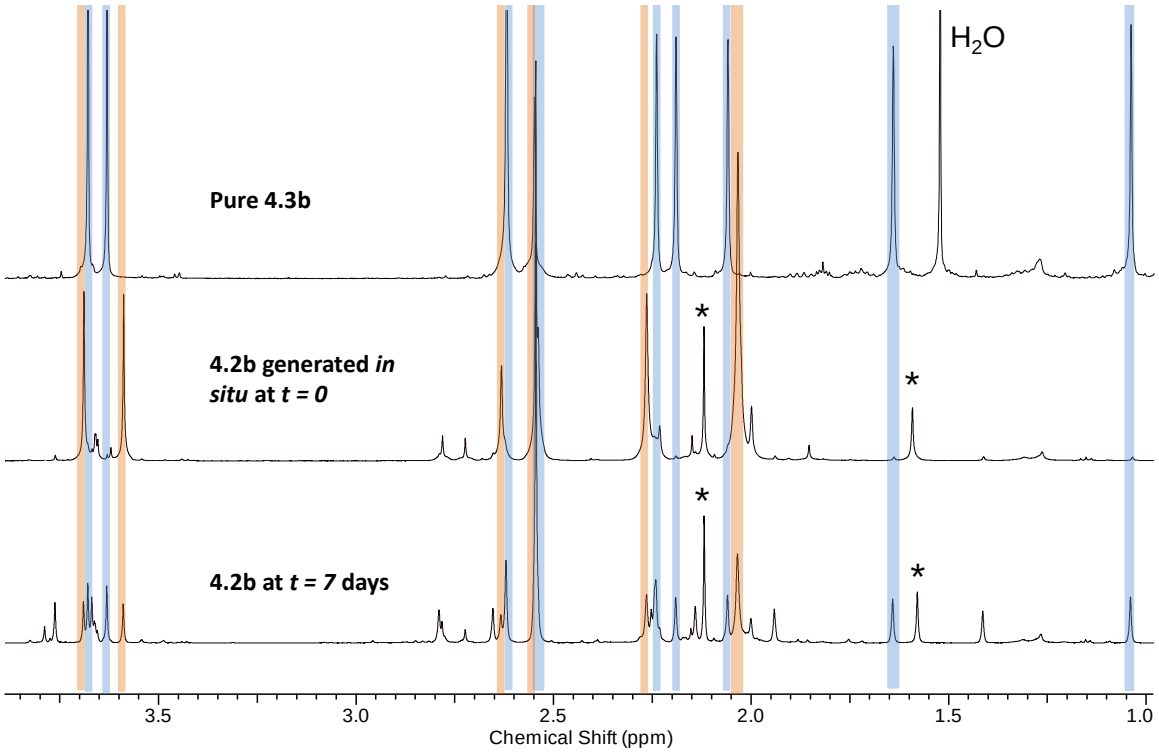

Figure 4.7 The aliphatic region of ^{1}H NMR spectra (CD_2Cl_2, RT) showing the clean conversion of **4.2b** to **4.3b**. Impurity peaks from solvents are marked by "*". Peaks highlighted in orange belong to **4.2b**; peaks highlighted in blue belong to **4.3b**.

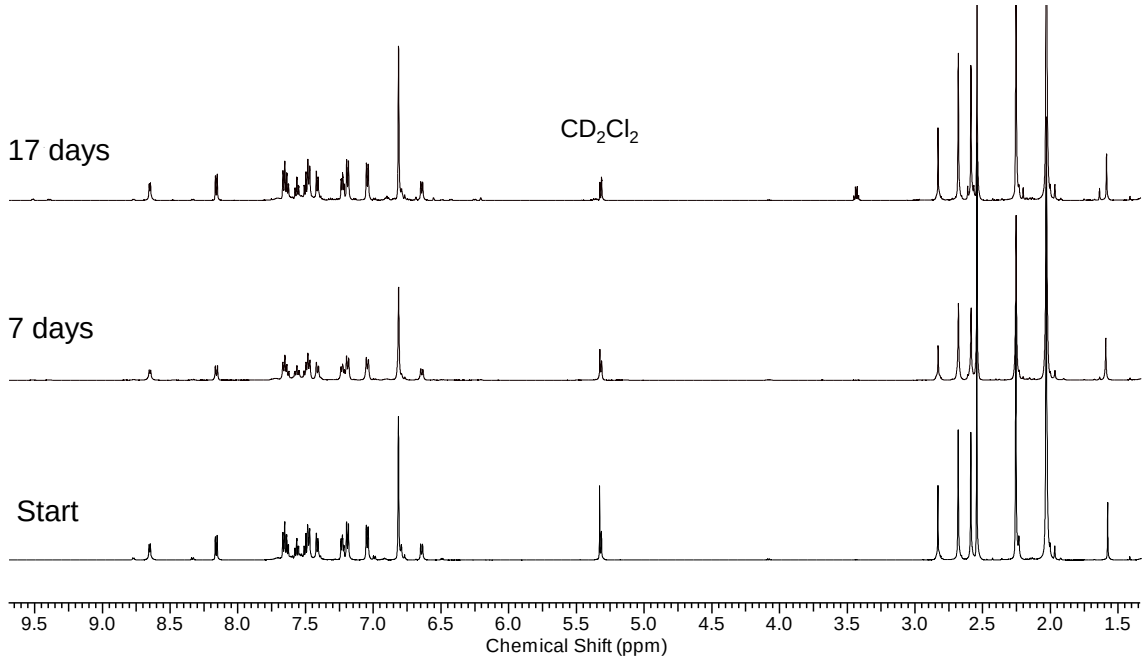

Figure 4.8 ^{1}H NMR spectra of **4.2c** (CD_2Cl_2, RT) showing no change after 17 days.

4.2.4 Control reactions using 4.2d and 4.2e

To further determine the roles of both the boryl acceptor and the $PtAr_2$ group in this unusual transformation, we synthesized control compounds **4.2d** and **4.2e** and examined their reactivity. Compound **4.2d** lacks the $BMes_2$ group, while **4.2e** contains a considerably more electron-deficient $PtCl_2$ centre. The crystal structure of **4.2d** was determined successfully by single-crystal X-ray diffraction analysis and shows a separation distance of 3.230(6) and 3.834(6) Å between the Pt centre and the two alkyne carbon atoms, similar to the computationally optimized structure of **4.2a**. However, no reaction of compound **4.2d** was observed by ^{1}H NMR over 10 days in CD_2Cl_2 at ambient temperature, indicating that the $PtPh_2$ group is unreactive to the nearby alkyne in the absence of the boron acceptor. Similarly, **4.2e** does not demonstrate any reactivity under the same conditions, indicating that an electron-rich $PtAr_2$ group is necessary for the transformation to occur. The double–aryl migration and cyclization in the formation of **4.3a** and **4.3b** can therefore be considered as a synergistic action of both the $PtAr_2$ and $BMes_2$ groups.

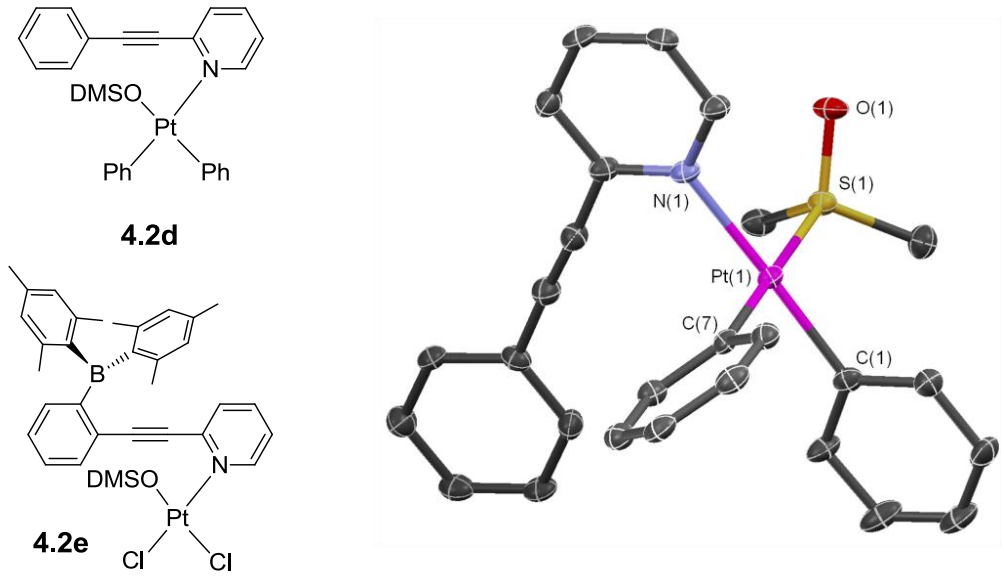

Figure 4.9 Left: structures of **4.2d** and **4.2e**. Right: crystal structure of compound **4.2d** with 50% thermal ellipsoids and labeling schemes.

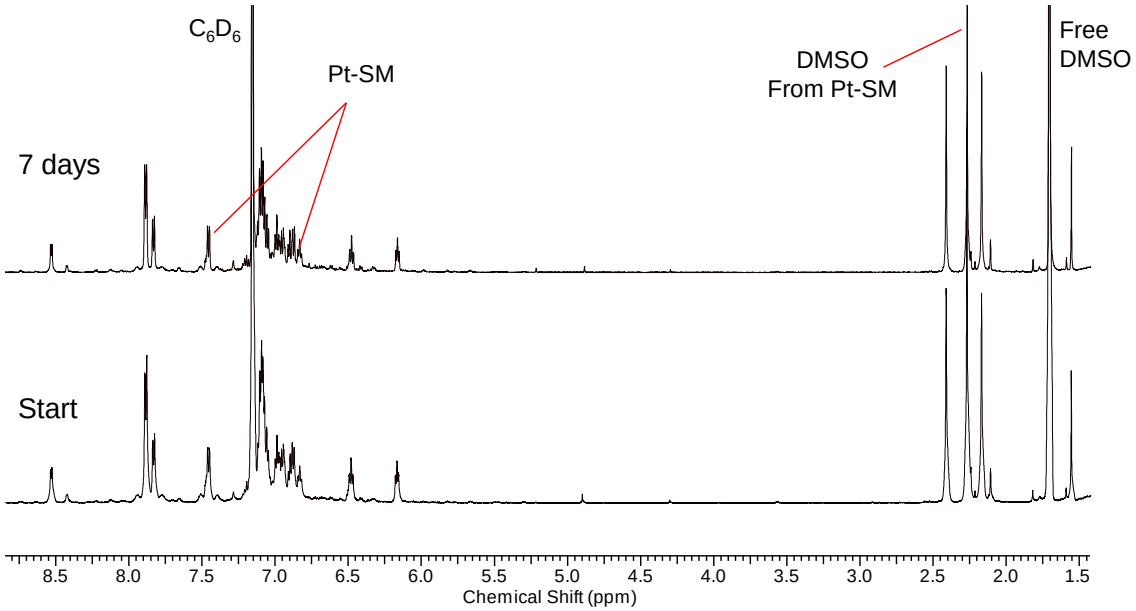

Figure 4.10 ^{1}H NMR spectra of **4.2d** (C_6D_6, RT) showing no change after 7 days. Compound **4.2d** was generated *in situ* by mixing **4.1** with $PtPh_2(DMSO)_2$ in 1:1 ratio.

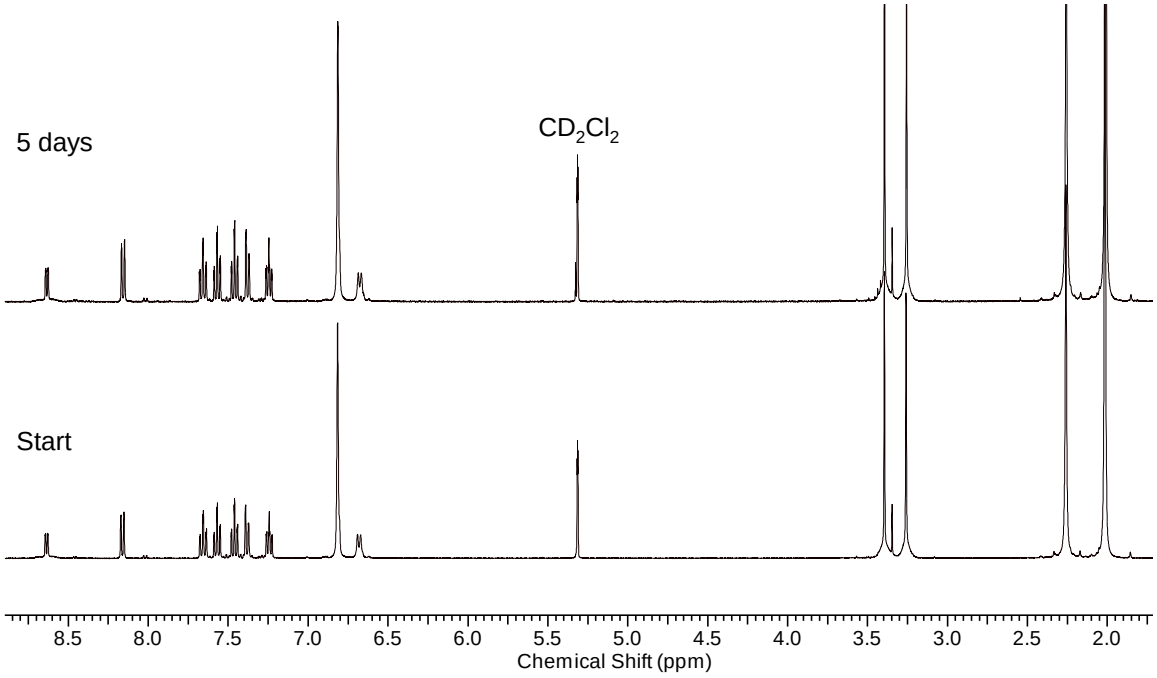

Figure 4.11 ^{1}H NMR spectra of **4.2e** (CD_2Cl_2, RT) showing no change after 5 days.

4.2.5 Mechanism of double cyclization/aryl migration

Alkynyltriorganylborates with the general formula Li[R'-CC-BR_3] are well known to undergo 1,2-migration reactions that transfer one R group from the borate to the alkyne α-carbon atom upon electrophilic attack at the β-carbon of the triple bond.[12] However, the precursors for such migration reactions are typically terminal alkynes. More recently, Erker and coworkers have shown that 1,2-alkyl or aryl migration from either a $B(C_6F_5)_3$ or $B(CH_3)(C_6F_5)_2$ group on an internal alkyne is also possible.[13] In contrast, remote migration of an aryl group from boron to a carbon center being four atoms away is highly unusual, and is facilitated in this case by cyclization of the molecular backbone. To the best of our knowledge, this is the first example of this type of remarkable transformation.

Based on the well-established mechanistic features of Pt(II) facilitated alkyl migrations to alkyne bonds[14] as well as the phosphine-borane cascade cyclization reported by Yamaguchi and coworkers,[5] we propose a plausible mechanism for the transformation of **4.2a** to **4.3a** (and **4.2b** to **4.3b**, Figure 4.12). Density functional theory (DFT) calculations on the reaction pathway were also performed, and support the proposed mechanism.

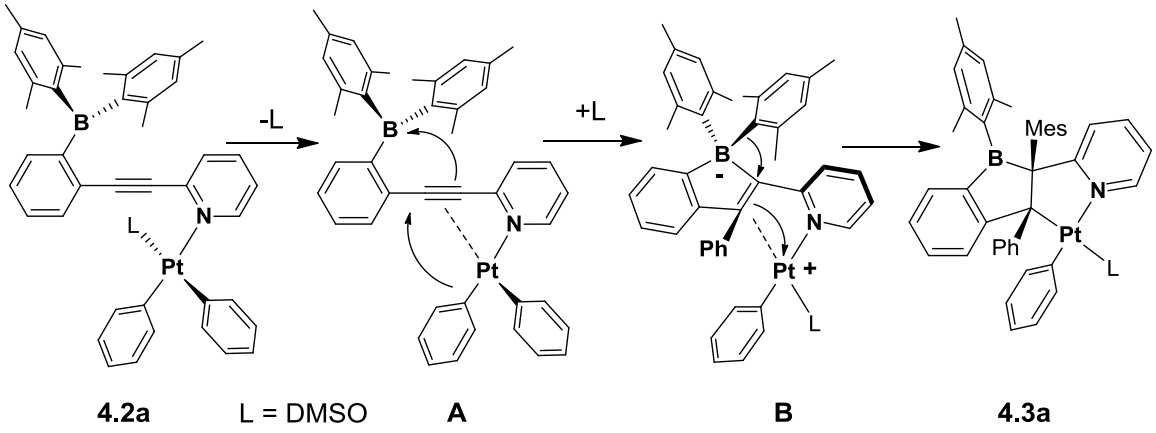

Figure 4.12 Proposed mechanism for **4.2a** to **4.3a** transformation.

The direct precursor for the transformation of **4.2a** to **4.3a** is species **A**, in which DMSO has dissociated from the Pt(II) centre, bringing the $PtPh_2$ unit much closer to the alkyne bond, with calculated Pt···C distances of 2.91 and 3.41 Å in **A** relative to 3.33 and 3.99 Å in **4.2a**. This activates the alkyne, promoting the migration of a phenyl group and cyclization of the π-system with the boron center. In this step, the electron-deficient $BMes_2$ group and the electron-rich $PtPh_2$ group act in synergy to promote the first cyclization/migration. DFT calculation (Figure 4.13) confirmed that the rate-determining step in the transformation of **4.2a** to **4.3a** involves simultaneous attack by Pt and B centres to the alkyne bond, and the migration of the phenyl ring. This is consistent with the lack of reactivity of species **4.2c** that contains a relatively electron-poor $PtAr_2$ group and a greater activation barrier. Re-association of DMSO gives species **B**, a key zwitterionic intermediate identified by DFT calculations. In this species, the electron-rich boryl and the electrophilic platinum centre enable a second migration step[15] – sigmatropic rearrangement of a boron-bound mesityl group, transferring it to the alkenyl carbon with formation of a Pt-C σ bond, yielding the final product **4.3a**.

This mechanism also explains the stereospecificity of the transformation of **4.2a** to **4.3a**. As the Pt centre in **B** blocks one face of the alkene, only the mesityl group on the opposite face of the alkene can migrate. This results in a *syn* arrangement of the two migrated aryl groups in the final product, giving exclusively the *syn* diastereomers of **4.3a**. Computational results show that product **4.3a** is indeed more stable than the starting material **4.2a** by ~36.8 kJ mol^{-1}.

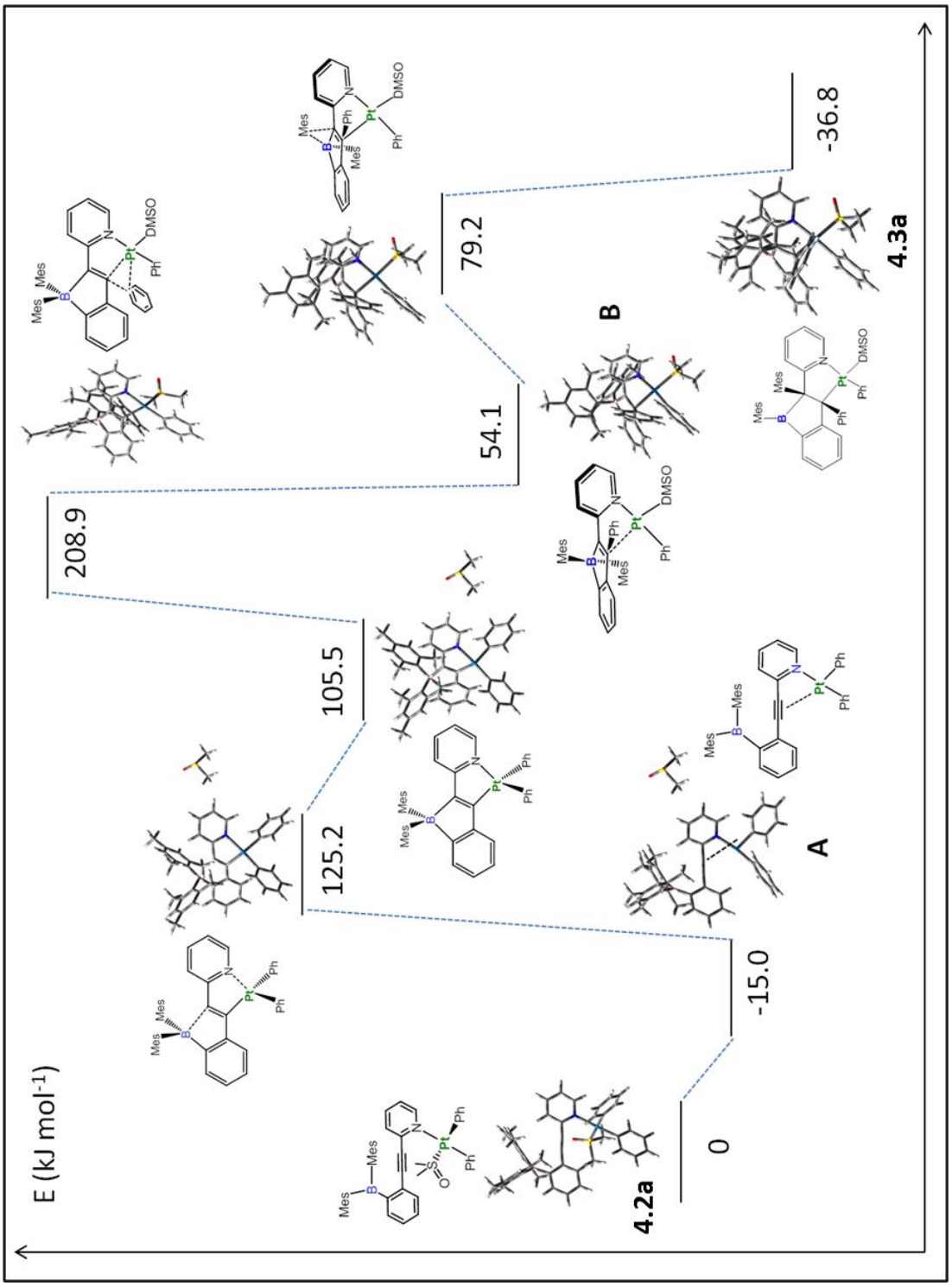

Figure 4.13 The intermediates/transition state structures and energies involved in the conversion of **4.2a** to **4.3a**, calculated by DFT.

4.3 Conclusions

In summary, we have demonstrated an unusual intramolecular double aryl migration/cyclization reaction involving complex **4.2a** and its analogue **4.2b**, resulting in the formation of a unique bicyclic organometallic scaffold. Furthermore, the complementary electronic properties of the electron-deficient borane and electron-rich platinum centres were found to play a key role in this unprecedented transformation. Future work will examine the application of this strategy to other polycyclic frameworks, as well as the incorporation of other electron-rich metal centers into boron-containing organometallic scaffolds.

4.4 Experimental

4.4.1 General considerations

All experiments were performed under a nitrogen atmosphere by standard Schlenk techniques unless otherwise noted. All reaction solvents were obtained from a Fisher Scientific SPS solvent column and dried over molecular sieves. Thin-layer and flash chromatography were performed on silica gel. Solution ^{1}H and ^{13}C NMR spectra were recorded on 400, 500 and 600 MHz Bruker Avance spectrometers. Deuterated solvents were purchased from Cambridge Isotopes and CD_2Cl_2 was further purified by distilling over P_2O_5. Elemental analyses were performed by the Laboratoire d'Analyse Élémentaire de l'Université de Montréal, Montréal, Québec, Canada. The compounds 2-(2'-(dimesitylboryl)phenylethynyl)pyridine (**4.1**)[9], 2-(phenylethynyl)pyridine (**4.4**)[16] and $PtAr_2(DMSO)_2$ compounds[10] were synthesized according to literature procedures. The yield of **4.1** was increased from 35% to 78% by extending the reaction time from 16 to 40 h.

4.4.2 Synthesis and characterization

4.2a: degassed CD_2Cl_2 (0.5 mL) was added to a vial containing **4.1** (5.0 mg, 0.012 mmol) and $PtPh_2(DMSO)_2$ (5.9 mg, 0.012 mmol) sealed under N_2. The starting materials were dissolved by gently shaking the vial, and the resulting yellow solution was allowed to stand for 4 hours at room temperature. The solution was then transferred to a degassed NMR tube for spectroscopic characterization. The solvent was removed *in vacuo* and washed with 0.2 mL of hexanes to afford the product as a yellow solid in nearly quantitative yield (> 90%). ^{1}H NMR (600 MHz, $CDCl_3$): δ 8.71 (d, J = 4.9 Hz, 1H, pyridine), 8.25 (d, J = 7.6 Hz, 1H, phenyl), 7.65 (dt, J = 7.6 Hz, J = 1.1 Hz, 1H, phenyl), 7.55 (dt, J = 7.8 Hz, J = 1.4 Hz, 1H, pyridine), 7.52 (d, J = 6.8 Hz, 2H, Pt-phenyl), 7.50 (dt, J = 7.6 Hz, J = 0.8 Hz, 1H, phenyl), 7.42 (d, J = 6.9 Hz, 1H, phenyl), 6.96 (t, J = 7.5 Hz, 2H, Pt-phenyl), 6.86 (t, 1H, Pt-phenyl), 6.83 (t, J = 7.4 Hz, 2H, Pt-phenyl), 6.72 (t, J = 7.3, 1H, Pt-phenyl), 6.64 (d, J = 7.7 Hz, 1H, pyridine), 2.67 (s, 3H, DMSO), 2.57 (s, 3H, DMSO), 2.29 (s, 6H, mesityl), 2.06 (s, 12H, mesityl) ppm. ^{13}C NMR (150 MHz, CD_2Cl_2): δ 152.4, 151.0, 149.6, 145.0, 141.5, 140.0, 138.4, 137.1, 136.9, 135.7, 134.3, 131.6, 130.2, 130.1, 129.0, 128.4, 127.7, 127.1, 126.3, 124.7, 124.1, 123.2, 122.8, 97.2 (alkyne), 91.1 (alkyne), 43.4 (DMSO), 43.3 (DMSO), 23.6 (mesityl), 21.5 (mesityl) ppm. CHN calc'd for $C_{45}H_{46}BNOPtS$•DMSO: C 60.51, H 5.62, N 1.50 %, found C 60.09, H 5.20, N, 1.31 %.

4.3a: compound **4.1** (35 mg, 0.082 mmol) and $PtPh_2(DMSO)_2$ (41 mg g, 0.082 mmol) in toluene (5 mL) were stirred over 3 days at room temperature under N_2. Toluene was slowly removed under reduced pressure without heating, and the residue was washed with hexanes and dried under vacuum. The residue was re-dissolved in ~3 mL of toluene and layered with hexane; the solution was stored at -23°C in a sealed flask to afford **4.3a** as dark yellow crystals.

NMR-scale reaction: 0.5 mL CD_2Cl_2 was added to a vial containing **4.1** (5.0 mg, 0.012 mmol) and $PtPh_2(DMSO)_2$ (5.9 mg, 0.012 mmol) under N_2. The starting materials were dissolved by

gently agitating the vial, and the resulting yellow solution was transferred to an NMR tube sealed under N_2. The conversion yield was determined by ^{1}H NMR, integrating the 2-pyridyl peak of **4.3a** in reference to that of **4.2a**. After 30 days, the NMR spectrum showed 56% conversion.

^{1}H NMR (600 MHz, CD_2Cl_2): δ 9.52 (d, J = 5.4 Hz, 1H, pyridine), 9.28 (d, J = 7.7 Hz, 1H, phenyl), 7.34, (d, J = 7.3 Hz, 1H, phenyl), 7.28, (dt, J = 8.4 Hz, J = 1.4 Hz, 1H, pyridine), 7.18 (t, J = 7.2 Hz, 1H, phenyl), 7.14 (d, J = 7.6 Hz, 1H, Pt-phenyl), 7.08 (d, J= 8.2 Hz, 1H, pyridine), 6.89 (t, J = 7.3Hz, 1H, phenyl), 6.86 (dt, J = 7.4 Hz, J = 1.2 Hz, 1H, pyridine), 6.84 (t, J = 7.4 Hz, 1H, phenyl), 6.77 (s, 1H, mesityl), 6.69 (t, J = 7.2 Hz, 1H, Pt-phenyl), 6.67 (s, 1H, mesityl), 6.63 (dt, J = 7.8 Hz, J = 1.0 Hz, 1H, phenyl), 6.60 (dt, J = 7.5 Hz, J = 1.1 Hz, 1H, Pt-phenyl), 6.57 (t, J = 7.5 Hz, 1H, Pt-phenyl), 6.54 (s, 1H, mesityl), 6.50 (t, J = 7.5, 1H, phenyl), 6.24 (d, J = N/A, 1H, Pt-phenyl), 6.23 (s, 1H, mesityl), 5.44 (d, J = 7.9 Hz, 1H, phenyl), 2.64 (s, 3H, DMSO), 2.61 (s, 3H, mesityl), 2.54 (s, 3H, DMSO), 2.24 (s, 3H, mesityl), 2.20 (s, 3H, mesityl), 2.04 (s, 3H, mesityl), 1.65 (s, 3H, mesityl), 1.03 (s, 3H, mesityl) ppm. ^{13}C NMR (125 MHz, CD_2Cl_2): δ 149.8, 148.4, 144.4, 143.8, 140.9, 140.6, 139.9, 139.5, 139.1, 138.6, 137.9, 137.8, 136.2, 135.4, 132.29, 132.26, 131.9, 130.6, 129.5, 129.2, 129.0, 128.9, 128.7, 127.9, 126.03, 125.98, 125.84, 125.81, 125.6, 125.4, 125.1, 123.2, 122.5, 120.4, 45.0 (DMSO), 44.2 (DMSO), 35.2 (fused ring), 34.6 (fused ring), 26.5 (mesityl), 26.3 (mesityl), 25.8 (mesityl), 24.6 (mesityl), 21.2 (mesityl), 20.5 (mesityl) ppm. CHN calc'd for $C_{45}H_{46}BNOPtS$: C 63.23, H 5.42, N 1.64 %, found C 62.70, H 5.26, N 1.57 %.

4.2b: synthesized in analogy to **4.2a**, **4.1** (7.8 mg, 0.018 mmol) and Pt(*p*-OMe-$C_6H_4)_2(DMSO)_2$ (10.4 mg, 0.018 mmol) in CD_2Cl_2 were mixed and allowed to stand for 4 hours at room temperature. Removal of solvent following characterization afforded the product as a yellow solid in near quantitative (> 90%) yield. ^{1}H NMR (600 MHz, CD_2Cl_2): δ 8.68 (d, J = 5.0 Hz, 1H, pyridyl), 8.20 (d, J = 7.6 Hz, 1H, phenyl), 7.63 (t, J = 7.3 Hz, 1H, phenyl), 7.54 (t, J = 7.5 Hz, 1H,

pyridyl), 7.48 (t, J = 7.4 Hz, 1H, phenyl), 7.41 (d, J = 7.4 Hz, 1H, phenyl), 7.36 (d, J = 8.3 Hz, 2H, C_6H_4), 7.18 (d, br, J = 7.8 Hz, 3H, pyridyl and C_6H_4), 6.83 (s, 4H, mesityl), 6.64 (d, J = 7.4 Hz, 1H, pyridyl), 6.62 (d, J = 8.4 Hz, 2H, C_6H_4), 6.46 (d, J = 8.2 Hz, 2H, C_6H_4), 3.70 (s, 3H, methoxy), 3.60 (s, 3H, methoxy), 2.65 (s, 3H, dmso), 2.55 (s, 3H, dmso), 2.28 (s, 6H, mesityl), 2.05 (s, 12H, mesityl) ppm. ^{13}C NMR (150 MHz, CD_2Cl_2), δ 156.6, 156.4, 152.5, 145.0, 141.5, 140.0, 139.1, 138.0, 137.0, 136.9, 136.4, 135.7, 134.2, 131.6, 130.2, 130.0, 129.9, 129.0, 126.3, 124.6, 114.2, 113.8, 112.9, 97.1 (alkyne), 91.2 (alkyne), 55.4 (methoxy), 55.2 (methoxy), 43.5 (dmso), 43.3 (dmso), 23.6 (mesityl), 21.5 (mesityl) ppm. CHN calc'd for $C_{47}H_{50}BNO_3PtS$: C 61.70, H 5.51, N 1.53%; found C 61.24, H 6.04, N 1.46 %.

4.3b: compound **4.1** (35 mg, 0.082 mmol) and Pt(*p*-OMe-$C_6H_4)_2(DMSO)_2$ (46 mg g, 0.082 mmol) in 5:1 toluene/CH_2Cl_2 (6 mL) were stirred over 3 days at room temperature under N_2. The solvent was slowly removed under reduced pressure without heating, and the residue was washed with hexanes (2 × 3 mL). The hexane solution was stored under ambient conditions to afford **4.3b** as a dark yellow powder.

NMR-scale reaction: 0.5 mL degassed CD_2Cl_2 was added to a vial containing **4.1** (4.4 mg, 0.010 mmol) and Pt($C_6H_4OMe)_2(DMSO)_2$ (5.8 mg, 0.010 mmol) under N_2. The starting materials were dissolved by gently agitating the vial, and the resulting yellow solution was transferred to an NMR tube sealed under N_2. After 7 days, the NMR spectrum showed 37% conversion.

^{1}H NMR (400 MHz, CD_2Cl_2): δ 9.51 (d, J = 6.0 Hz, 1H, pyridyl), 9.16 (dd, J = 8.6 Hz, J = 2.3 Hz, 1H, C_6H_4), 7.33 (d, J = 7.0 Hz, 1H, phenyl), 7.28 (dd, J = 8.6 Hz, J = 1.7 Hz, 1H, pyridyl), 7.09 (d, J = 7.8, 1H, pyridyl), 7.03 (dd, J = 8.3 Hz, J = 1.8 Hz, 1H, C_6H_4), 6.84 (t, J = 7.2 Hz, 2H, pyridyl & phenyl), 6.76 (s, 1H, mesityl), 6.72 (dd, J = 8.3 Hz, J = 2.8 Hz, C_6H_4), 6.67 (s, 1H, mesityl), 6.67 (dd, J = 7.6 Hz, J = 1.3 Hz, 1H, phenyl), 6.54 (s, 1H, mesityl), 6.33 (dd, J = 8.3 Hz, J = 3.0 Hz, 1H, C_6H_4),6.28 (s, 1H, mesityl), 6.27 (dd, J = 8.3 Hz, J = 3.0 Hz, 1H, C_6H_4), 6.08 (dd,

J = 8.1 Hz, J = 1.8 Hz, 1H, C_6H_4), 6.07 (dd, J = 8.8 Hz, J = 2.8 Hz, 1H, C_6H_4), 6.01 (dd, J = 8.8 Hz, J = 2.3 Hz, 1H, C_6H_4), 5.46 (d, J = 8.1 Hz, 1H, phenyl), 3.68 (s, 3H, methoxy), 3.63 (s, 3H, methoxy), 2.62 (s, 6H, DMSO & mesityl), 2.55 (s, 3H, mesityl), 2.24 (s, 3H, mesityl), 2.19 (s, 3H, mesityl), 2.06 (s, 3H, mesityl), 1.64 (s, 3H, mesityl), 1.04 (s, 3H, mesityl) ppm. ^{13}C NMR (125 MHz, CD_2Cl_2): δ 157.4, 156.4, 149.8, 144.9, 143.9, 141.2, 140.9, 140.8, 139.7, 139.6, 139.5, 138.5, 137.6, 137.5, 137.4, 136.1, 135.4, 133.2, 133.0, 132.2, 131.8, 131.2, 131.1, 130.5, 129.2, 128.9, 126.0, 125.4, 123.1, 120.3, 114.2, 111.6, 111.0, 110.7, 55.5 (methoxy), 55.4 (methoxy), 44.9 (DMSO), 44.2 (DMSO), 35.2 (fused ring), 34.6 (fused ring), 26.5 (mesityl), 26.2 (mesityl), 25.8 (mesityl), 24.6 (mesityl), 21.2 (mesityl), 20.5 (mesityl) ppm. CHN calc'd for $C_{47}H_{50}BNO_3PtS$: C 61.70, H 5.51, N 1.53%; found C 62.77, H 4.34, N 1.51 %.

4.3c: synthesized in analogy to **4.2a**, **4.1** (8.3 mg, 0.020 mmol) and Pt(*p*-CF_3-$C_6H_4)_2(DMSO)_2$ (12.5 mg, 0.020 mmol) in CD_2Cl_2 were mixed and allowed to stand for 5 hours at room temperature. Removal of solvent following characterization afforded the product as a pale yellow solid in near quantitative (> 90%) yield. ^{1}H NMR (500 MHz, CD_2Cl_2): δ 8.66 (d, J = 5.0 Hz, 1H, pyridyl), 8.17 (d, J = 7.6 Hz, 1H, phenyl), 7.68 (d, J = 7.9 Hz, 2H, C_6H_4), 7.64 (t, J = 7.6 Hz, 1H, phenyl), 7.57 (t, J = 8.3, 1H, pyridyl), 7.51 (t, J = 7.6 Hz, 1H, phenyl), 7.49 (d, J = 7.4 Hz, 2H, C_6H_4), 7.42 (d, J = 7.4 Hz, 1H, phenyl), 7.23 (t, J = 7.4 Hz, 1H, pyridyl), 7.20 (d, J = 7.7 Hz, 2H, C_6H_4), 6.82 (s, 4H, mesityl), 6.65 (d, J = 7.9 Hz, 1H, pyridyl), 2.69 (s, 3H, dmso), 2.60 (s, 3H, dmso), 2.26 (s, 6H, mesityl), 2.04 (s, 12H, mesityl) ppm. ^{13}C NMR (150 MHz, CD_2Cl_2): δ 154.7, 152.3, 151.2, 147.1, 145.0, 143.2, 141.5, 140.1, 138.4, 137.6, 136.9, 136.7, 135.8, 134.0, 131.6, 130.5, 130.4, 129.1, 126.0, 125.0, 124.6, 123.9, 123.2, 97.7 (alkyne), 90.6 (alkyne), 43.7 (dmso), 43.5 (dmso), 23.6, 21.5 ppm. CHN calc'd for $C_{47}H_{44}BF_6NOPtS$: C 56.97, H 4.48, N 1.41 %; found C 57.14, H 5.33, N 1.37 %.

4.2d: compound **4.4** (18 mg, 0.10 mmol) and $PtPh_2(DMSO)_2$ (50 mg, 0.10 mmol) in toluene (3 mL) was stirred for 4 hours at room temperature under N_2. The resulting precipitate was filtered, washed with toluene (1 mL) and hexanes (3 × 2 mL), and dried to yield a white powder (40 mg, 67%). Colourless crystals were obtained in toluene (**4.2d** is sparingly soluble in toluene).

^{1}H NMR (600 MHz, CD_2Cl_2): δ 8.82 (dd, J = 5.5 Hz, J = 0.8 Hz, 1H, pyridine), 7.90 (dd, J = 6.6 Hz, J = 4.8 Hz, 2H, phenyl), 7.73 (dt, J = 7.7 Hz, J = 1.6 Hz, 1H, pyridine), 7.63 (d, J = 7.9, 1H, pyridine), 7.54 (dd, J = 5.3 Hz, J = 4.6 Hz, 3H, phenyl), 7.50 (dd, J = 7.9 Hz, J = 1.2 Hz, 2H, Pt-phenyl), 7.42 (dd, J = 7.9 Hz, J = 1.2 Hz, 2H, Pt-phenyl), 7.31 (dt, J = 5.7 Hz, J = 1.3 Hz, 1H, pyridine), 6.93 (t, J = 7.5 Hz, 2H, Pt-phenyl), 6.84 (t, J = 7.6 Hz, 2H, Pt-phenyl), 6.81 (t, J = 7.4 Hz, 1H, Pt-phenyl), 6.71 (t, J = 7.3 Hz, 1H, Pt-phenyl), 2.76 (s, 3H, DMSO), 2.61 (s, 3H, DMSO) ppm. ^{13}C NMR (100 MHz, CD_2Cl_2): 152.8, 149.6, 145.1, 141.0, 137.8, 136.6, 132.5, 130.5, 129.9, 129.5, 129.3, 128.4, 137.8, 127.1, 125.1, 124.2, 123.2, 122.8, 122.4, 96.1 (alkyne), 88.3 (alkyne), 43.4 (DMSO), 43.2 (DMSO) ppm. CHN calc'd for $C_{27}H_{25}NOPtS$: C 53.46, H 4.15 N 2.31 %, found C 53.54, H 4.00, N 2.22 %.

4.2e: compound **4.1** (30 mg, 0.070 mmol) and $PtCl_2(DMSO)_2$ (30 mg, 0.070 mmol) in toluene (5 mL) were stirred overnight at 60°C under N_2 to afford a white precipitate. Toluene was slowly removed under reduced pressure, and the residue was washed with hexanes and dried under vacuum (55 mg, 57%). ^{1}H NMR (500 MHz, $CDCl_3$): δ 8.66 (d, J = 5.8 Hz, 1H, pyridine), 8.22 (d, J = 7.5 Hz, 1H, phenyl), 7.61 (dt, J = 7.8 Hz, J = 1.2 Hz, 1H, pyridine), 7.55 (dt, J = 7.4 Hz, J = 1.5 Hz, phenyl), 7.44 (dt, J = 7.8 Hz, J = 0.9 Hz, 1H, phenyl), 7.42 (dd, J = 7.5 Hz, J = 1.1 Hz, 1H, phenyl), 7.21 (dt, J = 7.5 Hz, J = 1.4 Hz, 1H, pyridine), 6.80 (s, 4H, mesityl), 6.66 (d, J = 7.5 Hz, pyridine), 3.44 (s, 3H, DMSO), 3.31 (s, 3H, DMSO), 2.27 (s, 6H, mesityl), 2.02 (s, 12H mesityl) ppm. ^{13}C NMR (125 MHz, $CDCl_3$): δ 153.1, 145.9, 139.4, 137.9, 135.2, 134.2, 131.4, 130.1, 129.7, 128.5, 124.7, 124.6, 109.6 (alkyne), 99.4 (alkyne), 90.1 (mesityl), 86.6 (mesityl),

44.8 (DMSO), 44.2 (DMSO), 23.3 (mesityl), 21.2 (mesityl) ppm. CHN calc'd for $C_{33}H_{36}BCl_2NOPtS$: C 51.37, H 4.70, N 1.82 %, found C 50.86, H 4.61, N 1.77%.

Pt(*p*-OMe-C_6H_4)$_2$(DMSO)$_2$: Pt(*p*-OMe-C_6H_4)$_2$(COD) (0.50 g, 0.97 mmol) was dissolved in 10 mL of DMSO and the solution stirred at 80°C for 1 h. The solvent was removed via vacuum distillation at 70°C, and recrystallization of the residue from CH_2Cl_2/hexane gave the desired product as a white solid (0.36 g, 68%). Pt(*p*-OMe-C_6H_4)$_2$(COD) was prepared in using the procedure described by Shekhar and Hartwig[4]. ^{1}H NMR (400 MHz, $CDCl_3$): δ 7.16 (d, sat J_{Pt-H} = 34.5 Hz, J = 8.0 Hz, 4H, C_6H_4), 6.64 (d, J = 8.0 Hz, 4 H, C_6H_4), 3.68 (s, 6H, methoxy), 2.82 (s, 12H, dmso) ppm. ^{13}C NMR (100 MHz, $CDCl_3$): δ 156.4, 135.6, 135.3, 113.8, 54.9, 43.4 ppm.

Pt(*p*-CF_3-C_6H_4)$_2$(COD): 4-bromobenzotrifluoride (0.29 g, 1.3 mmol) was dissolved in 20 mL Et_2O and cooled to -78°C under N_2. To the solution was added *n*-butyllithium (0.8 mL, 1.3 mmol) in dropwise fashion. After 45 min, $PtCl_2$(COD) (0.22 g, 0.58 mmol) was added and the mixture continued to stir for 3 h at -78°C. The reaction was allowed to warm to room temperature and left to stir overnight. The product was extracted using Et_2O/dilute NH_4Cl, the combined ether extracts were dried over $MgSO_4$ filtered through a 1 cm pad of Celite and a 2 cm pad of decolorizing carbon. Ether was evaporated from the filtrated *in vacuo*, and a white solid was obtained after washing the residue with hexanes (0.17 g, 49%). ^{1}H NMR (300 MHz, $CDCl_3$): δ 7.38 (d, sat J_{Pt-H} = 33.7 Hz, J = 7.7 Hz, 4H, C_6H_4), 7.24 (d, J = 7.4 Hz, 4H, C_6H_4), 5.09 (s, sat J_{Pt-H} = 18.9 Hz, 4H, cod), 2.57 (s, 8H, cod) ppm.

Pt(*p*-CF_3-C_6H_4)$_2$(DMSO)$_2$: Pt(*p*-CF_3-C_6H_4)$_2$(COD) (0.36 g, 0.62 mmol) was dissolved in 10 mL of DMSO and the solution stirred at 80°C for 1 h. The solvent was removed via vacuum distillation at 70°C, and recrystallization of the residue from CH_2Cl_2/hexane gave the desired

product as a white solid (0.32 g, 80%). ^{1}H NMR (400 MHz, $CDCl_3$): δ 7.44 (d, sat J_{Pt-H} = 34.7 Hz, J = 7.8 Hz, 4H, C_6H_4), 7.23 (d, J = 7.6 Hz, 4H, C_6H_4), 2.82 (s, 12H, DMSO). ^{13}C NMR (100 MHz, CD_3Cl): δ 150.6, 135.8, 126.2, 124.5, 124.2, 43.5 ppm.

4.4.3 ^{1}H NMR Spectra

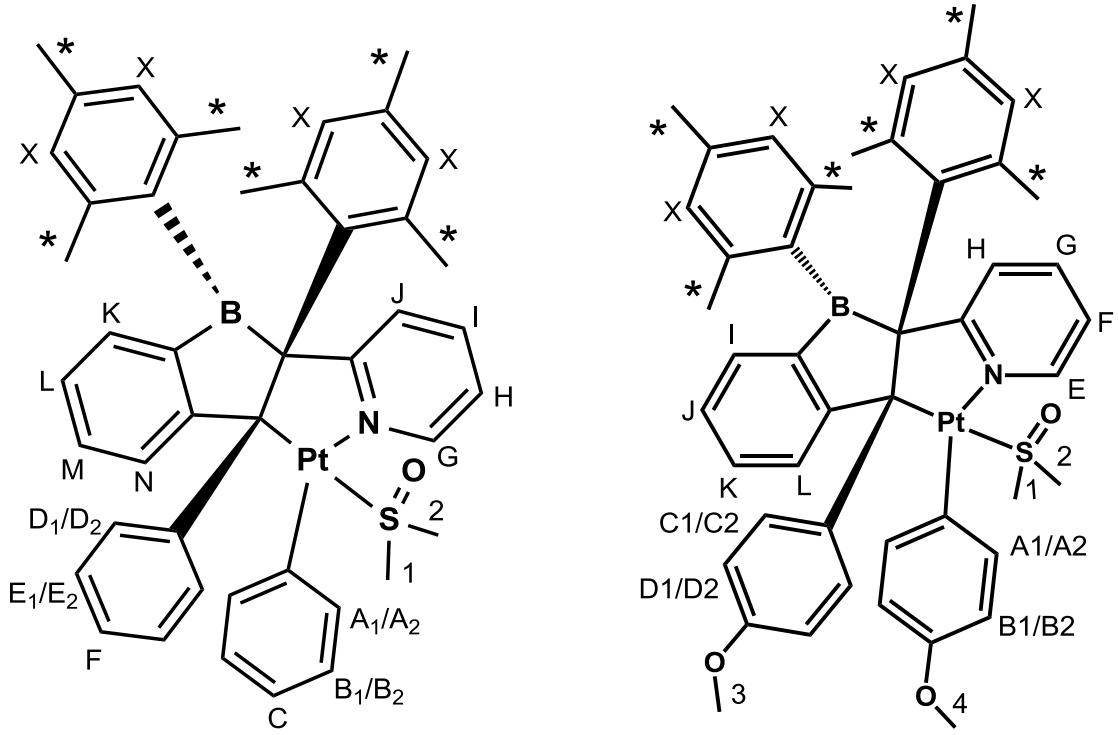

Figure 4.14 Structures of **4.3a** and **4.3b** with labeling scheme.

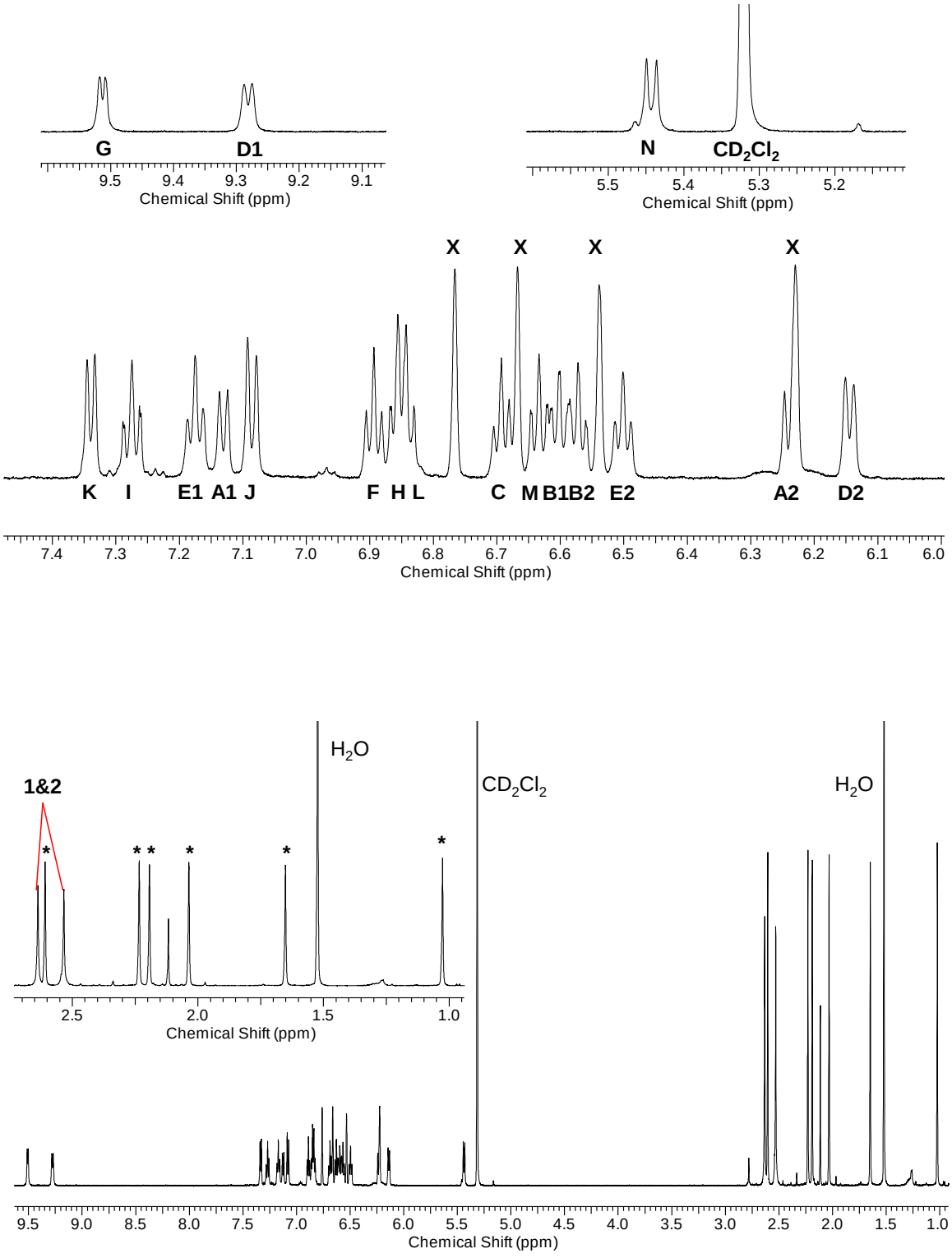

Figure 4.15 ^{1}H NMR spectrum of **4.3a** (bottom) and expanded aromatic region (top) in CD_2Cl_2.

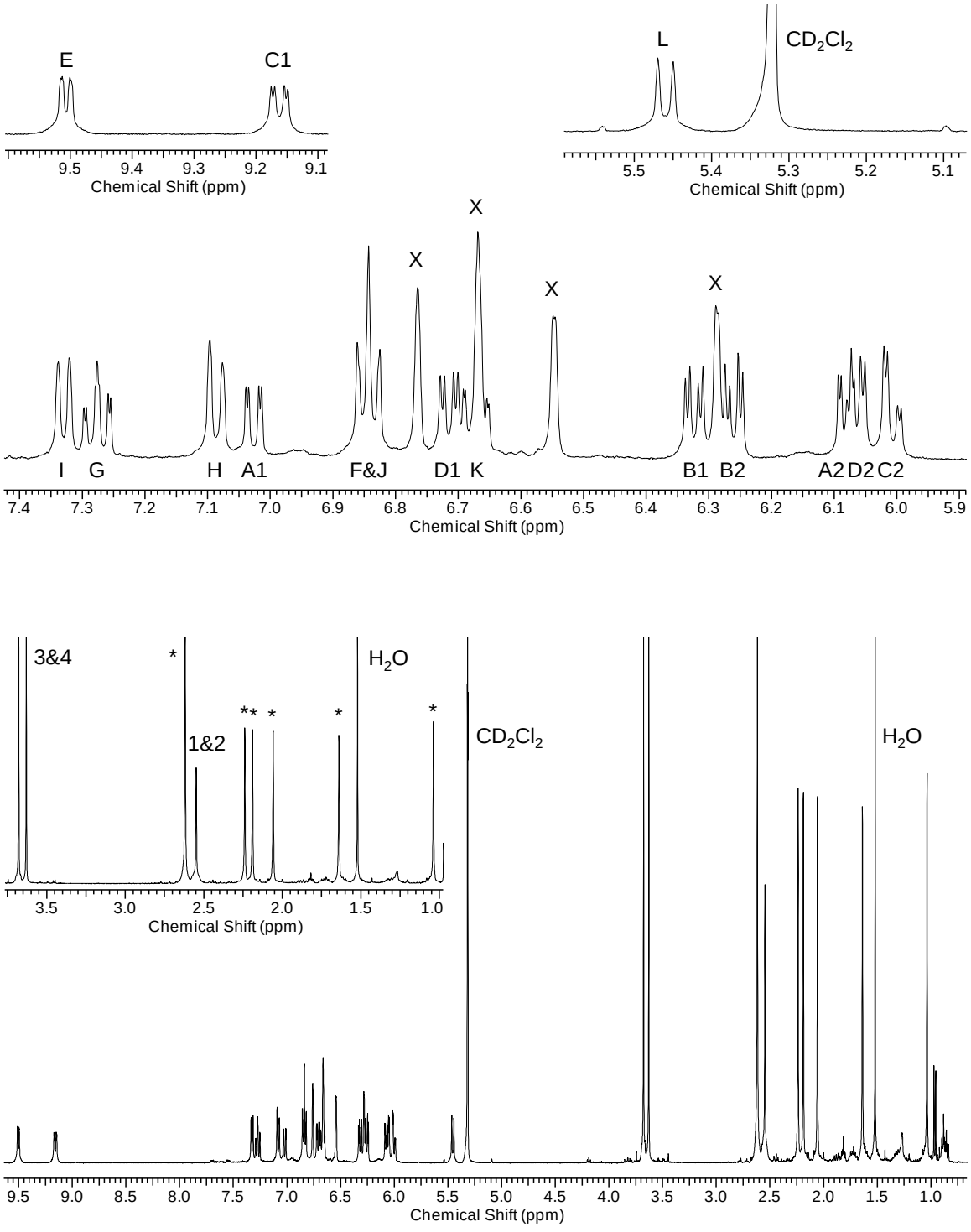

Figure 4.16 ^{1}H NMR spectrum of **4.3b** (bottom) and expanded region (top) in CD_2Cl_2.

4.4.4 Density functional theory calculations

The DFT study of the mechanism was done using the Becke three-parameter Lee-Yang-Parr (B3LYP) functional.[17] The basis sets used were 6-31G(d, p) for atoms C, H, B, N, O, and S, and LanL2DZ for Pt. The differences in reactant and product structures were examined and several pathways explored by scanning across the bonds reasoned to be relevant from this information. The characterization of stationary points along the reaction pathway was achieved by optimizing promising structures using standard methodology for local minima and transition state methodology for local maxima. The structures with lowest energy were taken to be the most likely pathway. The transition state structures were also verified with intrinsic reaction coordinate (IRC) calculations to confirm connections between forward and backward intermediates (minima). All geometry optimizations and IRC calculations were performed with the Gaussian 09 software package. Computing resources were provided by SHARCNET and WestGrid.

4.4.5 X-ray diffraction analysis

Single crystals of **4.3a**, and **4.2d** were mounted on glass fibers for data collection. Data were collected on a Bruker Apex II single-crystal X-ray diffractometer with graphite-monochromated Mo Kα radiation, operated at 50 kV and 30 mA and at 180 K. Data were processed on a PC with the aid of the Bruker SHELXTL software package (version 6.14)[18] and corrected for absorption effects. No significant decay was observed.

Table 4.1 Crystallographic data for compounds **4.3a** and **4.2d**

Compound	**4.3a**	**4.2d**
Formula	$C_{45}H_{46}BNOPtS$	$C_{27}H_{25}NOPtS$
FW	854.79	606.63
Space Group	P-1	P2(1)/c
a, Å	11.615(3)	12.9799(4)
b, Å	12.039(3)	13.2628(3)
c, Å	13.482(4)	14.7986(4)
α, °	93.144(3)	90
β, °	98.670(3)	114.901(2)
γ, °	96.355(3)	90
V, $Å^3$	1847.4(9)	2310.74(11)
Z	2	4
D_{calc}, g cm^{-1}	1.537	1.744
T, K	180(2)	180(2)
μ, mm^{-1}	3.891	6.182
$2\theta_{max}$, °	54.46	54.54
Reflns measured	19911	14815
Reflns used (R_{int})	8020(0.0302)	5095(0.0507)
Parameters	860	1184
Final R Values [I > 2σ(I)]:		
R_1[a]	0.0249	0.0410
wR_2[b]	0.0530	0.00930
R values (all data):		
R_1[a]	0.0309	0.0609
wR_2[b]	0.0553	0.1021
Goodness-of-fit on F^2	1.039	1.006

[a] $R_1 = \Sigma[(|F_0| - |F_c|) / \Sigma |F_0|$

[b] $wR2 = [\Sigma w[(F_0^2-F_c^2)^2] / \Sigma[w(F_0^2)^2]]^{1/2}$

$w = 1 / [\sigma^2(F_0^2) + (0.075P)^2]$, where $P = [Max (F_0^2, 0) + 2F_c^2] / 3$

Table 4.2 Selected bond lengths (Å) and angles (°) for compounds **4.3a** and **4.2d**

4.3a			
Pt(1)-C(3)	2.025(3)	C(3)-Pt(1)-N(1)	174.04(10)
Pt(1)-N(1)	2.113(2)	C(3)-Pt(1)-C(1)	91.85(11)
Pt(1)-C(1)	2.120(3)	N(1)-Pt(1)-C(1)	83.07(10)
Pt(1)-S(1)	2.3026(9)	C(3)-Pt(1)-S(1)	86.28(8)
C(1)-C(2)	1.627(4)	N(1)-Pt(1)-S(1)	98.87(7)
B(1)-C(10)	1.528(5)	C(1)-Pt(1)-S(1)	177.69(8)
B(1)-C(17)	1.587(5)	C(10)-B(1)-C(17)	125.1(3)
B(1)-C(2)	1.656(4)	C(10)-B(1)-C(2)	106.0(3)
		C(17)-B(1)-C(2)	127.1(3)

4.2d			
Pt(1)-C(1)	2.026(6)	C(1)-Pt(1)-C(7)	86.4(2)
Pt(1)-C(7)	2.030(6)	C(1)-Pt(1)-N(1)	176.6(2)
Pt(1)-N(1)	2.150(5)	C(7)-Pt(1)-N(1)	90.2(2)
Pt(1)-S(1)	2.2955(16)	C(1)-Pt(1)-S(1)	93.85(18)
C(18)-C(19)	1.197(9)	C(7)-Pt(1)-S(1)	178.94(19)
		N(1)-Pt(1)-S(1)	89.54(14)

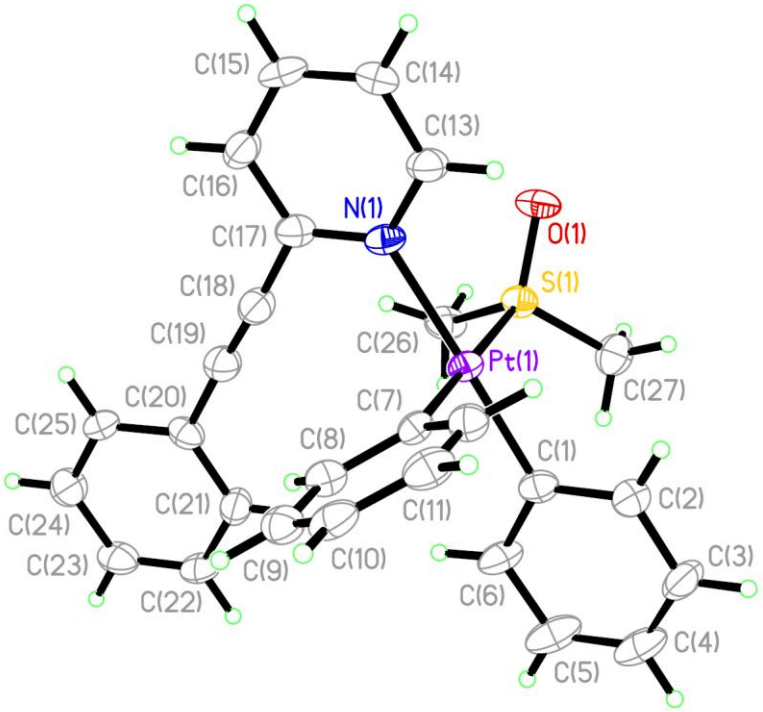

Figure 4.17 Crystal structure of **4.2d** with 50% thermal ellipsoids and labeling scheme.

4.5 References

(1) (a) Entwistle, C. D.; Marder, T. B. *Angew. Chem., Int. Ed*. **2002**, *41*, 2927. (b) Entwistle, C. D.; Marder, T. B. *Chem. Mater*. **2004**, *16*, 4574. (c) Jäkle, F. *Chem. Rev*. **2010**, *110*, 3985. (d) Jäkle, F. *Coord. Chem. Rev*. **2006**, *250*, 1107. (e) Wade, C. R.; Broomsgrove, A. E. J.; Aldridge, S.; Gabbaï, F. P. *Chem. Rev*. **2010**, *110*, 3958.

(2) (a) Ansorg, K.; Braunschweig, H.; Chiu, C. W.; Engels, B.; Gamon, D., Hügel, M.; Kupfer, T.; Radacki, K. *Angew. Chem., Int. Ed.* **2011**, *50*, 2833. (b) Braunschweig, H.; Dewhurst, R. D. *Dalton Trans*. **2011**, *40*, 549. (c) Braunschweig, H.; Dewhurst, R. D.; Schneider, A. *Chem. Rev*. **2010**, *110*, 3924. (d) Piers, W. E.; Bourke, S. C.; Conroy, K. D. *Angew. Chem., Int. Ed.* **2005**, *44*, 5016. (e) Hübner, A.; Qu, Z. W.; Englert, U.; Bolte, M.; Lerner, H. W.; Holthausen, M. C.; Wagner, M. *J. Am. Chem. Soc*. **2011**, *133*, 4596.

(3) (a) Murakami, M.; Miura, T. *Chem. Commun.* **2007**, 217. (b) Suginome, M.; Yamamoto, A.; Murakami, M. *Angew. Chem., Int. Ed.* **2005**, *44*, 2380. (c) Suginome, M.; Yamamoto, A.; Murakami, M. *J. Am. Chem. Soc*. **2003**, *125*, 6358.

(4) (a) Rao, Y. L.; Amarne, H.; Zhao, S. B.; McCormick, T. M.; Martic, S.; Sun, Y.; Wang, R. Y.; Wang, S. *J. Am. Chem. Soc*. **2008**, *130*, 12898. (b) Baik, C.; Hudson, Z. M.; Amarne, H.; Wang, S. *J. Am. Chem. Soc*. **2009**, *131*, 14549. (c) Baik, C.; Murphy, S. K.; Wang, S. *Angew. Chem., Int. Ed*. **2010**, *49*, 8224. (d) Amarne, H.; Baik, C.; Wang, R. Y.; Lu, J. S.; Wang, S. *Organometallics* **2011**, *30*, 665. (e) Rao, Y. L.; Wang, S. *Inorg. Chem*. **2011**, *50*, 12263.

(5) (a) Fukazawa, A.; Yamaguchi, E.; Ito, E.; Yamada, H.; Wang, J.; Irle, S.; Yamaguchi, S. *Organometallics* **2011**, *30*, 3870. (b) Fukazawa, A.; Yamada, H.; Yamaguchi, S. *Angew. Chem., Int. Ed.* **2008**, *47*, 5582. (c) Iida, A.; Yamaguchi, S. *J. Am. Chem. Soc*. **2011**, *133*, 6952. (d) Fukazawa, A.; Yamaguchi, S. *Chem. Asian. J*. **2009**, *4*, 1386.

(6) (a) Dureen, M. A.; Stephan, D. W. *J. Am. Chem. Soc.* **2009**, *131*, 8396. (b) Welch, G. C.; Juan, R. R. S.; Masuda, J. D.; Stephan, D. W. *Science* **2006**, *314*, 1124. (c) Dureen, M. A.; Brown, C. C.; Stephan, D. W. *Organometallics* **2010**, *29*, 6422. (d) Dureen, M. A.; Brown, C. C.; Stephan, D. W. *Organometallics* **2010**, *29*, 6594.

(7) For recent reviews see: (a) Stephan, D. W.; Erker, G. *Angew. Chem., Int. Ed.* **2010**, *49*, 46. (b) Voss, T.; Chen, C.; Kehr, G.; Nauha, E.; Erker, G.; Stephan, D. W. *Chem. Eur. J.* **2010**, *16*, 3005. (c) Stephan, D. W. *Dalton Trans.* **2009**, 3129. (d) Stephan, D. W. *Org. Biomol. Chem*. **2008**, *6*, 1535. (e) Stephan, D. W.; Greenberg, S.; Graham, T. W.' Chase, P.; Hastie, J. J.; Geier, S. J.; Farrel, J. M.; Brown, C. C.; Heiden, Z. M.; Welch, G. C.; Ullrich, M. *Inorg. Chem.* **2011**, *50*, 12338. (f) Piers, W. E.; Marwitz, A. J. V.; Mercier, L. G. *Inorg. Chem.* **2011**, *50*, 12252.

(8) (a) Hudson, Z. M.; Wang, S. *Dalton Trans*. **2011**, *40*, 7805. (b) Hudson, Z. M.; Sun, C.; Helander, M.; Amarne, H.; Lu, Z. H.; Wang, S. *Adv. Funct. Mater*. **2010**, *20*, 3426. (c) Hudson, Z. M.; Helander, M.; Lu, Z. H.; Wang, S. *Chem. Commun*. **2011**, *47*, 755. (d) Sun, Y.; Ross, N.; Zhao, S. B.; Huszarik, K.; Jia, W. L.; Wang, R. Y.; Macartney, D.; Wang, S. *J. Am. Chem. Soc.* **2007**, *129*, 7510.

(9) Sun, C.; Lu, J. S.; Wang, S. *Org. Lett*. **2011**, *13*, 1226.

(10) $PtPh_2(DMSO)_2$ and Pt(*p*-MeO-Ph)$_2$(DMSO)$_2$ are previously known compounds while Pt(*p*-CF_3-Ph)$_2$(DMSO)$_2$ is novel. $PtPh_2(DMSO)_2$ was synthesized using the procedure reported in (a) Klein, A.; Schurr. T.; Knodler. A.; Gudat, D.; Klinkhammer, K. W.; Jain, K.; Zalis, S.; Kaim, W. *Organometallics* **2005**, *17*, 4125. Pt(*p*-MeO-Ph)$_2$(DMSO)$_2$ and Pt(*p*-CF_3-Ph)$_2$(DMSO)$_2$ were synthesized using modified procedures reported in (b) Shekhar, S.; Hartwig, J. F. *J. Am. Chem.Soc.* **2004**, *126*, 13016., and (c) Yagyu, T.; Ohashi, J.; Maeda, M. *Organometallics* **2007**, *26*, 2383.

(11) Crystal data of **4.3a** and **4.2d** have been deposited at the Cambridge Crystal Data Center (CCDC 868871 & 868872).

(12) (a) Ishida, N.; Narumi, M.; Murakami, M. *Org. Lett.* **2008**, *10*, 1279. (b) Ishida, N.; Shimamoto, Y.; Murakami, M. *Org. Lett*. **2009**, *11*, 5434. (c) Ishida, N.; Ikemoto, W.; Narumi, M.; Murakami, M. *Org. Lett*. **2011**, *13*, 3008. (d) Ishida, N.; Shinmoto, T.; Sawano, S.; Miura, T.; Murakami, M. *Bull. Chem. Soc. Jpn*. **2010**, *83*, 1380. (e) Chen, C.; Eweiner, F.; Wibbeling, B.; Fröhlich, R.; Senda, S.; Ohki, Y.; Tatsumi, K.; Grimme, S.; Kehr, G.; Erker, G. *Chem. Asian. J.* **2010**, *5*, 2199. (f) Midland, M. M.; Brown, H. C. *J. Org. Chem.* **1975**, *40*, 2846. (g) Partyka, D. V. *Chem. Rev.* **2011**, *111*, 1529 and references therein.

(13) Chen, C.; Kehr, G.; Fröhlich, R.; Erker, G. *J. Am. Chem. Soc*. **2010**, *132*, 13594.

(14) (a) Davies, B. W.; Puddephatt, R. J.; Payne, N. C. *Can. J. Chem.* **1972**, *50*, 2276. (b) Ozawa, F.; Kamite, J. *Organometallics* **1998**, *17*, 5630. (c) Yamashita, H.; Tanaka, M.; Goto, M. *Organometallics* **1993**, *12*, 988.

(15) Chianese, A. R.; Lee, S. J.; Gagné, M. R. *Angew. Chem., Int. Ed.* **2007**, *46*, 4042 and references therein.

(16) Tuesuwan, B.; Kerwin, S. M. *Biochem*. **2006**, *45*, 7265.

(17) Frisch, M. J. *et al*. Gaussian 03, Revision C.02, Gaussian, Inc., Wallingford, CT, 2004.

Chapter 5

Summary and Outlook

In this work, we have demonstrated the use of a new triarylboron-containing 2,4,6-triphenyltriazine as an electron-transport material in OLEDs. This material was found to exhibit high triplet energy level, as well as low-lying HOMO and LUMO orbitals. Incorporation of this material into OLEDs using $Ir(ppy)_3(acac)$ as green phosphorescent emitter gave high-efficiency devices with performance appropriate for use in the display industry.

This strategy has proven to be highly successful; further optimization of devices incorporating this material will likely lead to significant improvements in turn-on voltage and efficiency. Further derivatives of triarylboron-containing materials based on a triazine core are also promising candidates for use as ETLs in OLEDs and should be explored. Finally, due to the high triplet energy of this material, investigation of its potential as a host for blue phosphorescent OLEDs is a promising avenue for further research.

We then discovered a facile hydration reaction for alkyne bonds based on the synergistic action of an intramolecular Lewis acid-base pair. The compound 2-(2'-(dimesitylboryl)phenylethynyl)pyridine contained an aromatic nitrogen atom that acted as an internal base to deprotonate water, which then allowed the coordination of hydroxide to the boron center. Association of Cu(I) catalyst to the alkyne bond then promoted the attack of hydroxide on the alkyne carbon, giving the hydration product. Due to the stabilization by the boron center, the product was isolated as an enol ester.

The reactivity we discovered was unique to the molecular geometry of this system, and will likely be difficult to reproduce in similar ambiphilic molecules. However, the insight gained from this reaction may prove useful in the development of new catalytic systems for hydration

reactions. In particular, exploration of catalysts incorporating both Lewis acidic and basic groups for the hydration of alkynes may lead to interesting synthetic routes to carbonyl compounds.

Finally, new and unusual reactivity was discovered from the reaction of 2-(2'-(dimesitylboryl)phenylethynyl)pyridine with Pt(II). Addition of this ligand to $PtPh_2(DMSO)_2$ resulted in a surprising double cyclization reaction accompanied by a double 1,2-aryl rearrangement. Furthermore, this transformation led to reduction of the central alkyne to a carbon-carbon single bond. The structure of this product was confirmed by single-crystal X-ray diffraction analysis, as well as by 1D and 2D NMR spectroscopy. The electronic factors governing the reactivity of this system were also studied using structurally related compounds.

This class of reactivity is unprecedented, and is likely to be specific to our ligand system. However, exploration of this reactivity using other electron-rich metals may result in new and exciting products. Incorporation of this ligand's structure into extended π-conjugated homologues may also result in a new and diverse class of compounds.